Development of Advanced ECAs with Micro/nano Hybrid Filler System: Filler Functionalization, Dispersion, and Conductivity Improvement

by

Behnam Meschi Amoli

A thesis
presented to the University of Waterloo
in fulfillment of the
thesis requirement for the degree of
Doctor of Philosophy
in
Chemical Engineering

Waterloo, Ontario, Canada, 2015

AUTHOR'S DECLARATION

I hereby declare that I am the sole author of this thesis. This is a true copy of the thesis, including any required final revisions, as accepted by my examiners.

I understand that my thesis may be made electronically available to the public.

Abstract

During the recent two decades, considerable efforts have been made to explore new generations of interconnecting materials and printed lines to replace the traditionally used toxic lead-based solders in electronic industries. Electrical conductive adhesive (ECA) which consists of conductive metallic particles and a polymeric matrix has attracted a great deal of attention as one of the most promising alternative materials. The conventional ECAs are typically made of silver micro flakes and epoxy resin. The low electrical conductivity of these ECAs is their main drawback compared to traditional lead-based solders, which hinders their applicability in today's blooming electronic industries. An enormous amount of research works have been conducted to enhance the electrical conductivity of the conventional ECAs, including increasing the polymer shrinkage, surface modification of silver flakes, introduction of low melting components to the ECA formulation, and the use of nano-sized conductive materials inside the formulation of the conventional ECAs. All of these approaches affect the quality of inter filler interaction inside the electrical network, in different ways.

The recent progress in nanotechnology helped material scientists to precisely design nanomaterials with different morphologies and surface chemistry. Owing to this capability, incorporation of nano-sized conductive fillers with different natures, morphologies, and surface properties inside the conventional formulation of ECAs has drawn considerable

attention to overcome the common drawbacks of conventional ECAs, such as poor electrical and mechanical properties, reliability issues, and large filler content. It has been reported that the introduction of conductive nanomaterials into the conventional ECAs can improve the electrical conductivity of ECAs if their size, morphology, and the ratio between nanofiller and silver flakes is carefully taken under consideration. In this project, we developed new generations of hybrid electrical conductive adhesives (ECAs) by introducing conductive nanofillers (spherical silver nanoparticles (Ag NPs), high aspect-ratio silver nanobelts (Ag NBs), and graphene) into the conventional formulation of ECAs. To harness the characteristic properties of the nanofillers and to facilitate their homogeneous dispersion inside the epoxy, nanofillers were functionalized.

In the first step of this project, spherical Ag NPs were synthesized and simultaneously functionalized with thiocarboxilic acids, resulting in the formation of NPs less than 5 nm. Two thiocarboxylic acids with the same chemical structure but different chain lengths (3 and 11 carbons) were used to functionalize the NPs. We showed that the size and the electrical properties of the NPs can be controlled by varying the chain length of their covering organic layer. The diameter of the Ag NPs functionalized with the short-chain acid was two times smaller than those with the long-chain acid. We also found that the short-chain functionalized NPs were electrically conductive while the long-chain functionalized ones were nonconductive. The short-chain functionalized NPs were incorporated into the conventional ECAs. We found that at low NPs contents (< 20 wt %) the electrical conductivity of the hybrid ECAs increased due to the filling of NPs into the interstices of the micron-sized silver

flakes, bridging of the NPs among separated flakes, and sintering of the NPs at relatively low curing temperature of 150 °C. However, higher NPs contents reduced the electrical conductivity because they may cluster and increase the gaps between the silver flakes. Furthermore, at higher NPs content, the number of contact points increases, which in turn decreases the electrical conductivity of the final ECAs.

The positive effect of the synthesized NPs on the electrical conductivity of the nanocomposite is basically attributed to the increased number of electrical pathways inside the electrical network due to the bridging of the NPs between separated silver flakes. However, a large amount of NPs are needed to form effective bridges inside the network, which increases the number of contact points inside the filler system and also increases the cost of the final ECAs. In the second step, we implement a novel type of high aspect-ratio silver nanostructure, silver nanobelts (Ag NBs), as co-filler inside the conventional formulation of the ECAs. The Ag NBs (10-40 nm thick, 100-400 nm wide and 1-10 μm long) were synthesized through self-assembly and room-temperature joining of hexagonal and triangular silver unit blocks which were synthesized by chemical reduction of silver nitride in the presence of poly(methacrylic acid). The incorporation of a small amount of the Ag NBs (2 wt%, NBs to flakes weight-ratio, K = 0.03) into a conventional ECA with 60 wt% silver flakes resulted in an electrical conductivity enhancement of 1550% in comparison to that of the conventional ECAs with the same total silver weight fraction, while addition of 2 wt% (K = 0.03) NBs into the conventional ECA with 80 wt% silver flakes enhanced the electrical conductivity of the hybrid ECA approximately 240%. These results imply high aspect-ratio

NBs are more effective to improve the electrical conductivity of ECAs at concentrations close to percolation threshold.

Considering the importance of the aspect-ratio of the nanofillers, in the next step, we implemented graphene, which is known for its exceptional electrical, mechanical and thermal properties, to further reduce the amount of silver flakes while maintaining a high electrical conductivity. Graphene, possessing the highest aspect-ratio among all the nanostructures and also due to its 2D structure, can provide extremely high surface area for electron transformation inside the electrical network. However, to exploit the interesting properties of the graphene, their single layer structure must be preserved inside the polymeric matrix. To achieve this goal, we applied two types of surface modification to exfoliate and stabilize graphene layers. First, we decorated graphene surface with Ag NPs, functionalized with a short chain length thiocarboxylic acid, and introduced this 2D nanostructure into the conventional ECAs. The electrical conductivity measurements revealed that the decorated graphene significantly improves the electrical conductivity of the conventional ECAs only at low filler concentrations, while to achieve high electrical conductivity, elevated curing temperatures are needed. This situation is a result of the increased number of contact points because of Ag NPs on graphene surface. Second, we used a non-covalent approach to stabilize graphene using the surfactant; sodium dodecyl sulfate (SDS). Our results showed that the stabilization of graphene with SDS noticeably enhance the electrical conductivity of the ECAs, which is attributed to the role of SDS in exploiting the high aspect-ratio of graphene. In order to examine this hypothesis, we used a larger size graphene and applied the

same SDS modification protocol. The electrical resistivity measurements showed that the electrical conductivity enhancement in the case of hybrid ECAs with large SDS–modified graphene was more significant than that with small SDS–modified graphene. The percolation threshold for the hybrid ECA with 1.5 wt% of both large and small graphene was reduced to an interestingly low value of 10 wt% while this value for conventional ECAs, and hybrid ECAs with non-modified graphenes was 40 wt%. Furthermore, adding 1.5 wt% of large SDS-modified graphene into the conventional ECA with 80 wt% silver flake content resulted in a very low electrical resistivity of 1.6×10^{-5} Ω.cm which is lower than that of eutectic lead-based solders.

Acknowledgements

First and foremost, I would like to express my deepest gratitude to my supervisor, Professor Boxin Zhao, for all his expert guidance, support, and encouragement throughout my PhD research. Without his help and incredible counsel my PhD project would have been a frustrating and overwhelming pursuit.

I would also like to pass my great appreciation to my co-supervisor, Professor Norman Zhou for his insightful guidance and support throughout these years. Many thanks go to my friends and colleagues at the University of Waterloo for their patience and support during the course of my PhD career.

I wish to acknowledge financial support from the Natural Sciences and Engineering Research Council (NSERC) of Canada.

Dedication

I dedicate this thesis to my beloved parents, Hassan Meschi Amoli and Manzar Karegar. I hope that this achievement will complete the dream that you always had for me all those many years ago when you chose to give me the best education you could.

Table of Contents

List of Figures

List of Tables

Chapter 1. Introduction, Motivation, and Thesis Outline

Lead-based solders are conventionally used as electrical interconnecting materials in electronic manufacturing, providing electrical paths between one circuit element and another upon their attachment to a system level board. However, lead has long been recognized as a hazardous material to human beings and our environment. The lead-based solders are mainly consumed in the production of electronic devices, which usually possess a life time of less than 5 years, which leads to a huge amount of lead accumulation in landfills each year. For instance, the total lead consumption in the US for 2000 was 52,400 metric tons of which more than 10% was used in production of lead-based solders [1]. Many countries have started to establish restricted regulations to abandon the application of lead in their electronic industries. This situation has inspired material scientists and researchers to find proper alternatives for the conventional eutectic solders. Today's blooming electronic technologies, e.g., multilayer printed circuits [2], thin-film transistors (TFTs) [3], transparent conductive coating [4], solar cells [5], and batteries, require advanced materials that offer high electrical conductivity, good flexibility, proper strechability, and satisfactory mechanical strength. In addition, these materials should be cost effective, environmentally benign, and easily processable. In this regard, electrically conductive adhesives (ECAs) are considered as the most promising alternative interconnection materials for future applications.

ECAs consist of a polymeric matrix, granting the physical and mechanical properties, and conductive fillers, providing the electrical pathways throughout the matrix. Depending on the

applications and desired electrical properties, different types of polymers and conductive fillers can be implemented. The conventional ECAs, which have already found their way into market, are usually based on epoxy as the polymeric matrix and silver flakes as conductive filler. Epoxy provides excellent adhesion, low shrinkage, superior resistance to thermal and mechanical shocks, and has a reasonable cost [6]. On the other hand, different types of metallic particle such as copper, nickel, and silver have been used as conductive fillers in the formulation of ECAs [7–10]. However, silver flake, due to its excellent electrical and thermal conductivities at room temperature, easy processability, and the conductive nature of its oxide has been the first and foremost utilized conductive filler inside the conventional ECAs [11].

Although the conventional ECAs (epoxy + silver flakes) offer several advantages over the traditional solders, including environmental friendliness, finer pitch printing capability, milder operating condition, fewer processing steps, and more flexibility [12,13], the complete replacement of the traditional solders with the conventional ECAs has not yet been achieved, mainly because of poor electrical conductivity. Despite all the progress, the electrical conductivity of the conventional ECAs (10^{-3}-10^{-4} Ω.cm) is still less than that of the eutectic solders ($\approx 2 \times 10^{-5}$ Ω.cm) [14]. This situation is related to their different working mechanism. In an ECA, electrons are transferred through the electrical network via the contact points between conductive fillers or by tunnelling effect. On the other hand, the eutectic solders work based on solder reflow in which current is passed through the metallic bonds [15]. In contrast to soldering, silver flakes inside the epoxy cannot render the metallurgical pathways

for electron transformation as metal solders do, but form a small contact point via the formation of a percolated network, which is more difficult for electrons to be transferred through.

It may seem one way to improve the electrical conductivity of the conventional ECAs is loading more silver flakes into epoxy to provide more electrical paths. However, after a specific concentration (i.e., percolation threshold) the electrical network becomes stable and adding more silver flakes to epoxy does not significantly affect the electrical conductivity. Besides, in order to fully replace traditional solders with ECAs, the satisfied electrical conductivity and good adhesive strength should be combined [16–18]. Adding more filler to epoxy decreases the mechanical strength of the final composite (due to the decreased volume fraction of polymeric matrix) and also negatively influences the processability, and the final cost of the composite [19].

In response to these concerns, research activities have stepped up to implement hybrid filler systems, i.e., the combination of nano-sized conductive materials and micron-sized silver flakes, as the conductive filler system inside the formulation of ECAs [15,20–22]. The recent progress in nanotechnology helps material scientists to precisely design nanomaterials with different morphologies and surface chemistry. Owing to this capability, incorporation of nano-sized conductive fillers with different natures, morphologies, and surface properties inside the conventional formulation of ECAs has drawn considerable attention to overcome the common drawbacks of the conventional ECAs, such as poor electrical and mechanical

properties, reliability issues, and large filler content. The utilization of nano-sized conductive material can enhance the electrical conductivities of ECAs at low filler content without sacrificing the mechanical and adhesive properties. Since the electrons are transferred through the electrical pathways inside epoxy and these pathways are formed via the linkage of conductive filler, the quality of contact between neighboring fillers are crucial issues affecting the final electrical performance of the hybrid ECAs [23]. To harness the characteristic properties of the nano-sized materials, different parameters such as their size, aspect-ratio, morphology, surface properties, the ratio of silver flakes to nanofillers, and the dispersion techniques should be taken under careful consideration. In current research, spherical silver nanoparticles (Ag NPs), high aspect-ratio silver nanobelts (Ag NBs), and graphene nanosheets were implemented as conductive co-fillers inside the conventional formulation of ECAs; the effect of these conductive nanomaterials, their morphology, and surface properties on the electrical conductivity of the resultant composites was investigated for each case.

The unique electrical [24–26], thermal [27], optical [28], and antibacterial [29] properties of Ag NPs have attracted extensive research interests with respect to their applications in the development of functional materials such as flexible electronic display [30], organic light-emitting devices [31] and biosensors [32] at ever smaller scales. During the past two decades, there has been increasing interest in the application of Ag NPs to enhance the electrical conductivity of conventional ECAs [15,19,21,26,33–35]. It has been reported that simply adding NPs has a negative effect on the overall electrical conductivity of ECAs because of

the increased number of contact points within an electrical pathway [36]. According to literature, a positive effect of NPs on the electrical conductivity of the polymer composite requires the sintering of NPs at high temperatures to reduce the number of contact points [19,21,23]. Many research works have been done to reduce the sintering temperature due to the thermal sensitivity of components in organic electronic devices [26,33,37,38]. To date, the major focus has been devoted to the application of Ag NPs bigger than 20 nm. One possible reason is that the surface organic layer of NPs should be readily removed from the surface during the curing process to trigger sintering at lower temperatures [21,35,39]. This condition usually needs the synthesis of NPs involving the physical adsorption of the organic layer on the surface of NPs, which usually leads to the formation of large NPs. In 2005, Jeong et al. investigated the incorporation of very small Ag NPs (5 nm) into the commercial ECAs and reported electrical conductivity improvement via incorporation of 2 wt% NPs without the need for sintering; Their study highlights the positive effect of small NPs ($\leq$ 10 nm) on the electrical conductivity of ECAs [15]. This progress was promising; however, the studies on Ag NPs less than 10 nm in the development of conductive polymer composites are scarce in literature.

In the first step of this project, we successfully synthesized and concurrently functionalized very small Ag NPs (smaller than 5 nm) using a simple wet chemistry approach. Two thiocarboxylic acids (11-Mercaptoundecanoic acid (MUA) and 3-Mercaptopropionic acid (MPA)) with the same chemical structure but different chain lengths were implemented to functionalize the NPs. We interestingly found that the chain length of organic layer has

significant impact on the size and the electrical conductivity of the NPs. Functionalization of the NPs using longer chain length acid (MUA) resulted in bigger (4.49±1.28 nm) and electrically insulating NPs, while surface coverage of the NPs with shorter chain length acid (MPA) led to formation of smaller (2.09±0.66 nm) and electrically conductive NPs. Although the chemically-stabilized NPs have low conductivity, (which limits their application for the development of conductive nanocomposites or ECAs), we postulated that by reducing the number density and the chain length of the stabilizing agent, the covering layer resistivity can be lowered and the NPs can be potentially used as reinforcing agents inside the ECA composites. Furthermore, we hypothesized that the chemically-stabilized NPs can be readily dispersed into epoxy and can be fused into the conductive network at a low temperature because of their small size. Hence, we introduced the smaller Ag NPs into conventional ECAs, consisting of 60 wt% silver flakes, and investigated the effect of the NPs as well as the specific roles of their surface layer on the electrical conductivity of a nano/micro hybrid composite adhesive. Our research findings revealed, for the first time, the chemically-stabilized NPs can improve the electrical conductivity of the conventional ECAs at a relatively low curing temperature of 150 °C without the extra step of sintering at an elevated temperature.

In recent years, high aspect-ratio nanofillers have been proposed as alternative materials for spherical NPs to overcome the concern of excessive contact points between NPs and to reduce the amount of conductive fillers [16,17,40–48]. High aspect-ratio nanomaterials can establish more stable and effective electrical network at lower filler contents with less

number of contact points within an electrical path. Moreover, they can provide better electrical conductivity without sacrificing the integrity and adhesive strength of the polymeric matrix [40]. For instance, Wu et al. reported a significant electrical conductivity improvement for the ECAs filled with 56 wt% silver nanowires (NWs) compared to that of the ECAs filled with micron-sized and/or nano-sized spherical silver particles with similar filler concentration [40]. The same results were reported by Tao et al. [49] and Chen et al.[45]. However, most of the studies performed in this field have involved the direct addition of silver NWs into epoxy resin without silver flakes; this situation requires a large amount of silver NWs to achieve high electrical conductivities [18,40,45]. There are few research reports on the development of hybrid filler systems using high aspect-ratio silver nanomaterials as auxiliary fillers in the formulation of the conventional ECAs. To the best of our knowledge, only Zhang et al. [50] reported the use of silver NWs along with the silver flakes (weight ratio of 2:3) to develop a hybrid fillers system and found a significant improvement in electrical conductivity of the fabricated ECA. This study suggested a synergetic effect of silver NWs and silver flakes on the electrical conductivity improvement of the hybrid ECAs.

In the second part of this project, we incorporated a new class of high aspect-ratio nanofillers (i.e., Ag NBs) in the conventional formulation of ECAs to develop a novel type of hybrid ECA composite. The Ag NBs were synthesized through a high-yield chemical reduction method which was based on the self-assembly and room-temperature joining of the hexagonal and triangular silver NPs as structural blocks of the NBs. Compared to the

previously used silver NWs which are synthesized at high temperatures and long reaction times, the fabrication of this NBs is fast and occurs at room temperature [51]. In addtion, the Ag NBs have a low “weight to length” ratio, which can reduce the total mass of conductive fillers in the composite. Moreover, the high aspect-ratio NBs are able to form a percolated network at low concentrations. Our results revealed a significant improvement in the electrical conductivity of the hybrid ECA composites in comparison to the conventional ECAs, especially at concentrations close to the percolation value.

After we understood the importance of the aspect-ratio of conductive nanofillers on the electrical conductivity enhancement of hybrid ECAs at low filler content, we examined graphene, which has the highest aspect-ratio among all nano-structured materials, as conductive co-filler inside the formulation of ECAs. Graphene is a flat monolayer of carbon atoms, 0.335 nm thick, densely packed into a honeycomb 2-D lattice structure [52–54]. Luan et al., demonstrated the significant potential of graphene to reduce the percolation threshold of ECAs by decreasing the tunnelling resistance inside the electrical network [54]. However, one challenge with the use of graphene is its aggregation during mixing with polymers, as graphene nanosheets tends to attract one another with strong van der Waals forces [55,56]. In order to harness the characteristic properties of graphene, the nanosheets need to preserve their unique single layer structure [57]. Pasricha et al., reported that the decoration of graphene with Ag NPs is an effective way to exfoliate graphene nanosheets, and to prevent their aggregation [58]. Considering that and inspired by the research works performed by Biak research group, (reporting significant electrical conductivity improvement via addition

of Ag NP-decorated CNT into the commercial ECAs), some research groups applied this idea for graphene for ECA application [23]. They believe that because of the higher aspect-ratio of graphene compared to CNTs [59], the Ag NP-decorated graphene should be a more promising co-filler to improve the electrical conductivity of conventional ECAs. Peng et al, recently reported an electrical conductivity improvement of ECAs via addition of Ag NP-decorated graphene to the conventional ECAs [60]. However, we postulated that the surface decoration of graphene with Ag NPs significantly decreased the contact resistance between neighboring fillers only when sintering of Ag NPs on the graphene surface occurs.

In the third step of this project, we employed a simple wet chemistry approach to decorate the graphene surface with Ag NPs for electrically conductive adhesive applications and carried out a systematic investigation on the effect of NPs sintering on the electrical conductivity improvement of hybrid ECAs. The NPs were functionalized with MPA to control their size and to prevent their oxidation. The small size of the NPs covered by very short chain length organic layer (MPA with 3 carbon atoms chain length) makes the NPs dispersible in organic solvent and susceptible to be sintered at low temperatures. The electrical conductivity of the hybrid ECAs with decorated graphene were measured at different curing temperatures and compared to those of conventional ECAs and hybrid ECAs with non-modified graphene. Our results showed that the Ag NP-decorated graphene is only effective to improve the electrical conductive of ECAs at low silver flake content via decreasing the tunnelling resistance. At high silver flake contents, elevated temperature is needed to achieve high electrical conductivity. We discussed the mechanism of electrical

conductivity improvement according to the quality of filler-filler interaction at different temperatures. The sintering behavior of conductive fillers was investigated using morphological, electrical, and thermal studies. We were able to prepare a highly conductive hybrid ECA by introducing a small amount of Ag NP-decorated graphene nanosheets (1 wt%) to the conventional formulation of ECAs. The resultant hybrid ECAs were found to have a bulk resistivity of 4.6×10^{-5} Ω.cm which is close to that of lead-based solders [14].

As mentioned earlier, we demonstrated that the improved electrical conductivity of ECAs via addition of Ag NP-decorated graphene is mainly because of the increased surface area of electron transportation in which the increased number of contact points (due to the presence of Ag NPs on the graphene surface) may cancel out this positive effect [61]. In order to decrease the number of contact points sintering of NPs must occur which requires elevated curing temperatures (higher than 150 °C). We postulated that the single layer graphene without metallic decoration is a better option as auxiliary filler for ECA application if a proper exfoliation technique is applied to preserve its single layer structure within the epoxy matrix. Surface modification of graphene using organic materials is one approach to exfoliate graphene in which the interaction occurs via either covalent bonding or via π-π stacking. Although this technique is shown to be effective to exfoliate graphene layers [62,63], it hinders their electrical properties because it disturbs the π-electrons delocalization of graphene surface [56].

Another method to exfoliate graphene nanosheets is based on the use of third component, known as a surfactant. In this approach, graphene layers are exfoliated by the mechanical energy provided by bath or horn sonication which overcomes the van der Waals interactions between graphene layers. At the same time, surfactant molecules adsorb onto the graphene surface and prevent their re-stacking via steric repulsions [64,65] (see Figure 1-1A). Some research groups implemented this method to produce surfactant-stabilized graphene from graphite powder. For instance, Lotya et al. reported the production of a high-concentration aqueous solution of graphene stabilized by sodium cholate surfactant using a long time low power sonication of graphite, followed by centrifugation [64]. In this project, we used a simple surfactant-assisted approach to disperse graphene nanosheets inside the conventional formulation of ECAs based on the use of an ionic surfactant, sodium dodecyl sulfate (SDS). The main advantage of this approach, as illustrated in Figure 1-1B, is we are able to preserve the single layer structure of graphene inside the nanocomposite without disturbing its structure. The single layer graphene nanosheets can effectively bridge between separated silver flakes and provide more surface area for electron transportation inside the electrical network. The electrical resistivity measurements of the hybrid ECA with SDS-modified graphene showed that SDS modification of graphene has a significant effect on enhancing the electrical conductivity of ECAs and reducing the amount of silver flakes.

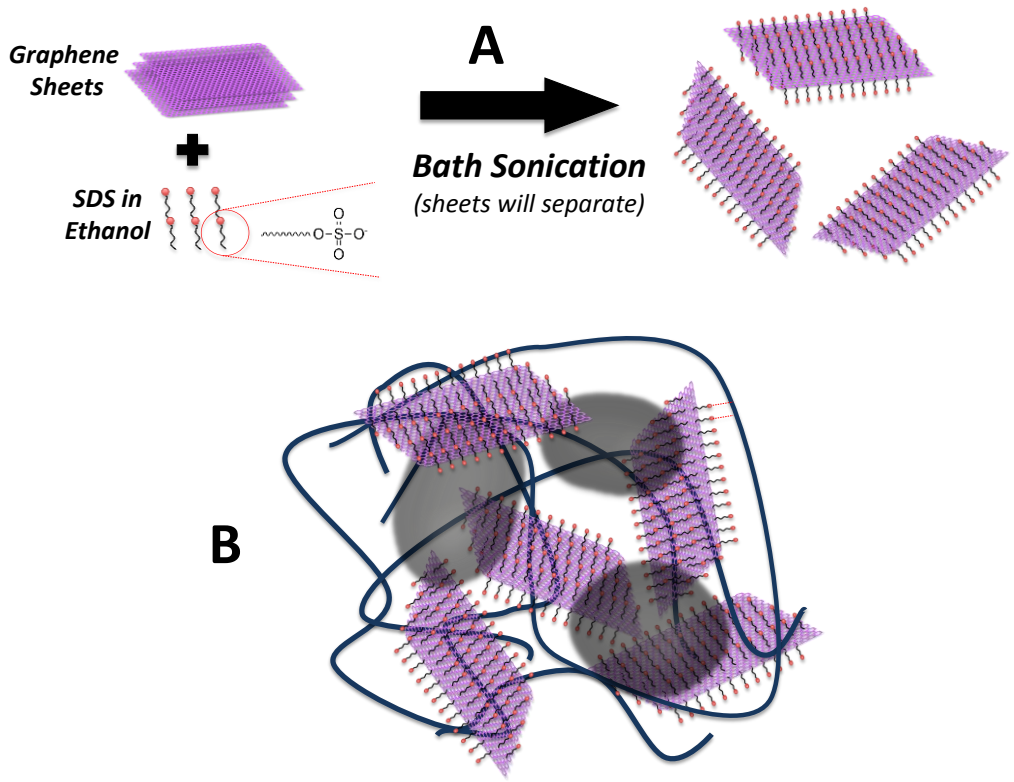

Figure 1-1 A) SDS modification of graphene leads to exfoliation of graphene flakes, B) the bridging of SDS-modified graphene between separated silver flakes establishes a compete electrical network inside epoxy

To shed further light on the effect of graphene aspect-ratio, we used graphene nanosheets with two different sizes (1 µm, and 5µm diameter) and applied the same SDS modification approach to exfoliate and disperse them inside the conventional ECAs. The electrical resistivities of the hybrid ECAs with small and large SDS-modified graphene were measured at different silver contents and compared to those of conventional and hybrid ECAs with non-modified graphenes. The results revealed that larger graphene are more effective to improve the electrical conductivity and reduce the amount of silver flakes than small

graphene. Highly electrical conductive ECA with a very low electrical resistivity of 1.6×10^{-5} Ω.cm was fabricated using 1.5 wt% of the SDS-stabilized large graphene and 80 wt% silver flakes. This fabricated ECA was more conductive than eutectic lead-based solder implying the great potential of the hybrid ECA with SDS-modified graphene to replace the traditional solders.

In the following chapter, the principle of ECAs working mechanism and their electrical conductivity measurements techniques will be explained. Moreover, the most recent literature on the development of hybrid ECAs using different types of conductive nanomaterials will be discussed. In Chapter 3, we will present our research findings on the effect of spherical Ag NPs, functionalized with chemically absorbed thiocarboxylic acids, on the electrical conductivity of hybrid ECAs. In Chapter 4, electrical conductivity enhancement of hybrid ECAs using a novel type of high aspect-ratio Ag NBs will be illustrated. The use of graphene as conductive co-filler with two different surface modification approaches inside the conventional ECAs will be discussed in details in Chapters 5 and 6. Finally, the thesis will be ended with Chapter 7, with the main concluding remarks based on the results obtained in this study, the main contributions of the thesis, and also both short-term and long-term recommendations for future work of this project.

Chapter 2. Literature Background

2.1 Electronic Packaging and Interconnects

Electronic packaging is defined as interconnections between a functional component (e.g., integrated circuits (ICs)) and other elements in a system-level board so as to make an electronic product. In order to make an electronic device, various levels of packaging are needed. Each level is connected to another level using interconnection materials [11]. The main purpose of these materials is to provide electrical connections between different levels in order to transfer power and signal. These materials also provide physical, mechanical, and electromagnetic protection and help with heat distribution. Figure 2-1 shows how interconnection materials are implemented to attach a functional component to a substrate.

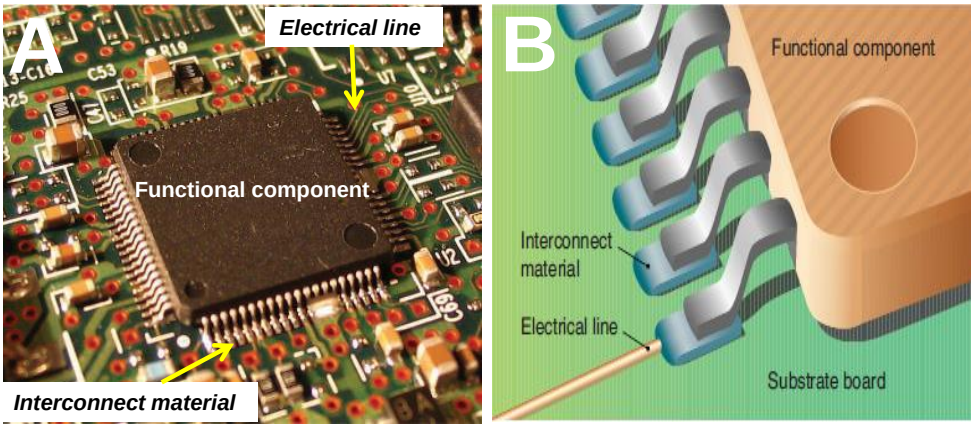

Figure 2-1. A) Attachment of a functional component on a substrate, B) a schematic of interconnection between a functional component and a substrate [1]

In the first level, after mechanical attachment to a substrate, a leadframe, bare dies or chip devices are electrically connected. For example, the interconnection between an IC and a package is provided in the first level of packaging, which acts as an IC carrier. Nowadays, wire bonding and flip-chip bonding (see Figure 2-2) have dominated the first-level interconnections. In wire bonding, a very fine gold or aluminum wire with typical diameter of 1 mm is utilized to electrically connect the IC and the substrate.

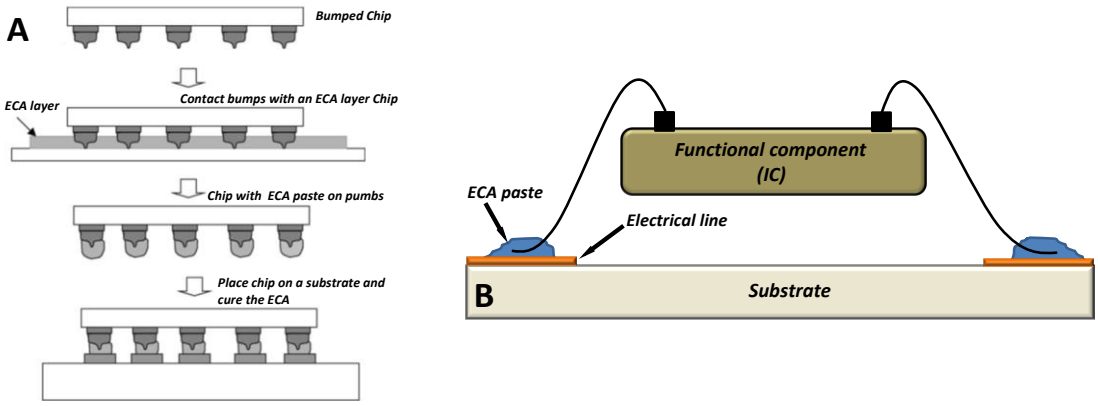

Figure 2-2.The schematic of two first level packaging techniques using ECA paste, A) filp chip, and B) wire bonding [11].

There are two common wire bonding techniques: Au ball-bonding (Figures 2-3A and 2-3B) and Al wedge-bonding (Figures 2-3C and 2-3D). In contrast to the wire bonding technique in which the active site of the chip is faced-up, in flip-chip bonding the active site is faced-down. In flip-chip bonding, the normal wire-bond pads at the perimeter of the die are replaced by solder balls or metal bumps. The schematic of flip-chip bonding is shown in Figure 2-4. Solder balls or bumps have different functionalities such as creating electrical

path from the chip to the substrate. They also play an important role in mechanical mounting of chips on the substrate. Moreover, they electrically separate the chip and the conductors of the substrate [66]. These days, flip-chip bonding, due to its superior technological advantages, such as small size, high speed, electrical performance, and low cost, has gained a foothold in electrical packaging industries [66,67].

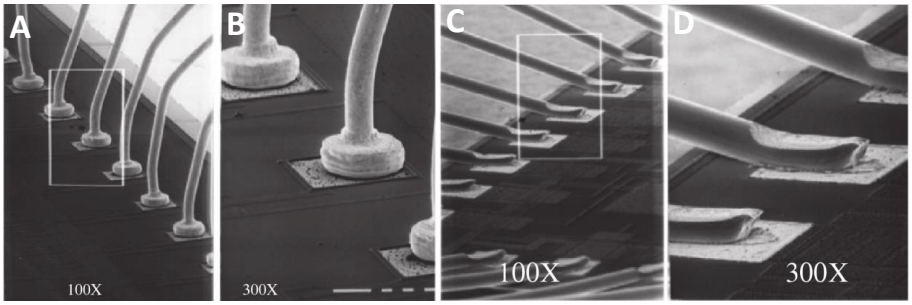

Figure 2-3. A), and B) The SEM images of Au ball-bonding; C), and D) The SEM images of Al wedge-bonding at different magnifications [66].

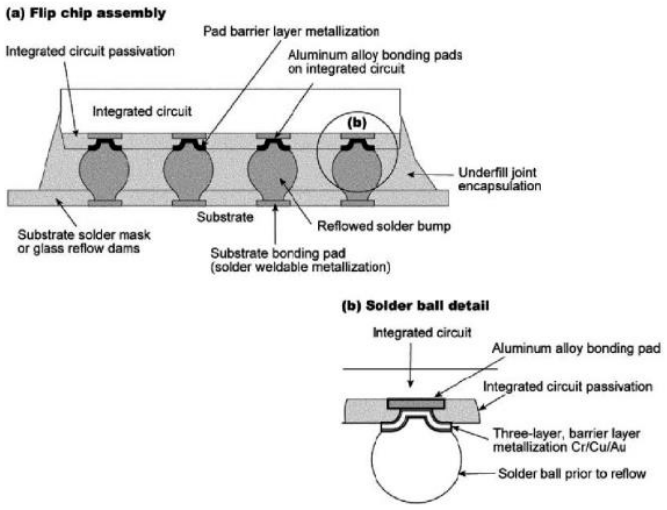

Figure 2-4. The detailed schematic of flip-chip bonding, A) A cross-section of assembly, B) Details of solder ball [66].

2.2 Interconnect materials

As mentioned earlier, interconnect materials are used to connect different levels of an electronic packaging to one another. Lead-based alloys, especially eutectic tin-lead solders, are traditionally employed as interconnect materials for this purpose. However, lead has long been recognized as a health threat to human beings and the environment. Accordingly, considerable efforts have been made to eliminate lead from the interconnection materials, and finding proper alternatives has is an urgent research project for material researchers working in electronic industries. Currently, two main types of alternative materials are being used to replace lead-based alloys: lead-free metal solders (e.g., Sn/Ag; Sn/Ag/Cu), and polymer-based electrical conductive adhesives (ECAs) [68].

2.2.1 Lead-free metal solders

Lead-free metal solders are already being used by many electronic industries as one of the alternatives for lead-based alloys. However, a lead-free solder should meet some basic requirements to achieve the expected performances to find their way in commercial products. For instance, the melting temperature of the solder should be low enough to avoid damaging the whole system and to decrease the operating cost. On the other hand, the melting temperature should be high enough so that the joint can tolerate the operating temperature at which the other parts of the system would be processed or the final product would be operated. Furthermore, solder melts should be able to wet the base metal to ensure an

intimate contact and good bonding strength. Tin (Sn), due to its relatively low melting temperature (232 °C), low cost, and the ability to wet most metal surfaces [11], has been considered as primary element in lead-free metal solders. Nowadays, eutectic Sn/Ag, eutectic Sn/Cu, eutectic Sn/Ag/Cu, and eutectic Sn/Zn are the most commonly used lead-free metal solders in industry [66]. However, the melting temperature of these metal solders is still higher than that of tin-lead solder (220 °C compared to 183 °C) which increases the solder reflow temperature from 230 °C to over 260 °C [19]. This high operating temperature can jeopardize the application of lead-free tin-based solders for organic/polymer packaged components and low-cost organic printed circuit boards/substrates. Although some research studies have been successfully performed on the production of low meting lead-free alloys, their mechanical properties and their processibility are not satisfactory for real applications [19]. In addition, the availability of the ingredients and the cost effectiveness of final solder are other important requirements influencing the potential of these materials for replacing the traditional solders.

2.2.2 Electrically conductive adhesives (ECAs)

Electrically conductive adhesives (ECAs), another alternative for replacing lead-based solders, are composite materials consisting of a polymeric binder and a conductive filler(s). The polymeric binder provides physical and mechanical strength to the adhesive, while the conductive fillers create an electrical network for the transfer of electrons. Easy processing,

unique mechanical and physical properties of polymers make them ideal structural materials in ECAs. In addition, the desired properties of the ECAs can be tuned by manipulating the structure of the polymers or by adding other materials to their formulation. Compared to the metallic and ceramic materials, ECAs can be fabricated by various processes with relatively low manufacturing cost; they have become one of the most widely-used materials in the field of electrical packaging [67]. A general comparison between some properties of the commercial ECAs and tin-lead (Sn/Pb) solders is presented in Table 2-1. It should be noted that the performance of ECAs depends on the properties of polymeric matrix, the type and surface properties of conductive fillers, the amount of conductive materials inside the composite, and also the quality of filler dispersion. Each of these parameters can significantly influence the final properties of the ECAs composite.

Table 2-1. General comparison between commercial ECAs and tin-lead solder [11]

Characteristic	Sn/Pb solder	ECA
Volume resistivity (Ω cm)	0.000015	0.00035
Typical junction R (mΩ)	10-15	<25
Thermal conductivity (W/m K)	30	3.5
Shear strength (psi)	>2200	2000
Finest pitch (mil)	12	<6-8
Minimum processing temperature (°C)	215	150-170
Environmental impact	Negative	Very minor
Thermal fatigue	Yes	Minimal

2.3 Chemistry, Formulation, and Properties of ECAs

2.3.1 Polymeric Matrix of ECAs

For an ideal polymeric matrix of an ECA, the properties such as long shelf life, easy and fast curing, relatively high glass transition temperature (T_g), good adhesion, and proper moisture resistivity are necessary [69]. Both thermoset and thermoplastic materials can be used as the polymeric matrix of ECAs. The main advantage of thermoplastic-based ECAs over thermoset-based ones is their reworkability, but their performance (i.e., mechanical and adhesion properties) declines considerably at elevated temperature [11]. On the other hand, thermoset polymers provide better adhesion compared to thermoplastic polymers and have better thermal and chemical resistances. In the following, we elaborate on epoxy's properties (as the polymer of interest of this project), and its synthesis procedure.

Epoxy is the most commercialized polymer used for ECA fabrication because of its excellent adhesion, low shrinkage, superior resistance to thermal and mechanical shocks, and reasonable cost. It also has good resistance to moisture, solvents, and chemical attack. Its properties may be further improved by a suitable choice of solvents, fillers, colorants, flame retardants, flexibilizers, and/or cure accelerators [66]. Bisphenol A epoxy is a hazardous material which should not be used in a direct contact with human body. However, as a polymeric matrix for interconnecting material, the contact of this material with human body is minimal which makes its environmental concern minimum. The commercial procedure of epoxy synthesis consists of a reaction between bisphenol A and epichlorohydrin in the

presence of sodium oxide which leads to production of bisphenol A epoxy with the structure presented in Figure 2-5. The physical state of epoxy resin depends on the repletion number (n) which varies from liquid (n = 0) to hard solid ($n \approx 30$). The viscosity of epoxy is determined by the ratio of bisphenol A to epichlorohydrin.

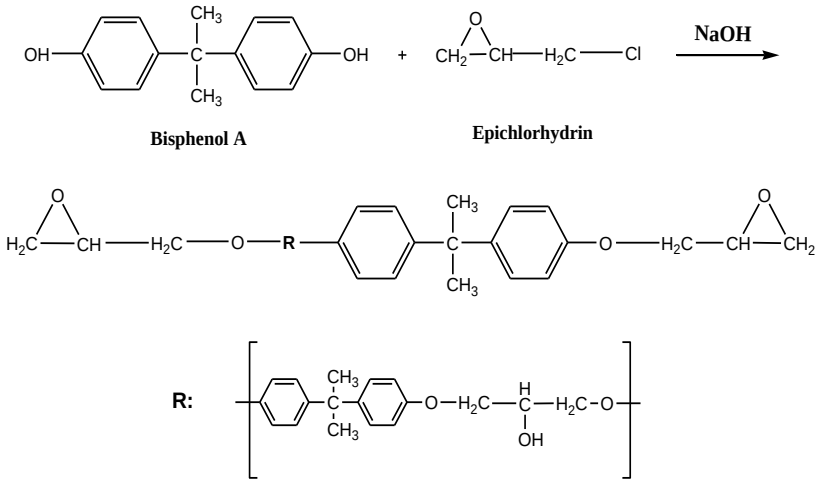

Figure 2-5. The mechanism of synthesis of bisphenol A epoxy.

2.3.2 The curing of epoxy

ECAs render electrical conductivity only when an epoxy is cured. Hence, understanding the curing behavior of epoxy is of significant importance. The desired properties of epoxy are obtained by reaction of the linear epoxy resin with suitable curing agents (known as curing reaction) to form three-dimensional cross-linked thermoset structures. Curing is an exothermic reaction and in some un-controlled cases may produce sufficient heat to cause thermal degradation. Curing may occur throughout epoxy homo-polymerization (reacting an

epoxy with itself) or via reacting with a curing agent or hardener. Depends on the application technique, curing condition, pot-life requirement and desired physical properties, the curing agent can be varied [66]. The common hardeners for epoxy resins include amines, acids, acid anhydrides, phenols, alcohols and thiols where the relative reactivity is approximately in the following order: phenol < anhydride < aromatic amine < cycloaliphatic amine < aliphatic amine < thiol. Here we elaborate on amines as the most used hardener for curing epoxy.

Figure 2-6 shows the curing reaction between an epoxide group of epoxy and an aliphatic amine. Primary amines are one of the most important parts of amine hardener. In a typical curing reaction between an aliphatic amine hardener and epoxy, primary amines react with the epoxide groups of epoxy to form a hydroxyl group and a secondary amine as shown in see Figure 2-6A. The secondary amine can further react with an epoxide to form a tertiary amine and an additional hydroxyl group (see Figure 2-6B). For aliphatic amines both primary and secondary amino hydrogens have approximately the same reactivity. Use of a di-functional or poly-functional amine along with a di-functional epoxy resin forms a three-dimensional cross-linked network. It should be noted that an amine type hardener will alter both the processing properties (viscosity, reactivity) and the final properties (mechanical, temperature and chemical resistance) of the cured copolymer network.

Although the curing of epoxy in the presence of hardener can happen at ambient temperature, for the most cases it requires heat to complete the curing reaction. Insufficient heat during cure will result in a network with incomplete polymerization, and thus reduced mechanical,

chemical and heat resistance. To obtain the best properties, the curing temperature should attain the T_g of the fully cured network. In some cases epoxy is cured in a step-wise fashion to control the rate of curing and prevent excessive heat build-up from the exothermic reaction.

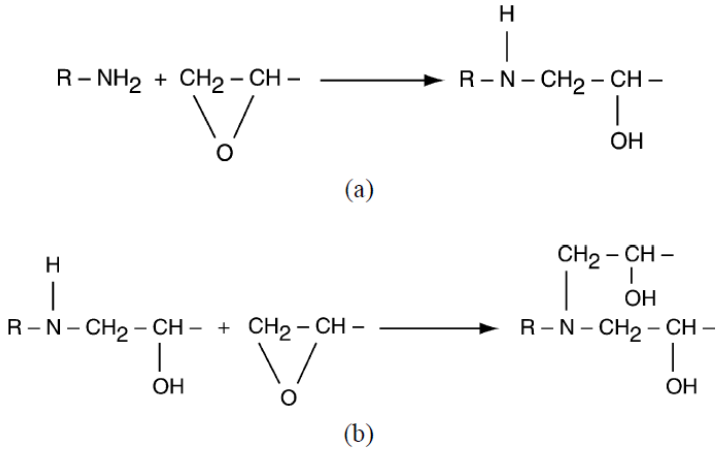

Figure 2-6. The curing mechanism of epoxy and a) a primary amine, b) secondary amine.

2.3.3 Conductive Fillers of ECAs

To make an insulating polymer electrically conductive, conductive fillers should be added to the polymer matrix of the ECAs; upon achieving the critical concentration of filler (percolation threshold), the insulating polymer will turn into a conductive one. Different materials such as metallic fillers (e.g., copper, nickel, gold, or silver particles), or carbon-based materials (e.g., carbon black, carbon nanotubes, and graphene) can be used as

conductive fillers. Among all these fillers, silver, due to its best electrical and thermal conductivity at room temperature, easy processability, and the conductive nature of its oxide has been the first and foremost utilized conductive filler in commercial ECAs. The SEM images of different types of silver fillers including flakes, NPs, and NWs are shown in Figure 2-7. Currently, in the most commercial ECAs silver flakes are being used as conductive filler because of their high conductivity, easy processing, and high surface area for electron transportation inside the electrical network. The size of silver flakes is usually between 1 to 20 μm. Bigger particles provide higher conductivity while delivering lower viscosity.

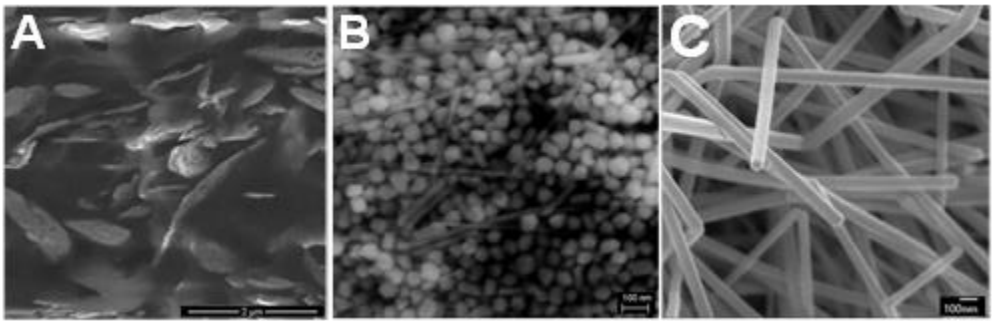

Figure 2-7. The SEM images of A) spherical silver flakes; B) silver NPs; and C) silver NWs.

2.4 The working mechanism of ECAs

The mechanism of electron transferring inside an ECA is usually explained by the percolation theory [70]. For each ECA, a specific concentration is defined as "percolation threshold". It is the concentration in which a continuous linkage of conductive particles occurs. Following the addition of conductive fillers to a resin, the electrical resistance of

ECA slowly decreases until the percolation point. Before percolation there is no practical connection between fillers. After the percolation threshold the resistivity of ECAs drops abruptly while beyond that adding more filler does not decrease the resistivity significantly [71]. The schematic of relation between the electrical resistivity of an ECA and filler content according to the percolation theory is shown in Figure 2-8.

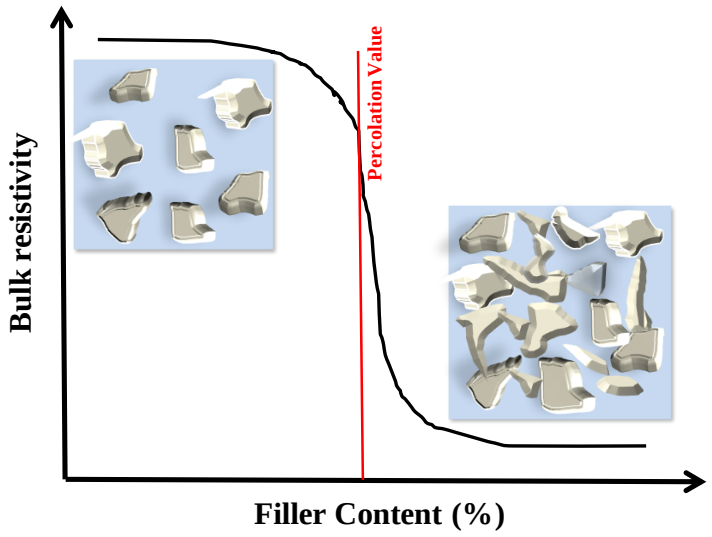

Figure 2-8. Typical percolation curve for an ECA based on the percolation theory.

Based on this theory, ECAs can be categorized into three major types, namely isotropically conductive adhesive (ICA), an-isotropically conductive adhesive (ACA), and non-conductive adhesive (NCA) (see Figure 2-9). ICAs are those adhesives which are able to transfer electrons in all directions, while ACAs transfer electrons only in one direction; NCAs are those adhesives which cannot transfer current in any direction [19]. In ICAs, the

concentration of conductive fillers is higher than the percolation threshold, making them able to transfer electrons in all directions. On the other hand, ACAs operates in the regions below the percolation threshold; conductive fillers in ACAs are separated from each other and can transfer electrons only in one direction, mostly upon applying high pressure, coupled with thermal treatments [19]. From now on, the word ECAs refer to ICAs as the conductive adhesive of interest in this project.

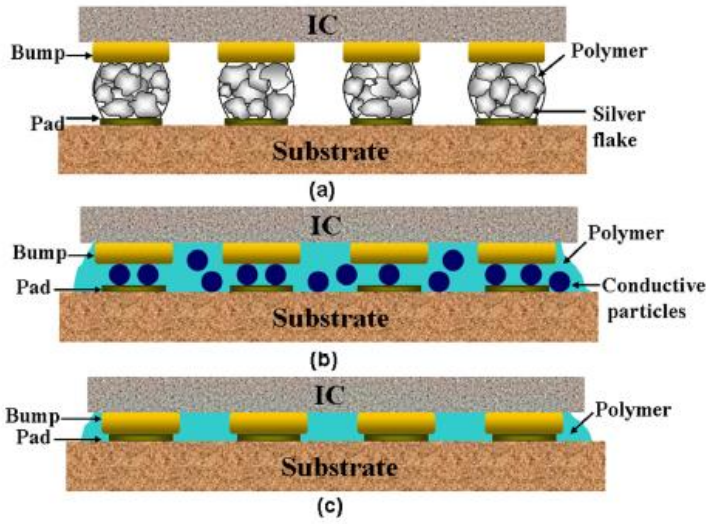

Figure 2-9. The schematic of application of different types of ECAs; a) ICA; b) ACA; c) NCA [19].

The percolation value depends on different parameters such as size [72], morphology [47], nature [73] and the dispersion state of conductive fillers. Each parameter influences the quality of conductive filler linkage in the electrical network, differently. The size of conductive fillers and their size distribution are important parameters affecting the

percolation threshold concentration. Wu et al filled epoxy with Ag NPs with different sizes (5-1000 nm) and studied the effect of the size of NPs on the percolation value [72]. They observed as the NPs size increased from 5 to 50 nm, the percolation concentration decreased to a minimum value of 63 wt%, which was 10 wt% less than that of conventional ECAs filled with micron-sized Ag particles. However, for the NPs bigger than 50 nm, the percolation concentration increased, suggesting there is an optimum particle size to form a percolated network. It has also been reported that the percolation value decreases with broad particle size distribution [74]. The percolation concentration also depends on the morphology of conductive fillers. Lower percolation threshold can be obtained using high aspect-ratio filler because they can provide more connected pathways at lower filler content [47,73]. The dispersion state of conductive fillers also has a significant effect on the percolation value. Presence of agglomerations in some level can be useful to form a percolated network at lower filler contents [75]. Li et al. prepared nanocomposites of CNT and epoxy using four different preparation conditions to provide different dispersion states of CNTs inside epoxy [76]. The reported percolation thresholds ranged between 0.1 wt% to 1 wt% in which the lowest value belonged to the nanocomposite with the second poorest dispersion state. They observed that the composite with the best dispersion state did not show any conductivity.

According to percolation theory, electrons are transferred through electrical pathways provided via the filler connections. Figure 2-10 schematically shows the mechanism of electron conduction throughout the electrical network. The overall resistance of an ECA can

be considered as the summation of series of resistivities, including the bulk resistance of filler (R_f), and filler-filler contact resistance ($R_{f\text{-}f}$) [22,74].

$$R_{overall} = R_f + R_{f-f} \qquad \textbf{Equation 2.1}$$

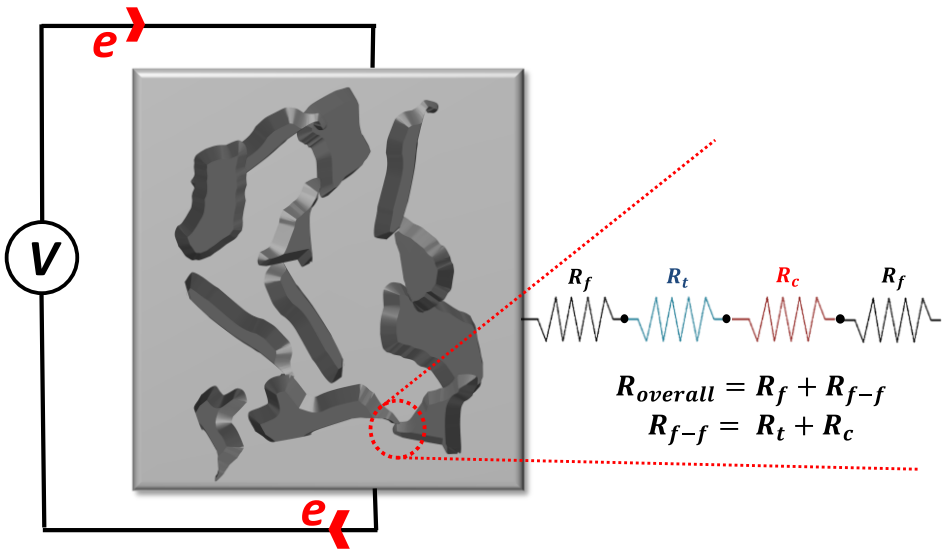

Figure 2-10. The mechanism of electrical conduction in an ECA; R_f, R_b and R_c are the bulk filler, tunnelling and constriction resistances, respectively.

For a specific filler system, the contact resistance ($R_{f\text{-}f}$), indicated by red circles in Figure 2-10, is the dominant factor that affects the overall resistance of an ECA. Therefore, to improve the electrical conductivity of ECAs with a specific material as conductive filler, the most effective way is to decrease the contact resistance between neighboring fillers [11]. The contact resistance itself is the summation of two basic resistances; "*constriction resistance*", and "*tunnelling resistance*" [77]. The former is related to the restrictions against free flow of electrons through sharp contact points; the lower number of contact points, the less constriction resistance. Compared to smaller ones, larger particles provide lower number of

contact points and larger contact area for electrons transportation inside the network [22]. Hence, micron-sized fillers, e.g., silver flakes, are preferred to be used as the main conductive filler inside ECAs. On the other hand, the tunnelling resistance comes from the spots where there are no direct connection between conductive fillers; and, electrons need to overcome a barrier energy to transfer through the network. This energy causes the tunnelling resistance. For a specific nanofiller, a cutoff distance is defined where the resistance between two parallel neighboring fillers is 30 times higher than the resistance of a single nanofiller [78]. The cutoff distance (*C)* varies for different types of nanofillers. For example, the cutoff distance for Ag NWs is approximately 150 nm while it is 1 nm for carbon nanotubes (CNTs) [79]. When the center line of two neighboring non-contact nanofillers (*d*) is larger than their diameter (*D*) and smaller than or equal to a cutoff distance, $D < d \leq C$, tunnelling of electrons occurs. Simmons in 1963 derived a generalized formula to quantify the tunnelling effect between similar electrodes separated by a thin insulating film [80]. Based on his method, the tunnelling resistance for two adjacent non-contact Ag NWs or CNTs can be approximately calculated as [78]:

$$R_{tunnel} = \frac{V}{AJ} = \frac{h^2 d}{Ae^2\sqrt{2m\lambda}} exp\left(\frac{4\pi d}{h}\sqrt{2m\lambda}\right) \qquad \textbf{Equation 2.2}$$

where *V* is the electrical potential difference, *J* is the tunnelling current density, *h* is the Plank's constant, *e* is the electron charge, *m* is the mass of electron, *A* is the cross-sectional area of tunnel, and λ is the height of the barrier energy (for epoxy is 0.5–2.5 eV). The barrier

energy depends on the materials that insulate the surface of the Ag NWs (e.g., the polymeric matrix, covering layer, or contamination on the surface of fillers) [74,77].

2.5 Electrical conductivity measurement of ECAs

The most important function of an ECA is to form electrical connections with desired electrical conductivity between different electronic parts to form a circuit. Hence, the main focus of the researchers working in this field is to decrease the electrical resistivity of ECAs (close to that of the traditional eutectic lead-based solders). Utilization of proper electrical resistivity measurement techniques is of significant importance to examine the efficiency of an ECA. There are two common ways to measure the electrical resistivity of an ECA: two-terminal (2T) sensing and four-terminal (4T) sensing methods. Figure 2-11 schematically shows the circuit configuration for each method. The 2T sensing method consists of a circuit in which current passes through both the resistor and the voltmeter (Figure 2-11A). In this method, the measured voltage is the summation of voltage drop in the resistor as well as the voltage drop in other parts of the circuit. This method is useful for the applications where high accuracy is not needed.

However, 4T sensing method, which is so called Kelvin method, is often employed when high accuracy and optimum performances are required. This method of measurement eliminates inaccuracy, attributed to wire resistances, which can be significant in very low resistivities. Figure 2-11B shows the connections of 4T sensing method which enables the voltage drop measurements exclusively across the resistor. The voltage circuit has high

impedance so that it draws no significant current. Since no current passes through the voltage sensor, one can measure the voltage drop between points a and b (resistor), exclusively (see Figure 2-11B).

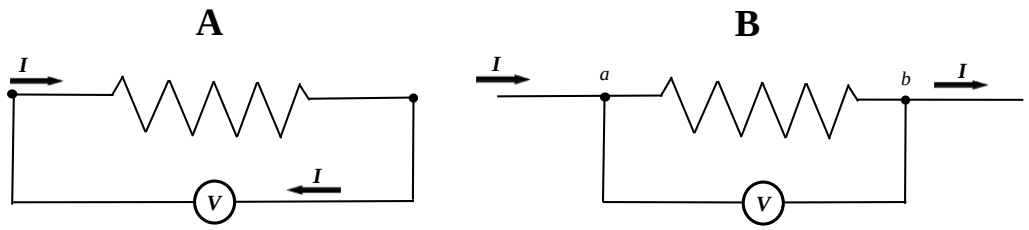

Figure 2-11. The circuit configurations of A) two-terminal and B) four-terminal sensing method.

The electrical resistivity measurement of ECAs is usually performed based on 4T sensing method rather than 2T sensing method. Four-point probe machine is often utilized for this purpose. In this technique, four probes touch a sample surface in which two of the probes are used to apply a specific amount of current through the sample while the others measure the voltage using a high impedance voltmeter (Figure 2-12). This method of measurement eliminates different sources of error such as the probe resistance, the spreading resistance under each probe, and the contact resistance between each metal probe and samples.

In 1957, Smits developed analytical calculations to evaluate correction factors for the bulk resistivity measurements on infinite and finite sheets using a four-point probe machine.

According to his work, in an infinite sheet, a current source causes a rise to the logarithmic potential,

$$\varphi - \varphi_0 = -\frac{I\rho_s}{2\pi}\ln r \qquad \textbf{Equation 2.3}$$

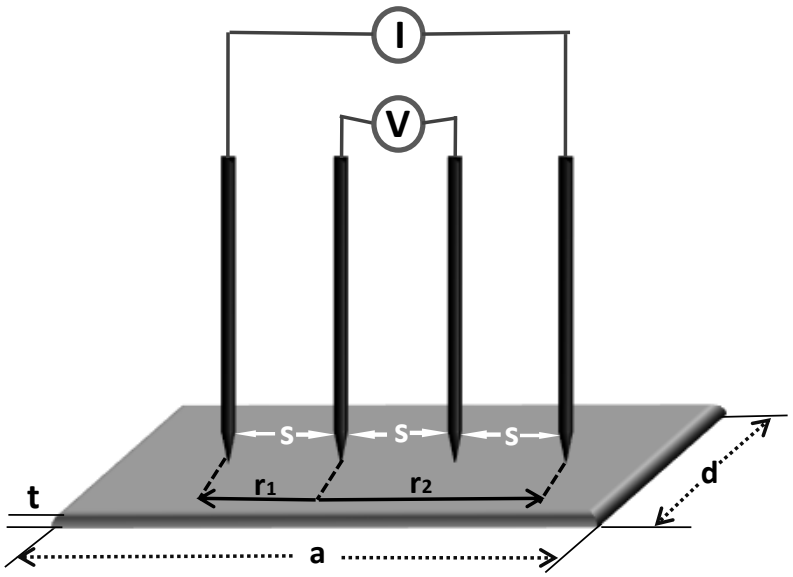

Figure 2-12. The configuration of a four-point probe technique for electrical conductivity measurements.

where φ is the potential, I the current, ρ_s the sheet resistivity, and r the distance from the current source. In particular, for a dipole (+ source and — source), Equation 2.3 can be rewritten as

$$\varphi - \varphi_0 = \frac{I\rho_s}{2\pi}\ln\frac{r_1}{r_2} \qquad \textbf{Equation 2.4}$$

For a four-point probe on a sheet, the two outside probes (current) are considered the dipole. Therefore, the potential difference between the two inner probes (voltage) with equal point spacing for an infinite sheet is

$$\Delta\varphi = V = \frac{I\rho_s}{\pi}\ln 2 \qquad \textbf{Equation 2.5}$$

Thus, the sheet resistivity can be calculated as

$$\rho_s = \frac{V}{I}\frac{\pi}{ln2} = \frac{V}{I}4.53 \ldots \qquad \textbf{Equation 2.6}$$

For a finite sheet with non-conductive boundaries Equation 2.6 is rewritten as

$$\rho_s = \frac{V}{I}C \qquad \textbf{Equation 2.7}$$

where *C* is a shape correction factor and depends on (*a/d*) and (*d/s*) ratios; where *a* and *d* are the length and width of the sheet, respectively, and *s* is the spacing between the probes (Figure 2-12). Table 2-2 presents the shape correction factor (*C*) for the sheet resistivity measurements of finite sheets.

For a sample with a finite thickness of *w*, the voltage gradient, perpendicular to the surface, must be considered while these gradients are negligible for a sheet with $w \rightarrow 0$. Smits related the bulk resistivity of an infinite sheet with a finite thickness of *w* to ρ_s as

$$\rho = \rho_s w = \frac{V}{I} w \frac{\pi}{ln2} F\left(\frac{w}{s}\right) \qquad \textbf{Equation 2.8}$$

where *F* is a correction factor because of the thickness of the sample. For a finite slice with the thickness of *w*, the shape correction factor, *C*, must be added to the Equation 2.8.

$$\rho = \rho_s \frac{V}{I} wCF\left(\frac{w}{s}\right) \qquad \textbf{Equation 2.9}$$

For $0.4 \leq w/s \leq 1$, *F* is close to 1.

It should be noted that the measurement using 4T sensing may be affected by the surface properties of conductive samples which may cause inaccuracy for bulk resistivity measurements.

Table 2-2. The shape correction factor (*C*) for sheet resistivity measurement of finite sheets using four-point probe technique.

d/s	***a/d* = 1**	***a/d* = 2**	***a/d* = 3**	***a/d* ≥ 4**
1.0			0.9988	0.9988
1.25			1.2464	1.2464

1.5		1.4788	1.4893	1.4893
1.75		1.7196	1.7238	1.7238
2.0		1.9454	1.9475	1.9475
2.5		2.3532	2.3541	2.3541
3.0	2.4575	2.7000	2.7005	2.7005
4.0	3.1137	3.2246	3.2248	3.2248
5.0	3.5098	3.5749	3.5750	3.5750
7.5	4.0095	4.0361	4.0362	4.0362
10.0	4.2209	4.2357	4.2357	4.2357
15.0	4.3882	4.3947	4.3947	4.3947
20.0	4.4516	4.4553	4.4553	4.4553
40.0	4.5120	4.5129	4.5129	4.5129
∞	4.5324	4.324	4.5325	4.5324

Table 2-3. Correction factor (*F*) for bulk resistivity measurement of finite sheets with thickness of *w* using four-point probe.

w/s	***F* (*w/s*)**
0.4	0.9995
0.5	0.9974
0.5555	0.9948
0.6250	0.9898
0.7143	0.9798
0.8333	0.9600
1.0	0.9214
1.1111	0.8907
1.25	0.8490

1.4286	0.7938
1.6666	0.7225
2.0	0.6336

2.6 Electrical conductivity improvement of ECAs

Since the invention of ECAs in 1950, [71] different approaches such as increasing the shrinkage of epoxy [81], surface engineering of silver flakes [82–84], adding low-melting components to provide metallurgical connection between silver flakes [85], and addition of nano-size conductive materials to the formulation of conventional ECAs [15,20,39,43,86], have been taken to improve the electrical conductivity of ECAs. Each approach is an attempt to decrease either the constriction or tunnelling resistances.

2.6.1 Increasing the shrinkage of epoxy

Before curing, ECAs, consisting of silver flakes and epoxy, do not show any conductivity; however, after curing, the conductivity dramatically increases [11]. Although the reason is not fully understood, it seems that shrinkage of the polymer is responsible for the enhanced electrical conductivity. In other words, curing causes a compressive stress on the filler particles, promoting better particle-to-particle contact thereby improving the conductivity [81]. It has been reported that increasing the crosslinking density increases the shrinkage of

the polymeric matrix, resulting in higher electrical conductivity of the ECAs. Therefore, polymer binders with higher degree of cross linking exhibit higher conductivity [81].

2.6.2 Surface treatment of silver flakes

Surface treatment of silver flakes has also been applied to improve the electrical conductivity of the ECAs. During the production of silver flakes, they are usually covered with a thin layer of organic lubricants, typically a fatty acid, having a long hydrocarbon chain. The purpose of this layer is to solve the dispersion and agglomeration issue of these metallic fillers, which arise mainly due to their high surface energy. However, these long-chain hydrocarbons are insulating materials, deteriorating the electrical properties of ECAs. Replacing the long-chain covering layer with short-chain layers can facilitate the access to the surface of silver flakes and provide more effective contact between them. In other words, by decreasing the thickness of the covering layer, the electrons can tunnel more easily between silver flakes. For instance, the electrical conductivity improvement of ECAs using in-situ replacement of long-chain stearic acid with some short-chain dicarboxylic acids has been reported [82]. Another approach to improve the electrical conductivity of an ECA via surface treatment of silver flakes is to reduce the silver oxide, which spontaneously forms on a silver surface, to pure silver. Although silver oxide, unlike other metal oxides, is conductive, its conductivity is still much lower than that of pure silver. For example, the application of reducing agents such as aldehydes to reduce silver oxide to silver (see

Equation 2.10) has been found as an effective way to improve the electrical conductivity of ECAs [87].

$$R - CHO + Ag_2O \rightarrow R - COOH + 2Ag$$ **Equation 2.10**

Other than reducing the silver oxide, the product of this reaction (i.e., R—COOH, which is a stronger acid in comparison to stearic acid) can replace the long-chain stearic acid molecules on the surface of silver flakes, leading to higher conductivity of silver particles.

2.6.3 Incorporation of nano-sized conductive particles

The extensive progress in nanotechnology has led to intensive interests to design nano-size materials with different shapes, and surface chemistries. Owing to the exceptional and fascinating characteristics of these nanomaterials, the introduction of nano-size conductive fillers inside the conventional ECAs has attracted considerable attention to improve the electrical conductivity of ECAs. The size [15,72], morphology [47], surface properties [20,21,39] and even the type of conductive nanofillers [84,88] have different impacts on the final electrical conductivity of ECAs by influencing the contact resistance inside the electrical network. One of the features of nanomaterials that significantly influences the properties of composites is their aspect-ratio. Figure 2.13 schematically shows the definition of the aspect ratio of different types of nanofillers. The aspect ratio of a particle can be defined as the ratio between the largest dimension to the smallest dimension of a particle. In

the following, we summarize the recent research activities which employed nano-size conductive materials (spherical Ag NPs (0-D), high aspect-ratio silver nanofillers (1-D), and graphene (2-D)) as auxiliary filler inside the conventional ECAs to develop new generations of hybrid ECAs.

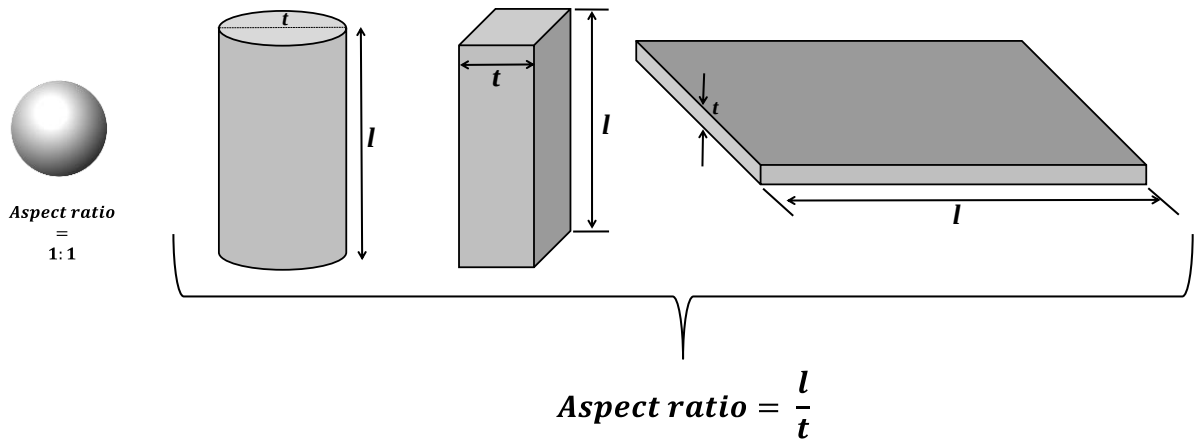

Figure 2-13. The aspect ratio of different morphologies of nanofillers

2.6.3.1 Spherical Ag NPs

The incorporation of spherical Ag NPs to the system of epoxy and silver flakes has been practiced by many research groups to develop new hybrid filler systems [15,20,25,26,34,35,37,39,49]; however, the role of NPs in modulating the electrical conductivity of ECAs is still controversial. Generally, it has been believed that adding Ag NPs at concentrations less than the percolation value improves the electrical conductivity of ECAs. Lee et al. reported a positive effect of Ag NPs on electrical conductivity when the filler concentration is less than the percolation threshold [89]. Chee and Lee anchored Ag

NPs on the surface of silver flakes by direct reduction of silver nitrite without using any capping agent [90]. Subsequently, they added the decorated silver flakes into epoxy and reported an electrical conductivity improvement at the beginning of the percolation regime. Since at concentrations less than percolation value silver flakes are not completely connected to each other, electron tunnelling is the dominant mechanism for electron transferring inside the network. Spherical NPs or their cluster by placing between separated flakes can make them connected and provide more electrical pathways inside the network which in turn reduces the tunnelling resistance.

On the other hand, simply adding Ag NPs after the percolation concentration may have negative effects on the electrical conductivity. In both previously mentioned studies, the NPs decreased the electrical conductivity beyond the percolation threshold. Fan et al. and Mach et al. also reported negative effect of Ag NPs on the electrical conductivity of a system of silver flakes and epoxy [91,92]. This situation can be explained by the concept of the constriction resistance [20]. As mentioned before, constriction resistance is one of the parameters affecting the total resistance of an ECA. This resistance is due to the restrictions against the free flow of electrons through a contact point (i.e., sharp contact); the higher the number of contact points, the higher the constriction resistance. Addition of NPs increases the number of contact points among fillers in the network, which in turn increases the contact resistance. Furthermore, the large amount of NPs (compared to silver flakes content) may increase the spacing gap between silver flakes and hindered their effective contacts, resulting in lower electrical conductivity values [36].

It should be noted that most research works, which were carried out to investigate the effect of Ag NPs on the electrical properties of ECAs, used NPs larger than 20 nm (see Table 2-4). However, it has been reported that very small Ag NPs, i.e., less than 10 nm, can have positive effects on the electrical conductivity of ECAs, even beyond the percolation contents [15,20]. Very small NPs can increase the surface area for electron transport inside the electrical network by filling the gaps and interstitial spaces between larger silver flakes (see Figure 2-14A). In a study by Jeong et al., the positive effect of very small Ag NPs (i.e., 5 nm) on the electrical conductivity of ECAs at the concentrations higher than percolation threshold was reported [15]. Using SEM images (Figure 2-14B and 2-14C), they showed that small Ag NPs filled the interstices between silver microparticles, which resulted in the bulk resistivity of 8×10^{-6} Ω.cm for the ECAs filled with 92 wt% of silver powder.

2.6.3.1.1 Sintering or metallurgical contact among silver flakes and NPs

As mentioned before, the increased number of contact points inside the electrical network is a challenge of using Ag NPs inside the ECA formulation. Sintering between Ag NPs is a potential approach that has been proposed to resolve this issue [20,21,34,35,37]. Sintering is a method to form an object from its powder and is based on diffusion between surface atoms. For metal particles, the atoms near the surface have fewer bonds with each other, thus, less energy is needed for them to leave the surface [93,94]. For metallic NPs, possessing a large surface area per given volume, the majority of atoms are present on the surface; this situation allows them to be sintered at temperatures far lower than their bulk melting temperature. This

phenomenon is called the "*depressed melting point effect*" [95,96]. Owing to this interesting feature, it is possible to form an electrical network with metallurgical connections between fillers by incorporation of nano-size materials inside the conventional formulation of ECAs where the formation of metallurgical contact between silver flakes at low temperatures is not possible.

As schematically shown in Figure 2-15A, sintering not only decreases the number of contact points between fillers, but also increases the contact area of electron transferring. Triggering sintering inside ECAs significantly helps to achieve higher electrical conductivity at low temperatures. Jiang et al. reported the electrical resistivity of 5×10^{-5} Ω.cm upon the incorporation of carboxylate functionalized Ag NPs to the system of silver flakes and epoxy (with total filler content of 80 wt%). They related the low electrical resistivity to the sintering of NPs at low curing temperature of 150 °C. Figures 2-15B and 2-15C show NPs morphological change after sintering [21].

The thermodynamic driving force for particle sintering of any size is based on the reducing their surface energy which can be expressed by [97]

$$\sigma = \gamma K = \gamma \left(\frac{1}{R_1} + \frac{1}{R_2}\right) \qquad \textbf{Equation 2.11}$$

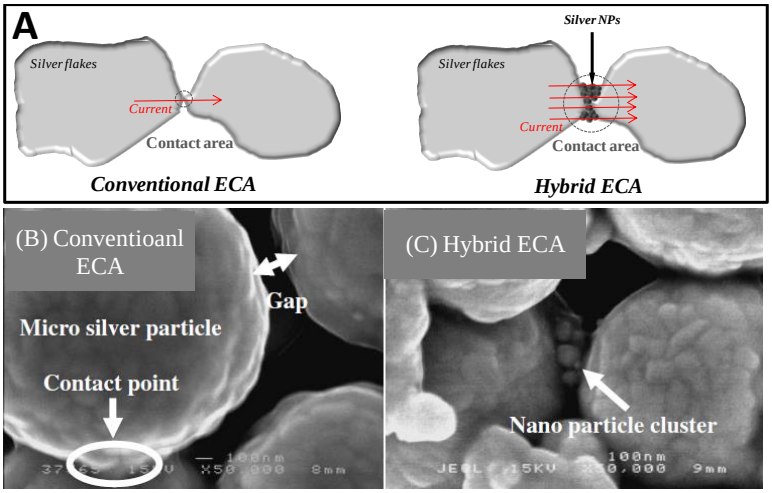

Figure 2-14. A) A schematic of electron conduction in conventional and hybrid ECAs, B) an SEM image of a conventional ECA, showing a gap between two silver micron-sized particles, C) an SEM image of a hybrid filler system, showing Ag NPs filling the gap between two [15]

where γ is the surface energy, K is the curvature of a surface, and R_1 and R_2 are the principle radii of the curvature. For a convex surface the curvature is taken to be positive and for a concave surface is negative. According to Equation 2.11, the driving force for particles sintering is inversely proportional to their size. Therefore, the driving force for the sintering of nano-sized particles is significantly larger than micro-sized particles. Apart from the surface energy driving force, there is another driving force for particle sintering which is related to mass transport phenomenon. The mass transport, occurring during sintering, is driven by the difference in the vacancy concentration ($\Delta C_v = C_v - C_{v0}$), where C_v is the vacancy concentration of a surface with the curvature of K, and C_{v0} is the vacancy concentration of a flat surface. The relation between C_v and C_{v0} is defined by Gibbs-Thomson equation

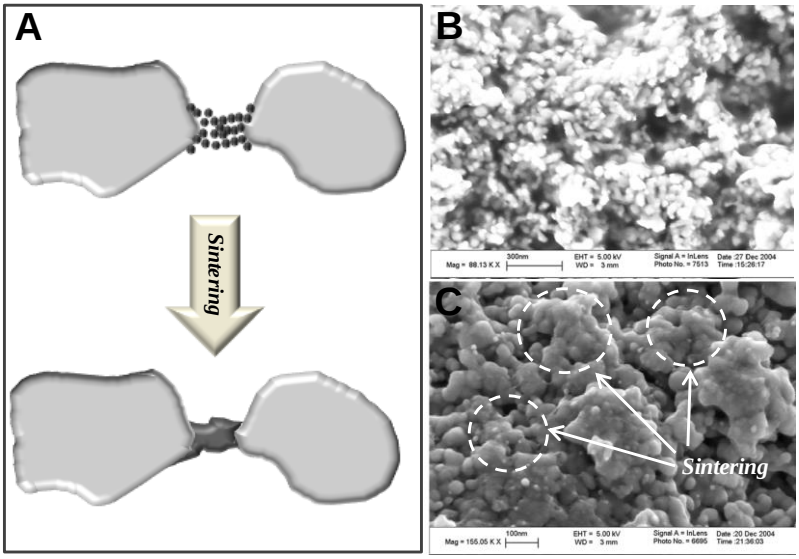

Figure 2-15. A) The schematic of sintering between Ag NPs, B) Ag NPs before sintering, and C) after sintering (figures B and C have been reproduced from copyright springer) [15]

$$C_v = C_{v0} \exp\left(-\frac{\gamma K \Omega}{kT}\right) \qquad \textbf{Equation 2.12}$$

where Ω is the atomic volume, k is Boltzmann's constant, and T is the absolute temperature. For micron-sized particles the term $\left(-\frac{\gamma K \Omega}{kT}\right)$ is smaller than 1, accordingly ΔC_v is equal to

$$\Delta C_v \approx -C_{v0} \frac{\gamma K \Omega}{kT} \qquad \textbf{Equation 2.13}$$

However, for nano-sized particle, the mass transport driving force is expressed by

$$\Delta C_v = C_{v0}\left[\exp\left(-\frac{\gamma K\Omega}{kT}\right) - 1\right]$$ **Equation 2.14**

Equation 2.14 shows when the particles size decreases to nanoscale the mass transport driving force increases, exponentially. All in all, the sintering driving force of any particle consists of two distinct parameters: surface energy driving force and mass transport driving force. For nano-sized particles, both of these parameters are significantly larger than micron-sized particles. This explains why the presence of nano-sized particles is necessary in the system of conventional ECAs to provide metallurgical connection among micron-sized silver flakes.

Rather than their size, sintering of NPs is affected by the covering layer on their surface [22,38,98]. NPs without any surface coverage can be sintered to each other even at room temperature [35,38]. Metallic NPs thermodynamically tend to form aggregates to reduce their surface energy. An organic layer over their surface can prevent the aggregation by providing large steric repulsion and also reducing their surface energy [96]. However, the presence of this organic layer is detrimental to the sintering at low temperatures which is a vital requirement for temperature sensitive devices. Hence, to make sintering happen at low temperature, the organic layer should be easily removed from the surface of NPs. The common stabilizing agents, such as polyvinylpyrrolidone (PVP), polyethylene glycol (PEG), long-chain alkanethiol, and amines usually form chemical bonds with NPs surface, which are hard to remove. In the most cases, a large amount of these stabilizing agents cover the surface of NPs. To detach these organic residues elevated temperatures (i.e., 200 °C or

higher) are often needed, which is usually higher than bearing temperature of the polymeric matrix or substrate.

Proper surface functionalization techniques can provide a controlled amount of organic material over the NPs surfaces with controlled de-bonding temperature. Remarkable efforts are in progress to reduce the sintering temperature due to the thermal sensitivity of components in organic electronic devices [26,34,35,37,99]. For instance, in a study by Zhang et al., they investigated the effect of different surface covering layers on the sintering temperature of Ag NPs, as well as the final electrical resistivity of nanocomposites [37]. They synthesized Ag NPs using combustion chemical vapor condensation (CCVC) method providing less amount of surface residue on NPs surface compared to the common wet-chemical methods. They used the same precursor but different reducing atmosphere, which led to the formation of NPs with carboxylate and oxidized surface. They reported that the complete removal of surface residue has a significant influence on the final electrical conductivity of epoxy filled with Ag NPs and silver flakes. To study the effect of surface residue on electrical conductivity, they cured the composite at 180 °C and achieved a bulk resistivity of 4.8×10^{-5} Ω.cm for the ECAs filled with 80 wt% of silver (flakes and NPs); this resistivity was three orders of magnitude less than that of the ECAs cured at 150 °C. This electrical resistivity difference is because at 150 °C some organic residues are still present on the NPs surface, inhibiting their complete sintering.

Some research groups tried to sinter Ag NPs inside epoxy by *in situ* synthesis method. Using this technique, one can generate Ag NPs without any surface residue during curing process, which in turn provides the chance to sinter at very low temperature. For instance, Gao et al., reported *in situ* synthesis of Ag NPs inside epoxy (filled with 80 wt% of silver flakes) during the curing process without the use of stabilizer; they reportedly reached a bulk resistivity of 7.5×10^{-5} Ω.cm [35].

2.6.3.1.2 The effect of covering layer chain length

As mentioned earlier, NPs are usually covered by an organic material to control their shape, properties, and also prevent their aggregation in different media. As reinforcing agent in nanocomposite fabrication, NPs must also be covered by some organic layer to make them compatible with their polymeric host. These layers (due to their insulating nature) inhibit the electrical performance of the final composite. The chain length of the organic layer over the surface of fillers is a critical parameter which influences the final electrical properties of ECAs; shorter chain lengths result in better electron transportation than the longer ones. Jiang et al. studied the effect of the introduction of Ag NPs treated by 5 different surfactants inside epoxy. Their results showed that the surfactant chain length has an important impact on the sintering initiation and consequently, the resistivity of ECAs (see Table 2-4), although it has not been mentioned what kind of surfactants were used [22].

Table 2-4. A comparison between different ECAs with hybrid filler systems of micro/nano silver particles

Research group	r_1 (wt%)*	r_2 (wt%)**	NP size (nm)	NP surface modification	r_3 (wt%)***	Bulk resistivity (Ω.cm)
Lee et al. [89]	—	98.2	50	none	98.2	1.93×10^{-4}
Fan et al. [91]	77.5	2.5	55	none	80	10^{-4}
Mach et al. [92]	75	3.5	80-100	none	~ 79	0.02
Jeong et al. [15]	90	2	5	none	92	8×10^{-6}
Jiang et al. [21]	48	32	16	Carboxylate group	80	5×10^{-5}
Jiang et al. [22]	—	70	N/A	N/A	70	2.4×10^{-4}
Gao et al. [35]	80	N/A	20-30	none	N/A	7.5×10^{-5}
Zhang et al. [34]	48	32	40-50	Carboxylate group	80	4.8×10^{-5}

*r_1 is the silver micro filler content.
**r_2 is silver NPs content.
***r_3 is total silver content.

2.6.3.2 High aspect-ratio silver nanofillers

The main drawback of conventional ECAs is that the electrical resistivity below 10^{-4} Ω.cm is unreachable even by using a large amount of silver flakes [14]. On the other hand, by increasing the amount of filler the volume fraction of epoxy decreases; consequently, the adhesive strength of the composite decreases. Recently, high aspect-ratio silver nanofillers are proposed as a promising option to overcome this issue. High aspect-ratio silver nanofillers can establish a percolated network at very low filler content [4,100,101]. Compared to spherical Ag NPs, these nanofillers provide lower number of contact points and larger surface area for electron transportation, which in turn decreases the constriction

resistance. Besides, the large aspect-ratio of these nanomaterials can provide more electrical paths inside the composite thereby significantly decreasing the tunnelling resistance (see Figure 2-16).

These interesting features of the high aspect-ratio silver nanomaterials have drawn considerable attention among the active research groups working in this field to exploit them as either the main or auxiliary filler inside the formulation of ECAs. For example, Wu et al., filled epoxy with 56 wt% of Ag NWs and reported four orders of magnitude electrical conductivity improvement compared to that of the one filled with the same amount of macro- and nano-size Ag particles [40] (see Table 2-5). It should be noted that the shear strength of the ECA filled with NWs was reported as ~17.6 MPa, showing a 0.3 MPa improvement compared to that filled with micro- and nano-size Ag particles. Tao et al. also reported the same results [49]. Yu et al., reported 13 orders of magnitude electrical conductivity improvement via the incorporation of 50 wt% of Ag NWs modified by (3-Aminopropyl)triethoxysilane (APTES) [46]. They related the electrical conductivity improvement to the homogenous dispersion of NWs inside epoxy, providing a percolated network inside polymeric matrix at low filler content.

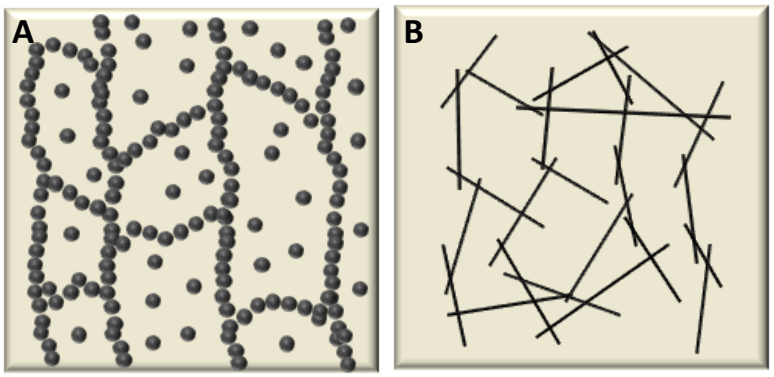

Figure 2-16. The establishment of electrical network using A) silver NPs, and B) high aspect-ratio silver nanofillers.

However, the direct addition of high aspect-ratio nanofillers into epoxy requires a large amount of materials to achieve the desired conductivities. Utilization of these nanomaterials as an auxiliary filler in conventional ECA can provide a synergetic effect of high aspect-ratio silver nanomaterials and silver flakes to improve the electrical conductivity of hybrid ECAs. Chen et al., studied the electrical conductivity of a system consisted of silver micron-sized particles, doped with Ag NWs and compared the results with an un-doped system [16]. According to their results, the doped system showed better electrical conductance compared to un-doped one while having the same amount of silver filler content. By using TEM and SEM images, they related the improved electrical conductivity to the bridging of NWs between separated micro-size silver particles. In another work in 2010, they incorporated Ag NWs inside the conventional formulation of ECAs and reported an improved electrical conductivity for the hybrid ECAs compared to the one with Ag NPs as co-filler [45].

2.6.3.2.1 Sintering of the high aspect-ratio silver nanofillers

Owing to their nano size scale, high aspect-ratio Ag nanofillers can provide the advantage of sintering and metallurgical contact between fillers at low temperature because of the "*melting point depression effect*" [95]. Similar to Ag NPs, the surface coverage has an important impact on the sintering temperature of these nanomaterials. Xiao's research group studied the effect of covering layer on the sintering behavior of Ag NWs, synthesized by a polyol process [102]. They functionalized NWs by a fatty acid (aliphatic acids) and polyvinyl pyrrolidone (PVP). They observed that the NWs functionalized by fatty acid began to sinter to each other at 200 °C, while sintering did not happen for those covered by PVP. Peng et al. showed that PVP can be washed out from the surface resulting in room temperature sintering of Ag NWs [38]. In another work by Xiao's group, they used di-carboxylic acids to functionalize Ag NWs. Di-carboxylic acids (due to their good affinity with metallic surfaces) are commonly used as shielding layer over the surface of Ag NPs to prevent their oxidation [103]. Since they chelate to the NPs surface, they can be easily detached from the surface, making the NPs able to be sintered at low temperatures [21]. It was observed that the functionalized NWs started to sinter to each other at 200 °C and gradually became shorter and thicker as temperature increased [50]. To trigger sintering inside ECAs, they incorporated the functionalized NWs into the conventional ECAs and reported an electrical resistivity of 5.8×10^{-6} Ω.cm for the epoxy filled with 75 wt% of the modified NWs and silver flakes (with the weight ratio of 2:3).

2.6.3.3 Graphitic nanofillers

Due to the exceptional mechanical and electrical properties of graphitic fillers, i.e., carbon nanotubes (CNTs) and graphene, recently, a considerable amount of attention has been drawn to utilize these nanomaterials in the field of electrical conductive nanocomposites. CNTs, first identified by Iijima, are sheets of graphite, rolled into seamless tube. They are categorized into single wall (SWCNT), double wall (DWCNT), and multi wall (MWCNT) carbon nanotubes [104,105]. On the other hand, graphene nanosheet is a flat monolayer of carbon atoms, 0.335 nm thick, densely packed into a honeycomb two-dimensional (2-D) lattice structure [53]. CNTs and graphene, possessing very large surface area per given volume and high aspect-ratio can create a percolated electrical network at very low filler content. By introducing these nanomaterials inside conventional ECAs, the density of the final ECAs is decreased, significantly [106]. In addition, compared to traditionally used metallic fillers, the exceptional mechanical properties of these nanomaterials can enhance the mechanical strength of the final ECAs drastically.

To harness the characteristic properties of these nanomaterials they must be efficiently dispersed inside their polymeric host. The bottleneck is that feeding polymers with as-prepared graphitic fillers usually leads to formation of aggregates as they tend to be held together (by van der Waals forces and/or entanglements) [56]. Stabilization of CNT/graphene by assistance of surfactant in liquid media [107], or surface functionalization via covalent bonding or π stacking [108] are the main approaches used to disperse and exfoliate these

nanomaterials inside a polymeric matrix. Both approaches have some drawbacks. Although the surface modification of graphitic fillers via covalent bonding may lead to better dispersion and interfacial interaction between nanofillers and polymeric chains [54], this method may hinder the electrical performance of nanofillers due to disturbance of π-electron delocalization [56]. On the other hand, dispersion of these nanomaterials by assistance of surfactant in organic solvents preserves their chemical structure. However, some issues challenge this approach for nanocomposite fabrication. First, a limited amount of CNT/graphene can be stabilized inside organic solvents by assistance of surfactants [65]. Second, residual surfactant removal is difficult in most cases [107].

Although some research has been conducted to fabricate epoxy filled with graphitic fillers [109], the nanocomposites with graphitic nanofillers as the main conductive filler cannot meet the minimum requirements of advanced ECAs due to the limited electrical conductivity of these nanomaterials compared to metallic fillers. However, their high aspect-ratio along with their conductive nature makes them a perfect option as auxiliary filler inside the system of epoxy and silver. In this case, the main part of electrical network is constructed by silver materials while the graphitic fillers help to establish the percolated network at lower filler content. In a study by Xuechun and Feng, they investigated the effect of MWCNTs on the electrical conductivity of ECAs filled with silver flakes [110]. They used surfactants to disperse MWCNTs in acetone. The results showed that adding MWCNTs, especially before percolation threshold, remarkably increased the electrical conductivity while beyond the percolation threshold, the influence of MWCNTs on electrical conductivity was not

pronounced. Marcq et al., also reported the synergetic effect of CNTs and silver flakes on electrical conductivity improvement of ECAs [43]. Luan et al., filled epoxy with a novel hybrid filler system, consisting of Ag NWs and 2-D chemically reduced graphene sheets (with hydroxyl groups over the surface) [54]. They observed that the percolation threshold decreased to a low value of 20 wt% and the electrical conductivity improved remarkably (see Table 2-5). Since the tunnelling resistance dominates the overall resistivity of the system, they attributed the electrical conductivity enhancement to the reduction of tunnelling resistance between NWs due to the presence of graphene nanosheets.

The efficiency of electrical pathways largely depends on the bulk conductivity of fillers as well as the quality of contact between neighboring fillers. Hence, the surface decoration of graphitic fillers using metallic NPs has been performed by some research groups as an attempt to increase their average electrical conductivity and also to decrease the contact resistance between fillers [23,41]. This approach is more effective for CNT because by surface metallization of CNTs, their average conductivity increases. Wu et al., decorated MWCNTs by Ag NPs and incorporated them as conductive filler inside epoxy. They also filled epoxy with non-modified MWCNTs. For the ECA filled with decorated MWCNTs, they reported a bulk resistivity of 2.21×10^{-4} Ω.cm at the percolation content, which showed one order of magnitude improvement compared to that of the ECAs filled with non-modified MWCNTs at the same concentration [48] (see Table 2-5). Baik and his co-workers modified the surface of CNTs with carboxylate groups as well as nickel and Ag NPs and incorporated them into silver pastes, consisting of silver flakes and epoxy. No matter which type of

surface-modified CNT was added to the silver paste, the electrical properties improved drastically while Ag-coated CNTs led to the most improved electrical conductivity (i.e., 83%) [41] (see Table 2-5).

It was mentioned that if sintering takes place between neighboring fillers, the contact resistance decreases dramatically. To take advantage of sintering and coalescence between fillers, Biak and his co-worker decorated CNTs by Ag NPs, functionalized with a di-carboxylic acid [23]. The presence of the di-carboxylic acid on the surface of small NPs prevented the oxidation of Ag NPs and also allowed the coalescence and sintering of NPs at a relatively low temperature of 180 °C. Incorporation of the decorated MWCNTs into the commercial silver paste (81 wt% of conductive filler) decreased the electrical resistivity of the hybrid ECA to 4×10^{-6} Ω.cm, showing a significant improvement compared to that of ECAs with non-modified CNTs. Self-assembly and coalescence of Ag NPs on the surface of MWCNTs resulted in better compatibility with micron-sized silver flakes. Silver-decorated MWCNTs construct electrical bridges between separated silver flakes during the curing step, and the NPs presented at the end of each tube sintered the MWCNTs to the neighboring silver flake (see Figure 2-17). The metallurgical connections between silver flakes and MWCNTs significantly decrease the tunnelling resistance and also provide more electrical pathways for electrons transportation inside the network.

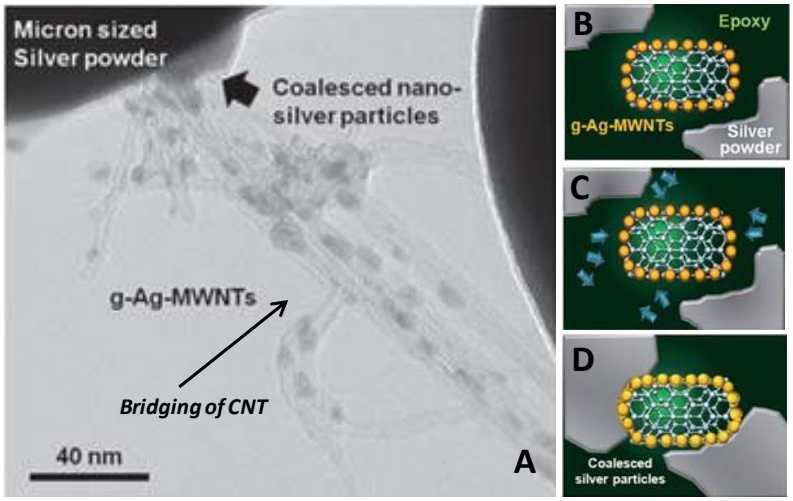

Figure 2-17. A) The bridging of CNT between separated silver flakes without epoxy, B, C, and D) schematics of electrical network formation via the bridging and coalescence of Ag decorated CNTs between silver flakes [23].

Compared to CNTs, graphene nano-sheets offer higher surface area for electron transportation inside the network due to their 2-D structure and higher aspect-ratio. Pu et al. used nitrogen-doped graphene inside the system of epoxy and silver powder and reported that the percolation of silver powder reduced to 30 wt% [59]. Their results confirmed that 2-D graphene is much more effective than other types of high aspect-ratio carbon-based fillers such as carbon nanotubes and carbon black. However, the challenge of attaining a homogeneous dispersion, as well as preserving its single-layer structure inside the composite acts as a bottleneck in ECA fabrication. Surface modification of graphene using organic materials is one approach to exfoliate graphene in which the interaction occurs via either covalent bonding or via π-π stacking. Although this technique is shown to be effective to exfoliate graphene layers, it hinders their electrical properties because it disturbs the π-electrons delocalization of graphene surface [56,62,63,111]. The surface decoration of

graphene with inorganic nanoparticles (NPs) such as Ag NPs is another approach that can effectively exfoliate graphene nanosheets. For example, Pasricha et al., reported that the decoration of graphene with Ag NPs is an effective way to exfoliate graphene nanosheets, and to prevent their aggregation [58]. Some research groups applied this idea into ECA application as an attempt to reduce the contact resistivity between conductive fillers. Peng et al. recently reported the positive effect of Ag NP-decorated graphene on the electrical conductivity of ECAs when they were added to the conventional ECAs. However, the final electrical conductivity was not that significant. The improved electrical conductivity of ECAs via addition of Ag NP-decorated graphene is mainly because of the reduction of the tunnelling resistance; however, the increased number of contact points (due to the presence of Ag NPs on the graphene surface) may cancel out this positive effect. If sintering of Ag NPs on the graphene surface occurs, it can significantly decrease the contact resistance between neighboring fillers via the formation of metallurgical contacts between silver flakes and graphene nanosheets. Recently, Liu's research group developed new *in situ* approaches to decorate the graphene surface with Ag NPs for ECAs application [112,113]. In their method, the formation of Ag NPs on graphene surface occurs during the curing process of epoxy, making the NPs size very sensitive to curing temperature. They reported high electrical conductivity for the fabricated ECAs using this method (see Table 2-5). Although *in situ* approaches eliminate the use of organic layer over NPs surface, it makes it difficult to keep the NPs size constant as the curing temperature changes. Furthermore, at temperatures less than NPs formation temperature, there would be no Ag NPs inside the nanocomposites,

thereby limiting the applications of the ECAs to those operating at temperatures higher than NPs formation temperature.

Table 2-5. A comparison between ECAs with high aspect-ratio nanofillers.

Research Group	Silver flakes (wt%)*	Silver NW (wt%)	CNT (wt%)	Graphene (wt%)	Total silver content (wt%)	Bulk resistivity (Ω.cm)
Wu et al. [40]	—	56	—	—	56	1.2×10^{-4}
Zhang et al. [102]*	—	76	—	—	76	7.1×10^{-4}
Zhang et al. [50]**	45	30	—	—	75	5.8×10^{-6}
Xuechun and Feng [110]	72	—	0.24	—	72	1.43×10^{-3}
Marcq et al. [43]	70	—	0.4	—	70	2×10^{-4}
Wu et al. [48]***	—	—	41	—	—	2.21×10^{-4}
Oh et al. [41]****	80	—	2	—	80	1.84×10^{-5}
Oh et al. [23]*****	79.5	—	1.5	—	81	4×10^{-6}
Luan et al. [54]	—	50	—	N/A	50	$\sim 10^{-3}$
Peng et al. [60] ******	65	—	—	15	65	2.37×10^{-4}
Liu et al. [113]*******	80	—	—	0.05	80	4.3×10^{-5}
Liu et al. [114]*******	80	—	—	N/A	80	3×10^{-5}

*The silver NWs were functionalized by an aliphatic acid.
**The silver NWs were functionalized by dicarboxylic acids (e.g., pentanedioic acid).
***The CNTs were coated with silver NPs of 5 nm.
****The CNTs were covered by silver NPs of 100-200 nm.
*****The CNTs were covered by silver NPs of 20 nm which were functionalized by glutaric acid.
****** The graphene nano-sheets were decorated by silver NPs of ~ 30 nm
******* The graphene nano-sheets were decorated by silver NPs of ~ 10 nm

Chapter 3. Spherical Silver Nanoparticles as Auxiliary Co-fillers for ECA Applications; The Effect of Surface Functionalization on the Electrical Properties of the NPs and the Polymeric Composite

3.1 Introduction

The unique electrical [24,25,33], thermal [27], optical [28,115] and antibacterial [29,116] properties of Ag NPs have attracted extensive research interest with respect to their applications in the development of functional materials such as flexible electronic display [30,117], organic light-emitting devices [31], and biosensors [32] at ever smaller scales. One critical step of many applications of NPs is to disperse them into a polymer matrix to fabricate nanocomposites; the NPs provide functionalities whereas the polymer matrix provides mechanical strength. A proper monolayer of surfactants is often needed to effectively cover the surface of NPs so as to reduce the surface energy, which in turn reduces the formation of aggregates and at the same time allows for loading more NPs in the polymeric matrix [21]. The surface layer, coated on NPs surface, usually negatively influences the desired functions of the NPs. For instance, the surfactant layers insulate NPs and reduce their intrinsic thermal and electrical conductivities; this situation limits the broader use of polymer nanocomposites as functional materials. In this chapter we focus on the surface functionalization of Ag NPs, and their corresponding effect on the electrical conductivity of the NPs as well as their polymer composites.

As mentioned in the previous chapter, silver-filled polymer composites have been utilized as electrical conductive adhesive (ECA) application for device assembly to eliminate the environmental concerns regarding traditional lead-based solder while providing other advantages such as milder processing conditions, fewer processing steps, and finer pitch capability [11,15,19,39]. During last decade, there has been increasing interest in the application of Ag NPs to enhance the electrical conductivities of conventional conductive adhesives filled with silver micro flakes [15,19,21,26,33–35,118]. However, simply adding NPs has negative effects on the overall conductivity of the ECAs because of the increased number of contact points. A positive effect of NPs on the electrical conductivity of the polymer composite requires the sintering of NPs at high temperatures to reduce the number of contact points [19,21,23]. Remarkable efforts have been performed to reduce sintering temperature due to the thermal sensitivity of components in organic electronic devices [37–39,94]. To date, the major focus has been on the application of Ag NPs bigger than 20 nm. One possible reason is that the surface organic layer of NPs should be readily removed from the surface during the curing process in order to sinter NPs at lower temperatures. This condition usually needs the synthesis of NPs involving the physical adsorption of the organic layer on the surface of NPs, which leads to the formation of large NPs. Jeong et al. investigated the incorporation of commercial 5 nm Ag NPs into the conventional ECAs with 90 wt% silver micro particle and reported that adding a small amount of the NPs (~2 wt %) improved the conductivity without the need for sintering, which highlights the positive effect of small NPs on the electrical conductivity of ECAs [15]. This progress was promising; however, the studies on Ag NPs less than 10 nm in the development of conductive polymer

composites are scarce in literature. It may be because of the need for chemical stabilization of NPs during their synthesis; the stabilizing agent could insulate the NPs, depending on its chain length and adsorption mechanism.

Varied chemicals including mono- or di-carboxylic acids [38], sodium citrate [94], amines [119], and alkanethiols [120,121] have been used to produce functionalized NPs; the functional groups prevent them from forming aggregates. Since Brust et al. [122] developed a two-phase liquid-liquid system to synthesize alkanethiol-stabilized gold NPs, the synthesis and characterization of thiol-capped metal NPs have been the subject of considerable research interest [123–126]. Chen and Kimura developed a large scale synthetic method for the production of carboxylate–modified gold and Ag NPs, which could be homogenously dispersed in water and organic solvents while they could also be re-isolated as pure powder without any aggregation [127,128]. Similar methods have been considerably used to synthesize metal NPs using thiocarboxylic acids [129–131]. One of the striking features of stabilizing metal NPs by thiocarboxylic acids is the production of very small (i.e., less than 5 nm) and mono-dispersed NPs. The characteristic properties of this type of NPs such as size, size distribution, thermal and electrical properties can be controlled by the chemistry and coverage of the functional groups on the NPs surface. Although many research works have been performed to synthesize and functionalize silver NPs using different organic layers, to our knowledge there is no systematic study on the effect of this surface layer on the electrical properties of Ag NPs and their corresponding polymer composites.

In this chapter, we investigated the effect of very small Ag NPs as well as the specific roles of their surface layer on the electrical conductivity of a nano/micro hybrid composite adhesive. To do so, the conventional ECA, consisting of 60 wt% Ag micron flakes in epoxy, was used as a base composite, because using only NPs lead to a non-conductive composite or it requires a large amount of the NPs to be conductive, which is costly and not practical. Thiocarboxylic acids with different chain lengths were implemented to stabilize Ag NPs. Although the chemically-stabilized NPs have low electrical conductivity, which limits their application for the development of conductive nanocomposites or ECAs, we postulated that by reducing the number density and the chain length of the stabilizing agent, the covering layer resistivity can be lowered and the NPs can be potentially used as reinforcing agents in ECAs. Furthermore, we hypothesized that the chemically-stabilized NPs can be readily dispersed into epoxy and can be fused into a conductive network at a low temperature because of their small size. Our research findings revealed, for the first time, the chemically-stabilized NPs can improve the electrical conductivity of the conventional ECAs at a relatively low curing temperature of 150°C without the extra step of sintering at an elevated temperature.

3.2 Experimental

3.2.1 Synthesis and Chemical Modification of Ag NPs

11-Mercaptoundecanoic acid (MUA, ≥95 wt % Aldrich) and 3-Mercaptopropionic acid (MPA, ≥99 wt % Aldrich) were used to stabilize Ag NPs. These two thiocarboxylic acids

differ in their chain lengths. The number of carbons in the backbone of MUA and MPA are 11 and 3 carbons, respectively. MPA-stabilized Ag NPs (Ag-MPA) were synthesized following the established procedure [127,128,130]. 40 mL of MPA (8 mmol) solution in tetrahydrofuran (THF) and 240 mL silver nitrate (340 mg, 2mmol) ($AgNO_3$, ≥99 wt% Aldrich) solution in THF/water (volume ratio: 5/1) were mixed drop-wise. After 5 min, the initially transparent solution became blurry whitish along with the formation of small white clusters, which is associated to the formation of Ag-S bonds [124,130]. Subsequently, 20 mL of aqueous solution of sodium borohydride (20 mmol) ($NaBH_4$, ≥99 wt % Aldrich) was added to the mixture, leading to an abrupt precipitation of a dark-gray solid. In order to remove the unreacted materials, the precipitated sludge was washed three times by repeatedly dispersing in water and precipitating in THF followed by centrifugation at 8000 rpm for 30 min to remove the supernatant. The resultant gray solid was dispersed in 20 mL deionized (DI) water. MUA-stabilized Ag NPs (Ag-MUA) were synthesized by the same procedure as Ag-MPA. 900 mg (4 mmol) of MUA was dissolved in 40 mL THF and added drop-wise to the solution of $AgNO_3$, leading to the formation of yellowish solution. The same $NaBH_4$ solution was used to reduce Ag+ ions, leading to the formation of a dark-brown solid. The same washing steps were applied for the synthesis of Ag-MPA. The final NPs were dispersed in 20 mL of DI water. All the glassware was cleaned prior to use; they were soaked in a 1 M solution of sodium hydroxide for 24 h, neutralized with acetic acid, and then rinsed with DI water. The DI water (resistivity > 10 MΩ.cm at 25 °C; total organic carbon < 20 ppb) was obtained using a RiOs-DI Clinical system (Milli-pore Corporation).

3.2.2 Nanocomposite preparation

Diglycidyl ether of bisphenol A resin (DERTM 322) and triethylenetetramine (TETA), supplied by DOW chemical company (USA), were used as the epoxy base and hardener, respectively. The weight ratio of hardener to epoxy was 0.13. Two types of samples were prepared. One type contained only silver flakes (Aldrich, 10 μm); the other contained a mixture of the synthesized NPs and silver flakes at different weight fractions. A small amount of isopropyl alcohol (6 wt% of the epoxy) was added to dilute the epoxy before adding silver fillers. The total weight fraction of the silver varied from 60 to 70 wt% as listed in Table 3-1. The paste was mixed for 30 min using a vortex mixer followed by 1 h mixing in an ultrasonic bath. Epoxy hardener was then added and mixed using the vortex mixer for 10 min. The resultant paste was filled into a mold of 7×7×0.7 mm^3 (L×W×D), made using pieces of adhesive tape on a pre-cleaned microscope glass slide. To make a smooth surface and control the sample thickness, a clean copper plate was placed on top of the mold and the extra paste was squeezed out. The samples were pre-cured for 30 min at 60 °C and then post-cured at 150 °C for 2 h. After curing, the copper plate and adhesive tape were manually peeled off.

Table 3-1. Weight fractions of silver NPs and flakes in nano-micro particles filled epoxy

Sample	Ag flakes (wt%)	Ag NPs (wt%)	$K = \frac{Ag\ NPs}{Ag\ flakes}$	Total weight fraction of fillers	Total volume fraction of fillers
1	60	0	0	60	18.0
2	53	11	0.2	64	19.2
3	48	19	0.4	67	21.4
4	44	26	0.6	70	22.6

3.2.3 Characterization

Fourier transform infrared spectroscopy (FTIR) was performed for the Ag NPs using a Varian 640-IR specttrometer to verify the chemical structure of the surface layer of Ag NPs. A high resolution transmission electron microscope (HRTEM, JEOL 2010F FEG) was used to characterize the size and size distribution of the chemically-stabilized Ag NPs. To prepare TEM samples, one droplet of dilute dispersion of the Ag NPs in water (1 mg/mL) was dropped on a lacey/holey carbon copper grid and dried for 1 h in air. The TEM was operated at 200 kV and equipped with a Gatan ultra scan imaging filter. Ultraviolet-visible spectroscopy (UV-Vis) (UV-2501 pc, Shimadzu) was performed to confirm the formation and size distribution of synthesized NPs. Weight-loss and surface coverage of the NPs with thiocarboxylic acids were studied using the thermogravimetric analysis (TGA) (TA instrument, Q500-1254). Samples of about 4 mg were placed in the TGA sample pans. Dynamic scanning was performed from 40 °C to 600 °C with a heating rate of 20 °C/min under nitrogen atmosphere. The morphologies of the NPs and cured nanocomposites were examined by Scanning Electron Microscope (SEM, LEO FE-SEM 1530, Carl Zeiss NTS) operating at 5 and 15 kV. The bulk resistivity of the samples was measured using a four-point probe setup consisting of a probe fixture (Cascade microtech Inc.) and a source meter (Keithley 2440 5A Source Meter, Keithley Instruments Inc.) (see Figure 3-1). The sheet resistance of the samples (R_s) was characterized by the drop in voltage when applying a constant current (10 mA). The electrical resistivity (ρ) of the nanocomposites was calculated using the following equation:

$$\rho = R_s t = \left(\frac{\pi t}{\ln 2}\right)\frac{V}{I} \quad \Omega.cm$$ **Equation 3.1**

where t is the thickness of samples; I and V are the applied current and the measured voltage, respectively.

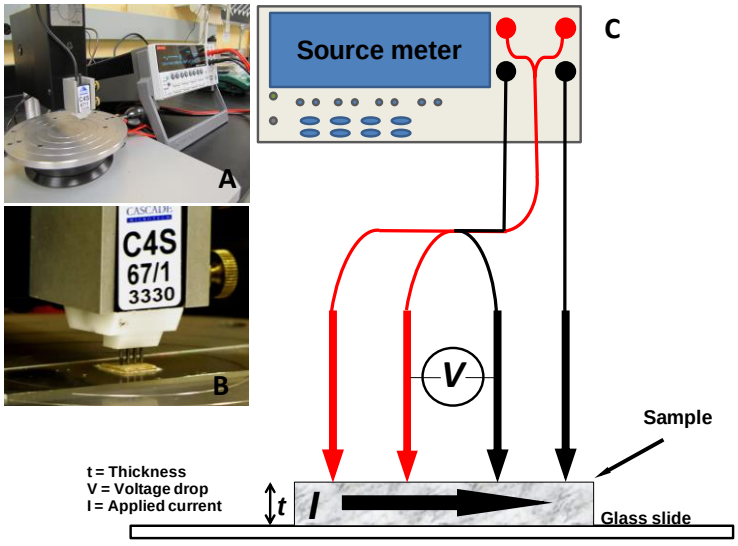

Figure 3-1. A) The electrical conductivity measurement setup consisting of a four-point probe and source meter; B) A close-up image of the four-point probe; C) a schematic illustration of measuring the bulk resistivity of nanocomposites.

3.3 Results and discussion

3.3.1 Synthesis and characterization of silver NPs

The chemically-stabilized Ag NPs were synthesized by the direct reduction of $AgNO_3$ using $NaBH_4$ in the presence of a thiocarboxylic acid. Figures 3-2A and 3-2B illustrate the

synthesis mechanism. In step 1, the thiocarboxylic acid was added into the solution of the silver salt in THF/water medium; the acid ($R\text{-}S^-$, Lewis base) partially reduces silver ions by donating one electron to Ag^+ (Lewis acid) ions, leading to the formation of silver atoms in the zero oxidation state (Ag°), which are chemically bonded to the hydrocarbon chains of the acid via Ag-S bond [127]. In step 2, a strong reducing agent, $NaBH_4$, was added to the suspension, which completely reduced the remaining silver ions into silver atoms (Ag°), resulting in the formation of Ag NPs, covered by thiocarboxylate groups. The silver-acid compound, formed in step 1, self-assembled over the surface of the growing Ag NPs and limited the growth of the NPs nuclei. The carboxylate functional groups provided a steric repulsion to prevent NPs from aggregating and at the same time enabled them to disperse in water and/or other polar solvents. Figure 3-2C shows typical TEM images of the MPA and MUA stabilized Ag NPs. Both NPs are spherical and well dispersed. We measured the size of 100 randomly-picked Ag NPs; the size distributions of those NPs were shown in the inserted histograms of Figure 3-2C. The diameter of Ag-MPA NPs ranged from 1 to 4 nm, while the majority was in the range of 1.5 to 3 nm, giving an average diameter of 2.09±0.66 nm. The diameter of the Ag-MUA NPs ranged from 2 nm to 8 nm, giving an average diameter of 4.49±1.28 nm. It is interesting to note that NPs capped with the short-chain acid (MPA) are smaller with a much narrower size distribution than the NPs capped with long-chain acid (MUA). Although the tuning of NPs size with the variation of the ratio of acid to NPs precursor ($AgNO_3$) has been known in literature [128,130], but to the best of our knowledge, there is no particular study of the effect of the chain lengths of covering layer on

the size of thiocarboxylate-stabilized Ag NPs. These results showed that the different chain lengths of the functional groups gave NPs of different sizes.

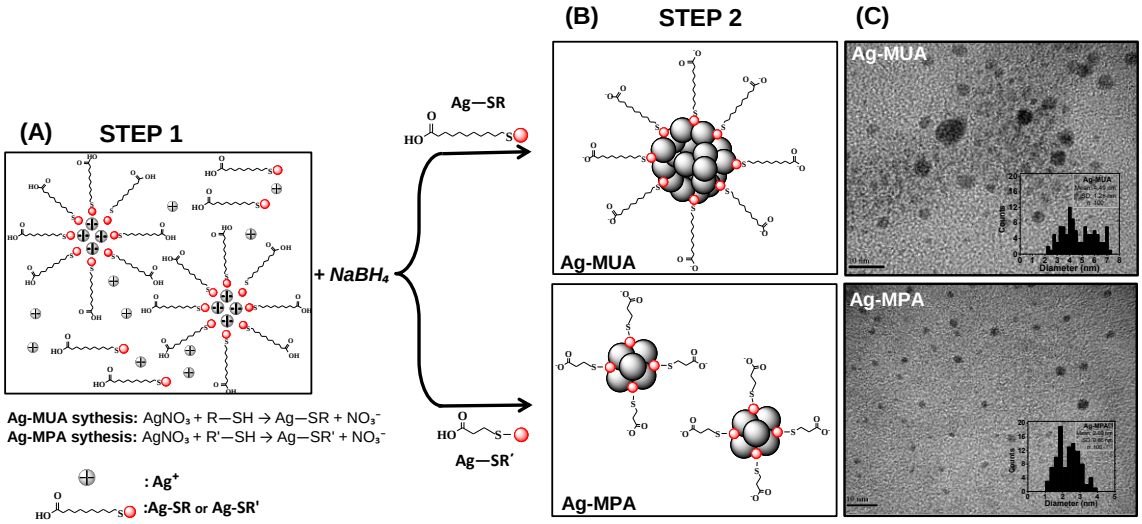

Figure 3-2. The synthesis of Ag NPs: A) step 1: the self-assembly of thiocarboxylic acids on the surface of growing Ag NPs and the partial reduction of Ag+ ions by thiocarboxylic acids, B) step 2: the formation of the Ag NPs, reduced by the strong reducing agent (the NPs were capped by self-assembled thiocarboxylate groups), and C) typical TEM images and histograms of the synthesized NPs.

We attribute the effect of chain lengths to the nature of the synthesis method. Two possible reasons may explain this situation. The first one is related to the strength of acids. The proton (attached to the sulfur) of MPA is much closer to the electronegative carboxylic group (located at the end of the chain) than that of MUA; this situation makes MPA a stronger acid than MUA. Thus, MPA can reduce a larger amount of silver ions at step 1; consequently less amount of silver ions remain in the system to grow the NP core. The second reason is related to the possible self-assembly mechanism of thiocarboxylic acids. The longer chain of MUA

can form a larger micelle-like structure compared to the shorter chain of MPA, providing a larger space for NPs to grow their nuclei.

UV-visible spectroscopic analyses were performed to further investigate the nature of the chemically-stabilized NPs. Figure 3.3 shows the optical spectra of both Ag-MPA and Ag-MUA NPs in aqueous solutions. Normally, metal NPs bigger than 2 nm have a strong and broad optical excitation peak in the UV-visible spectrum corresponding to the surface plasmon bonds (SPB) [132]. The symmetrical feature of the SPB for both Ag-MPA and Ag-MUA suggested a uniform and homogenous dispersion of the NPs in water; Ag NPs aggregates do not show a peak [133]. As shown in Figure 3-3, the SPB peaks were observed at the wavelengths of 412 nm and 436 nm for Ag-MPA and Ag-MUA, respectively. Note that the SPB peak of pure Ag NPs occurs between 380 nm to 390 nm [134]. These huge red shifts in the position of SPB peaks are caused by the presence of the attached organic layer on the surface of NPs [135]. The red shift in the position of the maximum absorption of Ag-MUA compared to that of Ag-MPA was also expected. Malinsky et al. studied the effect of the chain lengths on the optical properties of alkanethiol-capped Ag NPs and reported that the SPB peak would red shift 3 nm for every carbon atom in the alkane chain backbone [126].

It is also known that the features of SPB of metal NPs depend on their size and size distribution in which the SPB of larger NPs moves to higher wavelengths compared to that of smaller ones [136]. Hence, the observed red shift for Ag-MUA was attributed to the larger

size of these NPs compared to Ag-MPA [119,126]. Beside the peak at 436 nm, Ag-MUA has another peak at 342 nm. Dell' Eraba et al. reported a similar peak at 342 nm [130]. They attributed this small peak to the presence of some silver clusters in the system. But, this small peak was not observed in the spectrum of Ag-MPA, perhaps because the size distribution of Ag-MPA was narrower than that of Ag-MUA as estimated from the TEM results.

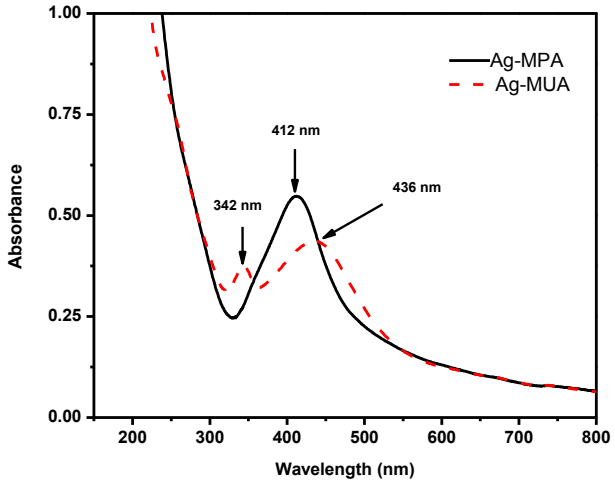

Figure 3-3. UV-visible spectra of Ag-MPA and Ag-MUA NPs.

Furthermore, we checked the stability of the NPs by comparing the UV-visible spectra of one-month aged samples with that of the fresh sample. As shown in Figure 3-4, the features of the spectra for both samples did not change after one month, suggesting the surface carboxylate groups formed strong hydrogen bonding with water molecules, which made NPs quite stable in aqueous medium [128].

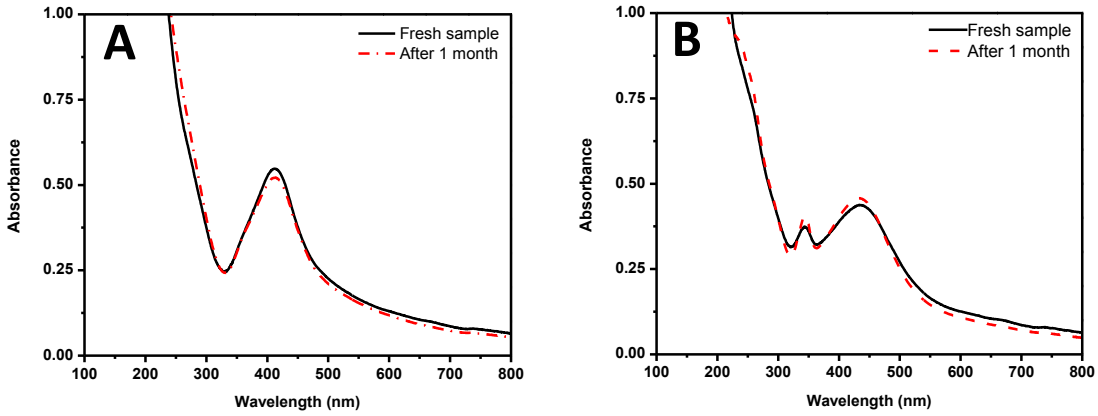

Figure 3-4. UV-visible spectra of fresh and one-month aged NPs aqueous dispersions: A) Ag-MPA NPs and B) Ag-MUA NPs.

The chemical adsorption or grafting of thiocarboxylic acids on the surface of NPs was examined by FTIR. With the exception of the liquid MPA, the analyses were performed in solid states for all the other samples. Figure 3-5 shows the spectra of pure acids and the functionalized NPs [137]. The broad peak at 3000 cm^{-1} for liquid MPA may relate to the presence free water, absorbed from the atmosphere. In the spectra of pure MUA and MPA, there are two small peaks, centered at 2543 and 2558 cm^{-1}, which belong to the S-H stretching bond; those peaks disappeared in the spectra of the grafted NPs. It confirms that sulfur groups of the acids were attached to the surface of the NPs via the formation of sulfur-silver bonds. The distinct peaks at 1691 and 1712 cm^{-1} for pure MUA and MPA (in the range of 1680-1720 cm^{-1}) correspond to the carbonyl group of the carboxylic acids. The peaks at 1559 and 1418 cm^{-1} for Ag-MUA, and at 1554 and 1403 cm^{-1} for Ag-MPA (Figure 3-5) are, respectively, assigned to asymmetric and symmetric vibrations of carboxylate groups,

confirming the existence of the mentioned groups on the surface of the Ag NPs, which was expected to be in the structure of the covering layer. The strong and sharp peaks at 2916 and 2845 cm^{-1} in the spectra of both pure MUA and Ag-MUA correspond to the asymmetric and symmetric stretching of methylene groups, respectively.

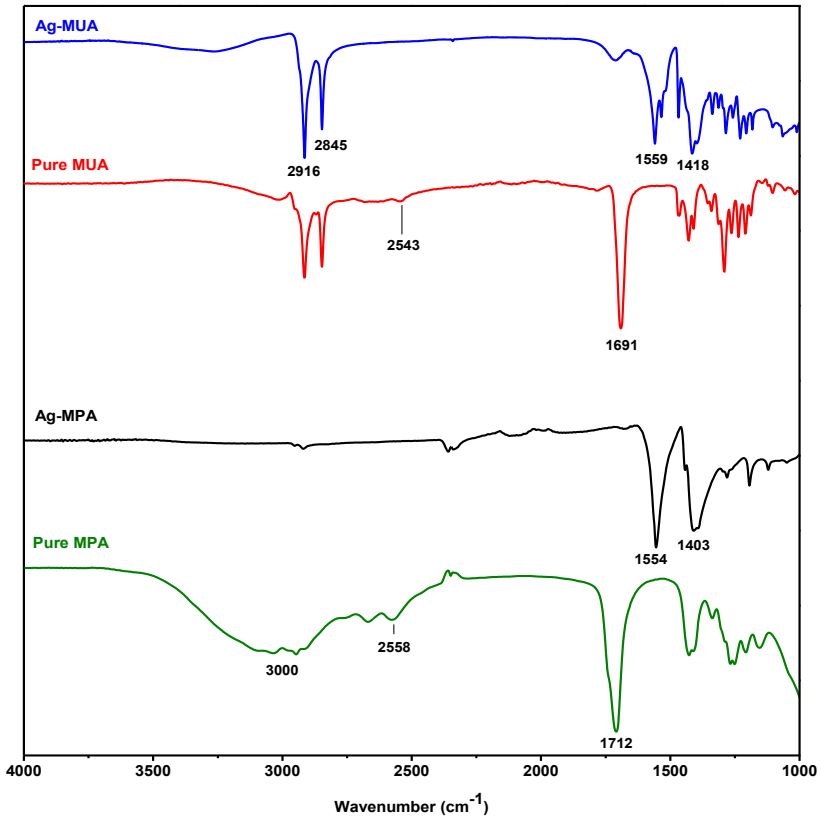

Figure 3-5. FTIR spectra of pure acids MUA and MPA and the corresponding stabilized silver NPs.

We took an analogy to the FTIR analysis of the typical hydrocarbons, such as polyethylene (PE), to obtain insights about the crystallinity of the surface layers on the synthesized NPs

[138]. For dissolved PE in a solvent, whose hydrocarbon chains are randomly oriented, asymmetric and symmetric stretches of methylene groups have broad peaks at 2928 and 2856 cm^{-1}, whereas for solid PE with a highly-packed and crystalline structure, these peaks become sharper and appear in lower wave numbers (i.e., 2920 and 2850 cm^{-1}) [138]. Applying the analogous information to the spectra of Ag-MUA, and considering the same methylene peak for Ag-MUA as the methylene peak of solid PE, it can imply that the long-chain, attached to the surface of Ag-MUA NPs, might be in a crystalline form. These two peaks are not significant for the Ag-MPA NPs. The crystalline structure of Ag-MUA were also reflected in the appearance of these NPs dry powder; the Ag-MUA NPs dry powders were shiny and rigid while Ag-MPA NPs were fluffy and soft as can be observed in Figure 3-6.

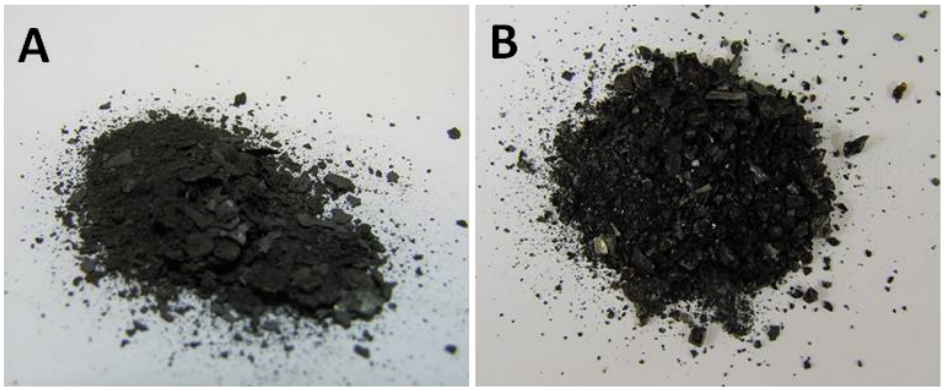

Figure 3-6. Digital images of dry powders of A) Ag-MPA and B) Ag-MUA NPs.

TGA was performed to investigate the thermal properties and the amount of stabilizing agents on the surfaces of Ag-MPA and Ag-MUA NPs. Figure 3-7 shows the weight-loss vs

temperature plots for the pure MUA, Ag-MPA and Ag-MUA. Note that the pure MPA is liquid at room temperature, so its analysis with TGA was not practical. The TGA of pure MUA showed thermal decompositions occurred between 130 °C and 300 °C, during which there was a 92 % weight-loss; the other 8 % weight loss occurred between 300 °C and 350 °C. There were two main weight-loss transition points for both Ag-MUA and Ag-MPA. Due to the presence of some pure MUA and moisture in the system, there was a small weight-loss before 300 °C for Ag-MUA. The first main transition of Ag-MUA occurred between 300 °C and 360 °C, having about 4% weight-loss which may attributed to the amount of MUA, physisorbed on the surface of the NPs. The second main transition of Ag-MUA, having a larger weight-loss (~ 24 wt%), was observed at 437 °C and continued up to 490 °C. This large amount of weight-loss at this stage is attributed to decomposition of chemisorbed organic materials [139]. As for the Ag-MPA, its thermal decomposition started at 130 °C; the weight decreased by only 3 wt% until 270 °C because of the decomposition of some un-bonded MPA or absorbed water in the system. As the temperature increased, similar to Ag-MUA, Ag-MPA displayed two main thermal decomposition steps. The decomposition of physically adsorbed MPA occurred between 270 °C and 350 °C, having an approximately 7 wt% of the total weight-loss. The decomposition of chemically adsorbed MPA occurred between 400 °C and 470 °C, having 11% weight-loss, which was almost half of that of Ag-MUA. A further comparison of the TGA curves of Ag-MUA and Ag-MPA shows that the thermal decompositions of Ag-MPA started and finished at lower temperatures. It appears that the chemical functionalization of the Ag NPs using the long-chain acid was more

effective than the short-chain acid, that is, the Ag-MUA NPs have a higher coverage of the organic layers than Ag-MPA NPs.

To obtain quantitative information, we estimated the number of functional groups per unit surface area from the weight-loss due to the decomposition of the chemisorbed acids. First, we calculated the mass of an individual NP (w_s) using the average diameter (d) of each NP (consequently volume of each NP, V), obtained from TEM images, and the density of silver (ρ).

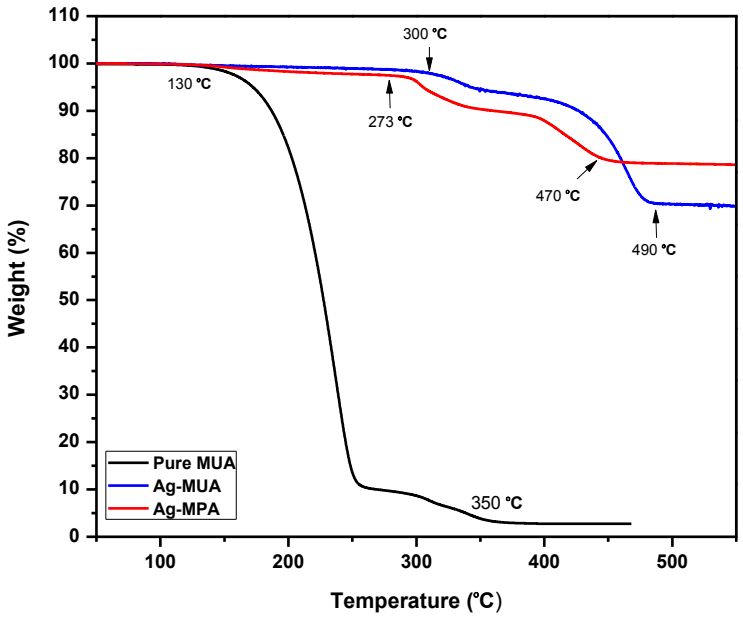

Figure 3-7. Thermogravimetric curves of pure MUA, MPA and MUA stabilized-silver NPs (or Ag-MPA and Ag-MUA).

$$V = \frac{\pi d^3}{6}$$ **Equation 3.2**

$$w_s = \rho . V$$ **Equation 3.3**

Second, the total amount of the organic layer in the system (W_o) was calculated by:

$$W_o = W . \phi$$ **Equation 3.4**

where W is the total mass of each sample subjected to the TGA, and ϕ is the weight fraction of chemisorbed acid on the surface of NPs, which were 24 wt% for Ag-MUA and 11 wt% for Ag-MPA. The total amount of pure silver (W_s) in the system is obtained as:

$$W_s = W - W_o$$ **Equation 3.5**

Third, the total number of NPs for each sample (N) subjected to TGA test is determined.

$$N = \frac{W_s}{w_s}$$ **Equation 3.6**

Fourth, the average number of functional groups or chains on an individual NP was determined.

$$n = \frac{W_o}{M_w \cdot N} N_a$$ **Equation 3.7**

Where M_w is the molecular weight of MPA or MUA, and N_a is the Avogadro number. n = 42 for Ag-MPA while n = 409 for Ag-MUA. Finally, the number of functional groups per unit surface area of the NP or the number density was determined.

$$n_o = \frac{n}{\pi d^2} \qquad \textbf{Equation 3.8}$$

$n_o \approx 2.6\ nm^{-2}$ for Ag-MPA, and $n_o \approx 6.4\ nm^{-2}$ for Ag-MUA. Thus, the long-chain functional groups grafted on NP are much denser than the short-chain functional groups.

3.3.2 Electrical properties of the functionalized NPs and the polymer composites

The electrical properties of the Ag-MUA and Ag-MPA were investigated by measuring the bulk resistivity of a sheet of NPs of 0.1 mm thick prepared by drying the dispersion of NPs in water on a microscope glass slide. Interestingly, Ag-MUA NPs did not show any conductivity whereas the bulk resistivity of the sheet of Ag-MPA NPs was approximately 1.02×10^{-3} Ω.cm. According to the information extracted from TGA results, the number density of the organic chains covering the surface of Ag-MUA is almost 3 times larger than that of Ag-MPA NPs (see Table 3-2). It seems that the denser and longer chains on Ag-MUA, which may have assembled on the surface into a crystalline structure as inferred from the FTIR analysis, effectively insulated the NPs surface; on the other hand, the shorter chain and lower density of the covering layer allow Ag-MPA NPs to be still conductive.

Table 3-2. A comparison of bulk resistivity of different types of silver fillers.

Material	Number of chain on the surface of each NPs	Number of chain per unit of surface area	Bulk resistivity of conductive fillers (Ω.cm)
Ag flakes	–	–	1.59×10^{-6}
Ag-MUA	409	6.4	-
Ag-MPA	42	2.6	1.02×10^{-3}

In order to understand how chemically-stabilized NPs influence the overall electrical conductivity of their polymer composites, they were added into a silver flake filled epoxy matrix at varied weight fractions to make a hybrid conductive adhesive. Due to the insulating nature of Ag-MUA, only Ag-MPA NPs were added to the system. The bulk resistivity of the conventional conductive adhesive, containing only silver flakes at weight fractions between 60 wt% to 70 wt%, were measured as a control for the hybrid adhesive. Figure 3-8 shows the bulk resistivity as a function of the total weight fractions of silver fillers for both types of nanocomposites. As can be seen in Figure 3-8, in the system, consisting of only silver flakes, addition of more fillers decreased the bulk resistivity; however, in the nano/micro hybrid filler system, in which the total amount of flakes was kept constant, the addition of a small amount of Ag NPs, (i.e. the weight fraction of NPs to silver flakes K = 0.2), reduced the resistivity of the nanocomposites by two orders of magnitude, while the resistivity started to increase by adding more NPs (i.e., K = 0.4, and 0.6), indicating that the NPs played a complex role in the system. For the sample with K = 0.4, the resistivity increased slightly compared to that of sample with K = 0.2, but still lower than the bulk resistivity of the conventional ECA (epoxy and silver flakes) with the same filler concentration. The addition

of more NPs (i.e., K = 0.6) further increased the resistivity to a value higher by one order of magnitude than that of the conventional ECA with the same filler concentration. In other words, the hybrid adhesive outperformed the conventional adhesive at the total weight fractions between 60 wt% and 67 wt% (K = 0.2, and 0.4) while adding more NPs did not improve the conductivity but resulted in a higher bulk resistivity than the conventional adhesive.

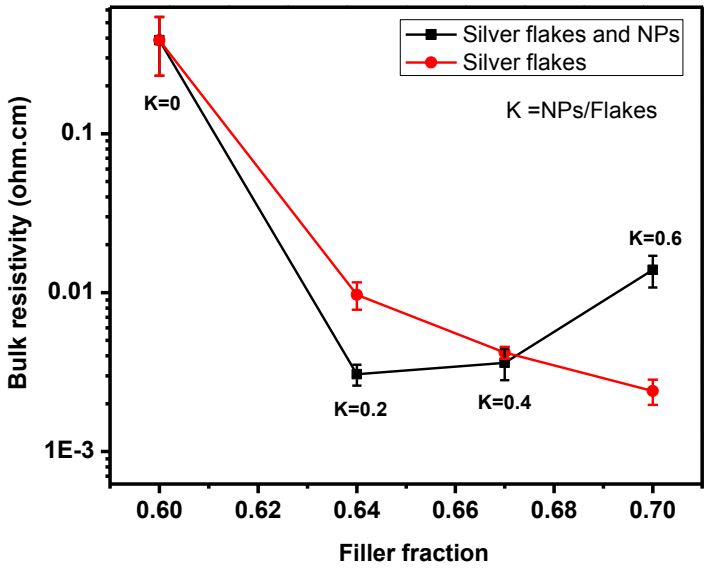

Figure 3-8. Bulk resistivity of conductive adhesives as a function of filler fraction for both the micro/nano hybrid configuration

To obtain some insights into the behavior of Ag-MPA NPs in the conducive composite, SEM images of the NPs and their nanocomposites were examined and discussed in terms of the effect of NPs on the overall conductivity of the nanocomposites. The performance of a conductive adhesive depends significantly on the quality of conductive fillers and the filler

network. The overall electrical conductivity of the filler networks in the adhesive matrix is determined by the intrinsic resistance of the fillers and the contact resistance of neighboring fillers. As for the filler-filler contact resistance, it is composed of two distinct resistances: constriction resistance and tunnelling resistance [77]. The former is related to the flow of electrons through contact points; the smaller the number of contact points, the lower the constriction resistance. It has been reported that the addition of NPs into the conventional conductive adhesive has a negative effect on the overall electrical conductivity because of the increased number of contact points, unless the NPs are sintered at an elevated temperature. Therefore, we suspected that the Ag-MPA NPs partially fused during curing because of their small sizes even though no particular sintering process was applied. The SEM images, shown in Figures 3-9A and 3-9B, confirmed that sintering occurred between NPs and silver flakes. Although the sintering of the chemically-stabilized silver NPs larger than 50 nm is not expected at this annealing condition (100 °C for 1 h), the small size of Ag-MPA NPs (< 5 nm) and short chain coverage may have allowed them to sinter at this relatively low temperature.

Adding a small amount of Ag-MPA might also help to reduce the tunnelling resistance, [77,140]. The tunnelling resistance is associated to the resistivity induced by the insulating materials including the surface layer of organics layer on filler surface or polymeric matrix [77]. One reason for the negative effect of NPs (> 50 nm) on the overall electrical conductivity is that they hinder the effective contacts between silver flakes and increase the tunnelling resistance [89]. However, for the 2 nm Ag-MPA NPs, we showed in Figures 3-9C

and 3-9D that they filled the gaps between silver flakes, which bridged the originally separated flakes. This bridging effect can significantly reduce the tunnelling resistance. Furthermore, the partially-fused NPs may also decrease the tunnelling resistance by creating new electrical paths throughout the epoxy. Figure 3-9E and 3-9F show SEM images of the composites before and after the addition of the NPs (weight fraction of NPs to silver flakes, $K = 0.2$). The area above the dash line is the top surface; the area beneath the dash line is the cross section of a fractured composite. As indicated by the arrows, clusters of NPs filled the interstices of silver flakes and caused the fillers to distribute more uniformly in the epoxy. Indeed, we observed in the four-probe measurements that the addition of NPs made the conventional micro-composite adhesive more electrically homogeneous. In other words, the NPs filled the gap between silver flakes and provided more electrically conductive paths. Finally, adding a larger amount of NPs ($K = 0.4$, and 0.6) may backfire because they form more and larger clusters, which may increase the gap distance between the silver flakes and consequently increased the tunnelling resistance. Besides, adding more NPs increases the contact resistance in the system. It is reasonable to conclude from these research findings that the chemically-stabilized NPs can improve the electrical conductivity of the conventional ECAs at a relatively low curing temperature of 150°C without the extra step of sintering at an elevated temperature. This improvement in the electrical conductivity of the ECAs at lower filler contents using the nano/micro hybrid filler system are attributed to the partial fusion of the NPs and the action of the NPs covered with the well-designed surface layer to fill the gaps between separated silver flakes due to their small size. Further studies are needed to elucidate the complex behaviors of NPs in the nano/micro hybrid conductive composites.

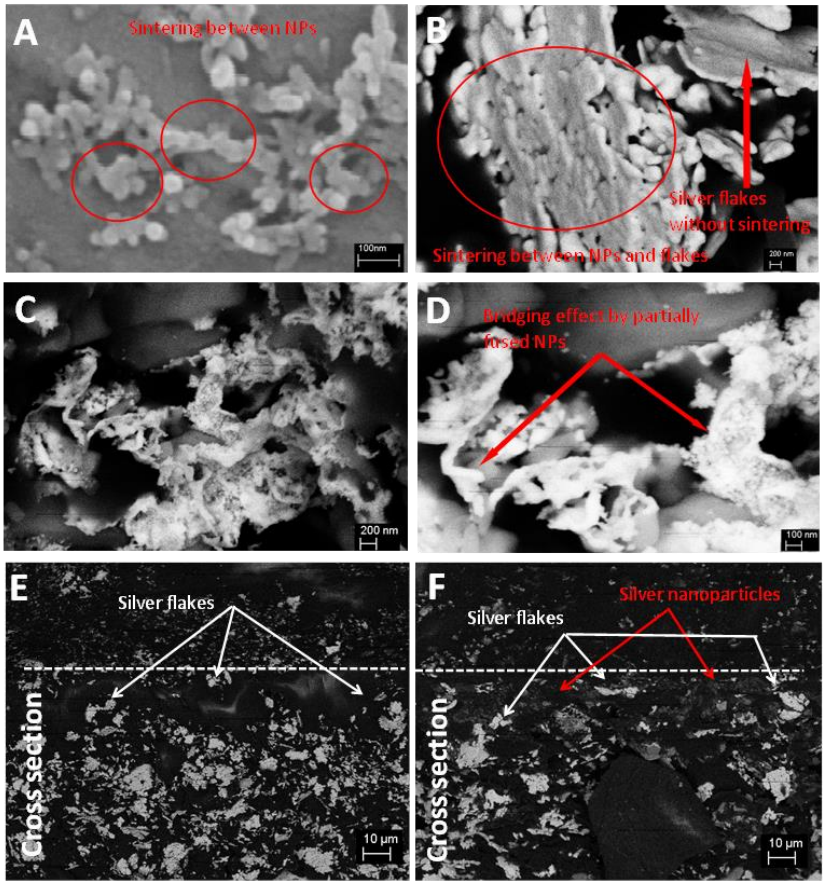

Figure 3-9. SEM images of A) sintered Ag-MPA NPs at 100 °C for 1 hr; B) sintering of NPs in nanocomposite structure after curing at 150 for 2 hr; C) bridging effect of NPs between silver flakes at a lower magnification; D) a higher magnification; and 45° views of the top and cross section of a fractured composite; E) separated silver flakes at the surface of composites without NPs; F) the filling of silver NPs into the gaps between the silver flakes creating news electrical paths

3.4 Summary

In summary, we synthesized novel thiocarboxylate-functionalized Ag NPs (less than 5 nm) by the direct reduction of silver nitrate in the presence of two different thiocarboxylic acids.

The well-controlled synthesis conditions allowed for a detailed investigation of the effect of the chain length of the functional groups on the thermal and electrical properties of the Ag NPs and their polymer composites. We found that the chain length had significant effects on the size and conductivity of the NPs; the NPs grafted with 3-carbon thiocarboxylic acid had an average size of 2.09 nm and were conductive while those with 11-carbon acid had an average size of 4.49 nm and were non-conductive. TGA analyses revealed the number density of short-chain acids, grafted on the NPs, were about three times smaller than that of long-chain acids. The FTIR analysis indicated that the long-chain acids might be assembled into a crystalline structure on the surface of NPs. It was proposed that the higher surface coverage and the crystalline structure of long-chain acids account for the non-conductive nature of the functionalized Ag NPs. The short-chain functionalized NPs were incorporated into a hybrid-designed composite adhesive, consisting of micron-sized silver particles and the NPs in an epoxy matrix. The electrical conductivity measurements and SEM images of the cross sections of cured hybrid composites showed that low NPs contents increased electrical conductivity due to the filling of NPs into the interstices of the microparticles and their low sintering temperature, whereas higher NPs contents reduced the electrical conductivity because they clustered and increased the gaps among the micro-particles. The relationship between the properties of the nanocomposites and the surface chemistry, size and amount of NPs were discussed, showing the complex role of NPs in the nanocomposites.

Chapter 4. Electrical Conductive Adhesives Filled with High-Aspect-Ratio Silver Nanobelts (Ag NBs)

4.1 Introduction

As mentioned in previous chapters, replacement of lead-based solders with ECAs requires advanced materials with desired electrical conductivity and mechanical strength, resembling those of the metallic solders. In conventional ECAs improvement of one of these fundamental properties (electrical vs. mechanical) essentially lead to sacrifice in the other. In other words, electrical conductivity enhancement of conventional ECAs requires more silver flakes to be added into the epoxy matrix; but the addition of a large amount of silver flakes is detrimental to the mechanical strength of the final composite due to the reduced volume fraction of the polymer matrix. In addition, as it has been said before, adding more conductive filler to epoxy after percolation threshold would not significantly improve the electrical conductivity. To address these concerns, research has been stepped up to implement hybrid filler systems (i.e., synergetic combination of nano-sized conductive materials and silver micro flakes) to develop cost-effective ECAs with desired properties.

The incorporation of spherical Ag NPs to the system of epoxy and silver micro flakes has been discussed in detail in previous chapters. Generally, it has been believed that adding Ag NPs in small amounts compared to silver flakes improves the electrical conductivity of the ECAs while beyond that it may reduce the electrical conductivity. This negative effect has

been found as a result of the increased number of contact points among the micro and nano-sized fillers [20,36]; a large number of contact points increase the contact resistance and reduce the efficiency of the electrical network to transfer electrons. To overcome the drawbacks in adding NPs, sintering between NPs during the curing of ECAs is suggested to decrease the number of contact points and subsequently to increase the electrical conductivity [21,39]. In Chapter 3 we showed that very small Ag NPs (less than 10 nm) can improve the electrical conductivity of the ECAs at a relatively low curing temperature (~150°C) because such small NPs can readily fill the gaps between the micro flakes while they also can be partially sintered because of their small size (less than 5 nm) [20]. However, a large amount of Ag NPs is still needed to form a percolated network which would increase the number of contact points within electrical pathways and decrease the electrical conductivity of ECAs. Besides, a large amount of NPs can negatively influence the mechanical strength, processability, and the final cost of ECAs.

In recent years, high aspect-ratio nanofillers have been proposed as alternative materials for spherical NPs to overcome the concern of excessive contact points between NPs and to reduce the amount of conductive fillers [16–18,40–44,46]. High aspect-ratio nanomaterials can establish more stable and effective electrical networks at lower filler contents with less number of contact points. Moreover, they can provide better electrical conductivity without sacrificing the integrity and adhesive strength of the polymeric matrix [40]. For instance, Wu et al. reported a significant electrical conductivity improvement for the ECAs filled with 56 wt% silver nanowires (Ag NWs) compared to that of the ECAs filled with micron-sized

and/or nano-sized spherical silver particles with similar filler concentration [40]. However, most of the studies performed in this field have involved the direct addition of Ag NWs into epoxy resin without silver flakes; this situation requires a large amount of Ag NWs to achieve the desired conductivities [18,40,45]. There is little research on the development of hybrid filler systems by using high aspect-ratio silver nanomaterials as auxiliary fillers in the formulation of the conventional ECAs. To the best of our knowledge, only Zhang et al. reported the use of Ag NWs along with the silver flakes (weight ratio of 2:3) to develop a hybrid fillers system and found a significant improvement in electrical conductivity of the fabricated ECA [50]. This study suggested a synergistic effect of high aspect-ratio Ag NWs and silver flakes on the electrical conductivity improvement of the hybrid ECAs.

In this chapter, we report the incorporation of a new class of high aspect-ratio nanofillers (i.e., silver nanobelts (NBs)) into the conventional ECA to develop a hybrid ECA composite. The Ag NBs were synthesized through a high-yield chemical reduction method, based on the self-assembly and room-temperature joining of hexagonal and triangular Ag NPs as structural blocks of the NBs. Compared to the previously used Ag NWs, which are synthesized at high temperatures and long reaction times, the fabrication of the NBs is fast and occurs at room temperature [51]. Besides, the Ag NBs have a low "weight to length" ratio, which can form a percolated network at low concentrations which consequently reduce the total mass of composites. Our results revealed a significant improvement in the electrical conductivity of the hybrid ECA composite in comparison to the conventional ECA.

4.2 Experimental

4.2.1 The Synthesis of Ag NBs

The Ag NBs were synthesized by chemical reduction of silver nitrate ($AgNO_3$, Sigma-Aldrich) in the presence of poly(methacrylic acid) (PMAA) according to our recent work [25]. In detail, 2.1 g of $AgNO_3$ was dissolved into 60 mL of de-ionized (DI) water and agitated in an ultrasonic bath for 10 minutes. Separately, 0.4-1 g reducing agent of ascorbic acid (Alfa Aesar) and a small amount of aqueous solution of PMAA sodium salt (40%, Aldrich Chemistry) were dissolved into 200 mL of DI water and agitated in an ultrasonic bath for 10 minute. The synthesis was started by adding the $AgNO_3$ solution into the reducing solution while it was stirred gently by a magnetic stirrer. After 10 min, solid precipitates were collected by vacuum filtering and dried in a vacuum oven at room temperatures.

4.2.2 Nanocomposite Preparation

The synthesized Ag NBs along with Ag flakes (Aldrich, 10 μm) at different weight fractions were added to epoxy (diglycidyl ether of bisphenol A, DERTM 322, Dow Chemical company, USA). The weight fractions of the Ag flakes and Ag NBs are listed in Table 4-1.

Table 4-1. Weight fractions of silver NBs and silver flakes in the conventional and hybrid ECA samples

	Sample #	Ag NB (mg)	Ag flake (mg)	NB content (wt%)	$K = \frac{Ag\ NB}{Ag\ flake}$	Total silver concentration (wt%)	Total silver concentration (Vol%)
Conventional ECA	1	0	200	0	0	60	18.0
	2	0	210	0	0	61	18.9
	3	0	220	0	0	62	19.7
	4	0	230	0	0	63	20.4
	5	0	240	0	0	64	21.1
	6	0	564	0	0	81	38.6
Hybrid ECA	7	7	200	2	0.03	61	18.9
	8	18	200	5	0.09	62	19.7
	9	30	200	8	0.15	63	20.4
	10	40	200	11	0.2	64	21.1
	11	17	547	2	0.03	81	38.6

To ensure a good dispersion of the NBs in the viscous epoxy, the NBs were first dispersed in isopropyl alcohol (IPA). The NBs suspension was then added into the mixture of Ag flakes and epoxy, which was slightly diluted by IPA. The mixture was then agitated for 30 min using a vortex mixer followed by 1 h of sonication; then, the mixture was degassed under vacuum for 1.5 h to remove the solvent from the system. After degassing, the curing agent

triethylenetetramine (TETA, Dow Chemical company, USA) was added to the mixture. The weight ratio of the curing agent to epoxy was 0.13. The final mixture was filled into a mold of 7 × 7 × 0.5 mm^3 (L × W × D) made on a pre-cleaned microscope glass slide using pieces of adhesive tape. To make a smooth surface and control the sample thickness, a clean copper plate was placed on top of the mold; the extra material was squeezed out. The samples were pre-cured for 30 min at 60 °C and then cured at 150 °C for 2 h. After curing, the copper plate and adhesive tape were manually peeled off. The same procedure was applied to prepare conventional ECAs (epoxy and Ag flakes) except, there were no Ag NBs in the system.

4.2.3 Characterization

A standard differential scanning calorimeter (DSC, TA Instruments, Q 2000) was used to estimate the de-bonding temperature between the covering layer (PMAA) and the Ag NBs. In DSC tests, a sample of about 6 mg of Ag NBs was placed into a hermetically-sealed pan and placed into the DSC cell under a nitrogen purge at 50 mL/min. The first heating scans were performed at a rate of 10 °C/min. After the first scan, the sample was cooled down to room temperature and then re-scanned at the same heating rate. The sample weight-loss and the NBs surface coverage with PMAA were studied using thermogravimetric analysis (TGA, TA instrument, Q500-1254). A sample of about 10 mg was placed into the TGA sample pan. Dynamic scan was performed from 40 °C to 700 °C with a heating rate of 10 °C/min under a 50 mL/min nitrogen purge atmosphere. The morphologies of the NBs and cured nanocomposites were examined by scanning electron microscope (SEM, LEO FE-SEM

1530, Carl Zeiss NTS) operating at 10 kV and high resolution transmission electron microscope (HRTEM, JEOL 2010F FEG) operating at 200 kV. For the cross-sectional analysis by SEM, samples were kept in liquid nitrogen bath for 10 min and gently broken while they were in the bath. The samples were mounted vertically on a SEM stub and SEM images were taken from the cross-section. The surface quality of the ECA nanocomposites was examined by water contact angle measurement tests along with surface roughness analysis. Water contact angle measurement tests were performed by placing 6 water droplets of ~3 μL on different spots on the sample surface. The static water contact angles on pure epoxy as well as on conventional and hybrid ECAs were measured by analyzing the image of each water droplet using a MATLAB code. The surface roughness of the samples was measured using a Veeco optical profilometer. The bulk electrical resistivity of the samples was measured using a four-point probe setup consisting of a probe fixture (Cascade microtech Inc.) and a source meter (Keithley 2440 5A Source Meter, Keithley Instruments Inc.). The sheet resistance of the samples (R_s) was characterized by the drop in voltage when applying a constant current (10 mA). The measurements were performed for four individual samples of a particular filler composition at 5 different spots; the average of all the readings was reported as the final value for that concentration. The electrical resistivity (ρ) of the nanocomposites was calculated using the following equation:

$$\rho = F.t\frac{\pi}{ln2}\left(\frac{V}{I}\right) \qquad \textbf{Equation 4.1}$$

where t is samples thickness, I is the applied current, and V is the voltage drop measured by the source meter. In equation 1, F is a correction factor for a finite sample with finite thickness. F is a function of the ratio of sample thickness (t) to probe spacing (s). For $0.4 < \frac{t}{s} < 1$, F is close to 1. In our system, in which the samples thickness is 0.5 mm and the probe spacing is 1 mm, F can be safely considered as 1.

4.3 Results and discussion

High aspect-ratio Ag NBs were fabricated by a facile chemical reduction approach based on the self-assembly and room-temperature joining of the hexagonal and triangular Ag NPs formed in the earlier stages of the synthesis. The synthesis mechanism is based on the reduction of silver ions by ascorbic acid to form initial silver crystals [51,141]. The PMAA covers the (111) planes of these initial crystals, making the growth rate in the [111] direction slower than that in the [100] direction. As a result, the initial crystals grow into a hexagonal morphology, as shown in Figure 4-1A [51,141–143]. The top and bottom planes of the hexagons are (111) planes while their edges are (111) and (100) planes [144–146]. However, throughout the synthesis process, some of the hexagons turn into triangles (see Figure 4-1B). The change in the morphology of hexagons is because of the difference between the growth rate of silver in [111] and [100] directions [145]. It should be noted that, despite the hexagons, the edges of the triangular Ag NPs only consist of (100) planes [145,147,148].

Since the top and the bottom flat faces of the hexagonal and triangular Ag NPs are covered by long-chain polymer molecules (PMAA), [25] they join to each other from the edges and assemble linearly to form high aspect-ratio belts [51,143]. Figure 4-1C and 4-1D clearly show the way the structural blocks (as pointed by arrows) were joined to each other and assembled into belt morphology. As can be seen in Figure 4-1D, the NBs are wavy and their edges are not flat. This interesting morphology is forming because of the shape of the structural blocks and also due to the way they join to each other.

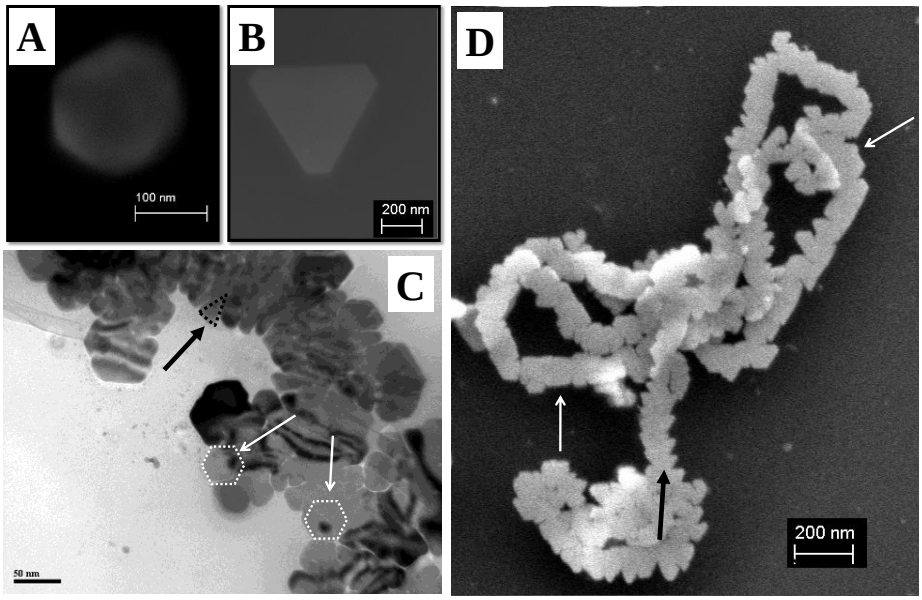

Figure 4-1. The SEM images of (A) a hexagonal silver NP; (B) a triangular silver NP; (C) A TEM image of the silver NB showing the self-assembly and joining of the structural blocks; (D) A SEM image of silver NBs. The white arrows point to hexagonal silver NPs and the black arrows point to triangular silver NPs.

The size analysis of the NBs was performed by measuring the length and width of 1700 randomly-picked Ag NBs, extracted from the SEM images. The width of the belts was in the range of 100 to 400 nm while the majority of the end-to-end length of the NBs, presented in Figure 4-2, was in the range of 1 to 10 µm.

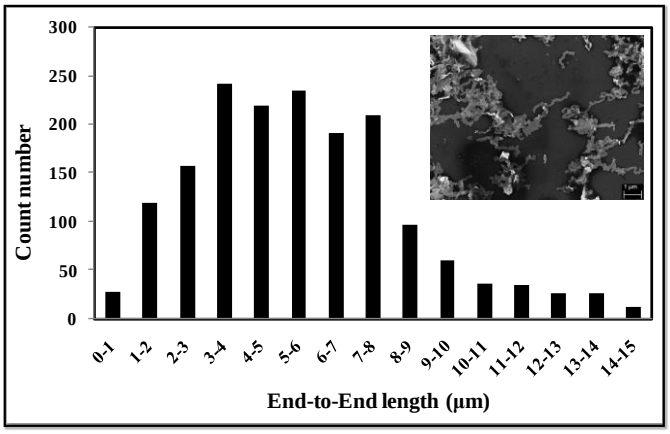

Figure 4-2. The end-to-end length distribution of the silver NBs. The inserted image is a typical SEM image of the silver NBs.

Although the presence of PMAA was crucial to control the shape of the NBs and prevent their aggregation, this layer, due to its insulating nature, may inhibit the electrical performance of the final nanocomposite. In other words, the amount of organic materials and their de-bonding temperature can largely affect the final electrical properties of the ECAs [21,39,50]. Hence, it is necessary to determine the amount of PMAA on the NBs surface and study its thermal properties. In this regard, DSC and TGA measurements were performed to determine the thermal behavior and amount of the organic layer on the NBs. Figure 4-3A represents the DSC curve for the Ag NBs. The first heating curve shows an endothermic peak

at 150 °C, which has disappeared in the second heating scan. This peak can be attributed to the de-bonding of PMAA from the NBs surface [21]. Thus, a minimum curing temperature of 150 °C is needed to detach the PMAA from the NBs surface so as to eliminate the negative effect of the covering layer on the overall conductivity of the nanocomposite. Figure 4-3B shows the TGA curves for both the synthesized NBs and pure PMAA. It can be seen that most of the pure PMAA (more than 95 wt%) was decomposed up to 200 °C. Regarding the TGA curve for NBs, there is a slight weight-loss (~0.1%) up to 150 °C, which can be related to water evaporation or the decomposition of other impurities. After 150 °C, an abrupt transition was observed, which finished at the temperature around 425 °C. This transition can be attributed to the thermal decomposition of the PMAA, adsorbed on the surface of the NBs [21]. The total weight-loss (excluding the initial weight-loss) for the Ag NBs was ~1.3 wt% up to highest applied temperature of 650 °C, which shows the amount of PMAA on the surface of Ag NBs. Having a small amount of PMAA over Ag NBs indicates that the PMAA was physically adsorbed at the surface, seeing that covalent bonding could generally lead to the attachment of a large amount of PMAA on the surface of NPs [127,139].

To investigate the effects of the Ag NBs on the electrical performance of the hybrid ECAs at low filler contents (close to the percolation threshold concentration), Ag NBs of different amounts (0-40 mg) were added to a control sample, which was a conventional ECAs containing a constant amount (200 mg, or 60 wt%) of silver flakes. The weight ratios of Ag NB and Ag micro flake (K) were calculated, which increased from 0 to 0.2. The addition of Ag NBs also increased the total amount or weight fraction of conductive silver fillers from

60 wt% to 64 wt%. In order to have direct comparisons, conventional ECAs of the same silver weight fractions as the hybrid ECAs were prepared and tested. All the samples and their composition are listed in Table 4-1.

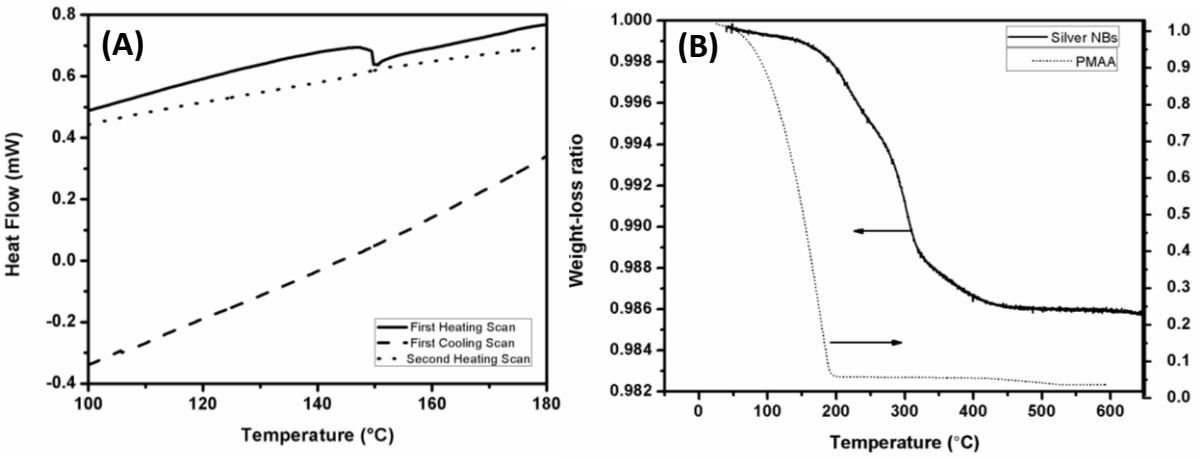

Figure 4-3. Thermal characterization of silver NBs, (A) DSC curves (heat flow vs. temperature) for silver NBs; (B) TGA curves (weight-loss vs. temperature) for both silver NBs and pure PMAA.

Figure 4-4 shows the changes in the bulk resistivity of the hybrid ECAs as well as that of the conventional ECAs (as control samples) as the total silver weight fractions increased from 60 wt% to 64 wt%; the weight ratio of Ag NBs to Ag flakes (K) are labeled beside each hybrid ECA composite. It can be seen that the adding a small amount of the Ag NBs (K = 0.03 – 0.09) into the conventional ECAs (K = 0) dramatically reduced the bulk resistivity of the conventional ECAs. The minimum bulk resistivity of the hybrid ECAs with K = 0.03 was approximately 6% of the resistivity of the conventional ECAs with the same filler content (61 wt% of silver), resulting in an electrical conductivity enhancement of 1550%. When more

NBs were added to the system (K = 0.15 and 0.20), the bulk resistivity of the hybrid ECAs started to increase, but only slightly. In contrast, bulk resistivity of the control conventional ECAs decreased slowly with the addition of more Ag flakes. At the weight fraction of 64%, the resistivities for the conventional and hybrid ECAs were close. These results show that adding more Ag NBs or increasing the K value did not improve ECAs further. Perhaps a large amount of nanoscale fillers caused a significant increase in the number of contact points or contact resistance among the fillers through currently existed electrical pathways which may cancel out the positive effect of Ag NBs on adding more electrical conductive paths inside the network [20].

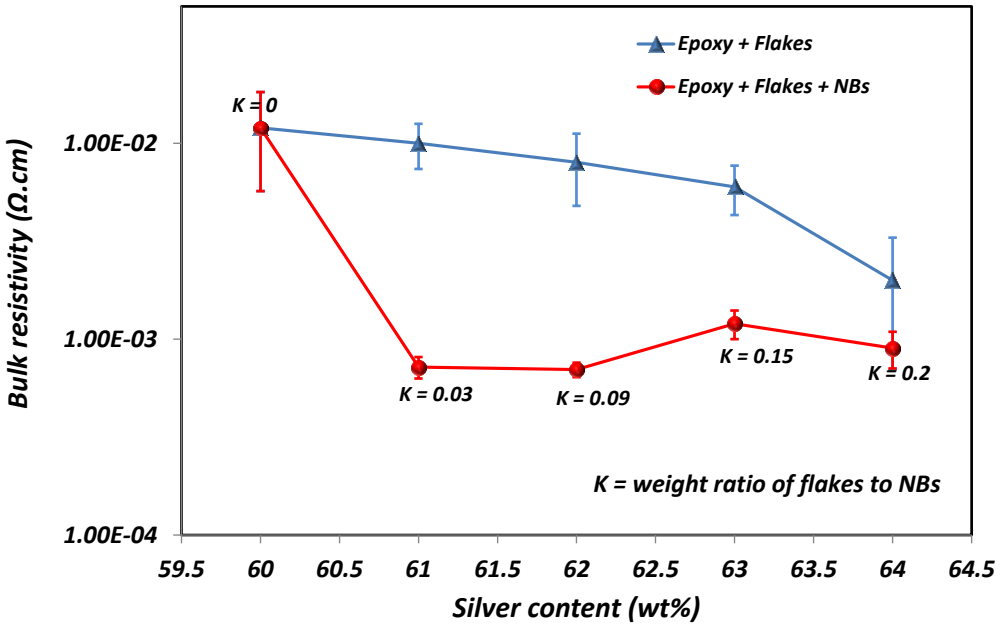

Figure 4-4. The bulk resistivity of the hybrid ECAs (solid line), and the conventional ECAs (dashed line) at various silver concentrations.

It is worthwhile mentioning that during electrical resistivity measurements, it was noticed that there were some non-conductive spots on the surface of the conventional ECAs because the ECA surface was not homogeneous and the non-conductive spots contain only epoxy. In contrast, the measurements for the hybrid ECAs were quite similar all over the surface. This observation is reflected by smaller error bars of the data points for the hybrid ECAs in Figure 4-4. It seems that the incorporation of the NBs into the conventional ECAs made the surface of nanocomposites more electrically homogeneous. Furthermore, both the conventional and hybrid ECAs were observed to bond well to the glass substrate surfaces; implying that the addition of the NBs in the system has no significant effect on the adhesive bonding strength.

To further evaluate the effectiveness of the hybrid filler system in the fabricated ECA composites, the weight fraction of silver in both the conventional and hybrid ECA composites was increased from the 61 wt% to 81 wt%. The bulk resistivity of the epoxy filled with 81 wt% of silver flakes was 4.5×10^{-4} Ω.cm, which is close to the bulk resistivity of the hybrid ECAs filled with 61 wt% of silver (NBs + silver flakes) (6×10^{-4} Ω.cm), as shown in Figure 4-5. These data clearly demonstrate that employing small amounts of Ag NBs is more effective in reducing the electrical resistivity than adding more Ag flakes to the system. We also added 2 wt% (equal to 0.64 vol%, $K = 0.03$) Ag NBs to the conventional ECAs, filled with 80 wt% silver flakes (total silver content of 81 wt%), which showed almost 246% better electrical conductivity (the reciprocal of the measured resistivity) in comparison to the conventional ECA filled with the same amount of silver flakes (81 wt%). These results show that the effect of the NBs on the electrical conductivity enhancement of the ECAs at 61

wt% filler content (close to the percolation threshold) is more pronounced than that at 81 wt% filler content, which is beyond the percolation threshold.

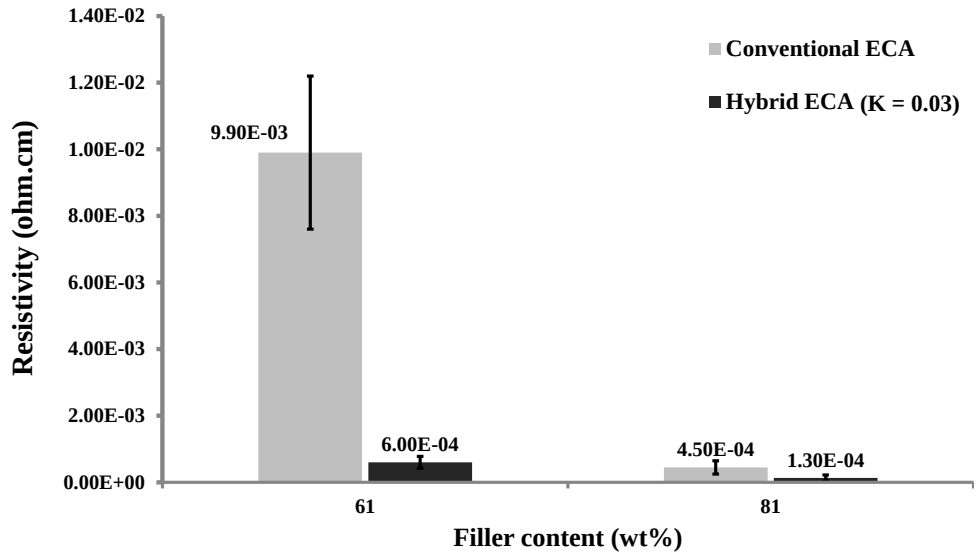

Figure 4-5. The comparison between the electrical resistivity of conventional and hybrid ECAs at different filler concentrations of 61 and 81 wt%.

To obtain more insights into the observed electrical conductivity improvement of the hybrid filler system, the total number of filler particles in a hybrid ECA is compared with that in the conventional ECA. Considering the NBs as a rectangular cubic with dimension of 5μm × 200 nm × 20 nm (length × width × thickness), and the flakes as a circular disc with radius of 5 μm and thickness of 500 nm, the number of Ag NBs and silver flakes per gram is about 5×10^{12} and 6×10^{8}, respectively. Thus, it can be stated that by adding similar amounts of NBs and silver flakes, number of NBs in the composite is almost four orders of magnitude larger

than that of silver flakes. Because of the smaller size of the NBs, they can readily fill in the interstitial space among the micro flakes to have a better filler distribution at small (submicron) length scales.

As mentioned in previous chapters, the overall resistance of an electrical network comes from the bulk resistance of fillers and the contact resistance between neighboring fillers as illustrated in Figure 4-6A1. The filler-filler contact resistance itself is composed of two distinct parameters: constriction resistance and tunneling resistance. In the ECA systems, the NBs can bridge the separated Ag flakes, helping the development of more electrical paths in the hybrid ECA and as a result, having lower tunnelling resistance in the case of hybrid ECA. On the other hand, a large amount of NBs may increase the number of contact points and subsequently increase the constriction resistance among the fillers, which can be detrimental to the quality of filler network. This is evidenced by the fact that increased ratio of NBs to micro flakes or the *K* values in Figure 4-4 did not improve the conductivity. Thus, the addition of an excessive amount of NBs should be avoided.

SEM analysis was performed to verify the bridging of the NBs between Ag flakes. Figures 4.6A1 and 4.6A2 show the typical SEM images of the cross-sections of both the conventional and hybrid ECAs with the same (i.e., 61 wt%) filler concentration, respectively. As can be observed in Figure 4.6A1, many silver flakes in the conventional ECA are separated by epoxy; thus, the electrical network has not been completely established. In contrast, Figure 4.6A2 shows that in the case of the hybrid ECA, NBs bridged those separate silver flakes and

made them connected (as pointed by the white arrow). It also shows that the NBs are evenly distributed throughout the epoxy; no noticeable aggregation can be observed. This observation evidenced the effectiveness of the dispersion method employed in the preparation of the hybrid filler system, which led to homogeneous dispersion of the NBs throughout the nanocomposite. The inserted image of Figure 4.6A2 is a higher magnification SEM image of the Ag NBs in the nanocomposite. It can be seen that the structure of the NBs was preserved during the nanocomposite preparation.

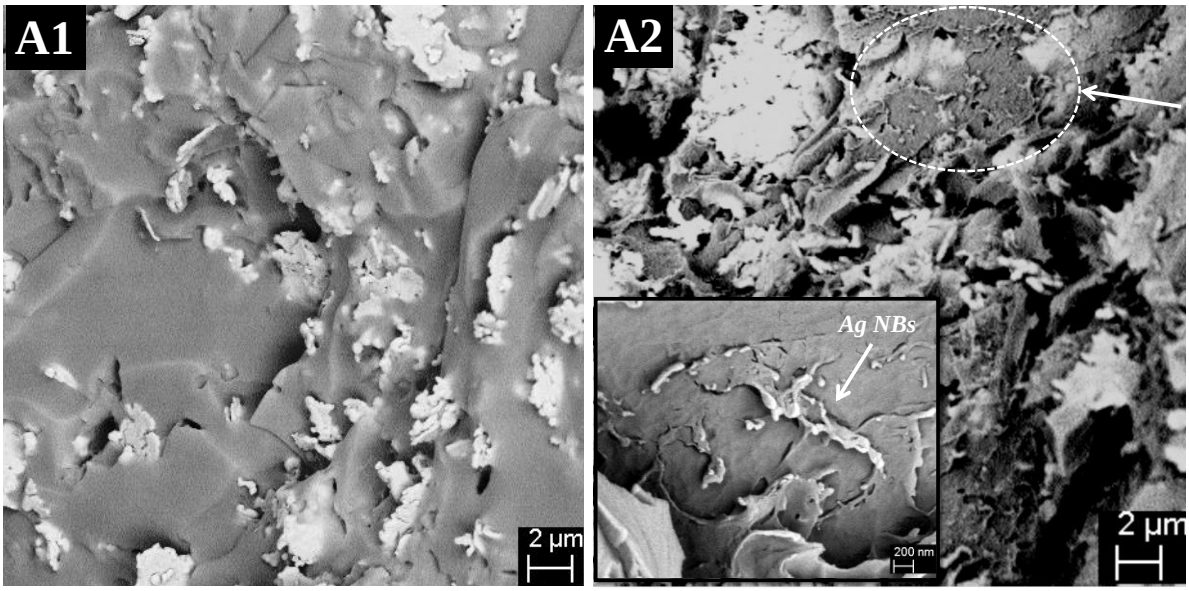

Figure 4-6. SEM images of the cross-sections of (A1) the conventional ECA; (A2) the hybrid ECA filled with the same amount of silver fillers (61 wt%). The inserted image is a high magnification SEM image of Ag NBs.

The surface properties of the hybrid ECAs might be another reason for the electrical conductivity improvement of the ECAs. They were investigated by performing water contact angle tests and roughness measurements. As can be observed in Figure 4-7A1 and 4-7B1,

adding 2 wt% Ag NBs to the conventional ECAs with 60 wt% Ag flakes (total silver content of 61 wt%) decreased the water contact angle from 105° ± 5.2° for the conventional ECA to 64° ± 7° for the hybrid ECA. The water contact angle measurements were also performed for other hybrid samples (with 62-64 wt% of silver), while pretty much similar results (ranging from 65° to 77°) were obtained. Given that the water contact angle can be significantly affected by the topographical structure of the surface (i.e., roughness), the average surface roughness (R_a) of the conventional and hybrid ECAs were measured by Veeco optical profilometer. The typical surface profiles of both samples (having R_a of 593 ± 61 nm and 516 ± 130 nm, respectively) are presented in Figures 4-7A2 and 4-7B2. The surface profile of the both samples is almost similar, demonstrating that the effect of surface roughness on the measured water contact angles is negligible.

The water contact angle on pure epoxy was measured to be 80° ± 5°. The water contact angle on the Ag flakes cannot be determined because of their discrete nature. In the literature, pure Ag has been reported to have a low contact angle close to 0° [149], while Ag covered with the common surfactant stearic acid has a water contact angle about 160° [150]. Recalling the effective contact angle of the conventional ECA as 105° ± 5.2°, it is obvious that the surface of the conventional ECA consisted of both epoxy and silver flake. However, the addition of Ag NBs with the low water contact angle of 0° to 49° [149,151] (depending on whether the PMAA was fully or partially decomposed from the NBs surface) to the conventional ECA led to a significant decrease in the water contact angle for the hybrid ECA (i.e., from 105° ± 5.2° for the conventional ECA to 64° ± 7° for the hybrid ECA). Considering the small

amount of Ag NBs added, it can be stated that NBs have significantly enriched the surface composition, leading to improved electrical conductivity of hybrid ECAs.

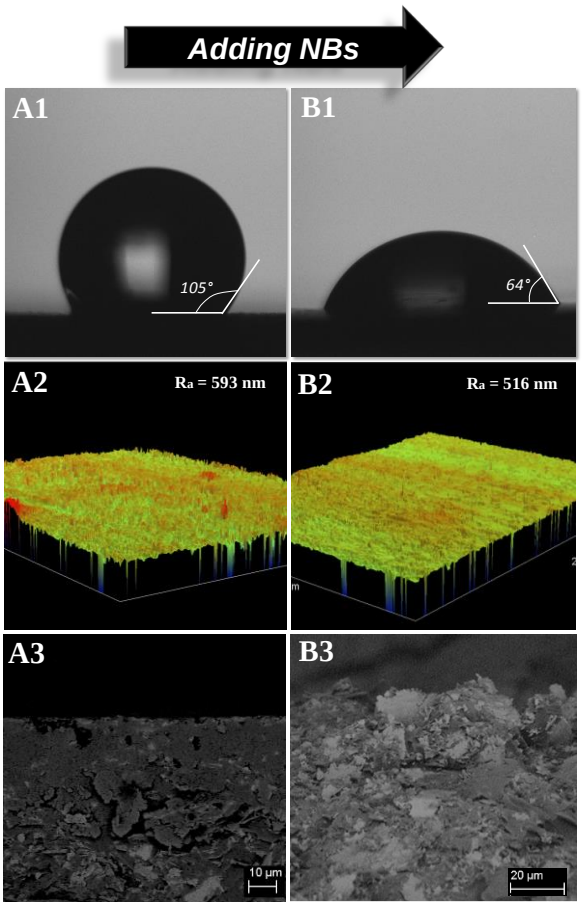

Figure 4-7. The water contact angles for (A1) a conventional ECA - sample 2 and (B1) a hybrid ECA- sample 7. Surface topography maps for (A2) the conventional ECA and (B2) the hybrid ECA. SEM images of the cross-sections of ECA showing the near surface composition for (A3) the conventional ECA and (B3) the hybrid ECA at a 90 degree view angle.

SEM morphological analyses were further performed on the cross-sections of the conventional ECA as well as that of the hybrid ECA (61 wt% silver) to evaluate filler distribution (shown in Figure 4-7A3 and 4-7B3, respectively). To avoid possible distortion of

filler distribution during the preparation of cross-sections, the ECA samples were frozen in liquid nitrogen and gently broken into two parts while in the liquid nitrogen bath. It can be observed in Figure 4-7A3 that the surface of the conventional ECA was partially covered by silver flakes. In contrast, in the case of the hybrid ECA (see Figure 4-7B3), the silver fillers (including both Ag flakes and NBs) are the dominant component occupying the near surface matrix of the composite. Although further surface analyses are needed to fully quantify the surface filler compositions the SEM images and the water contact angle analyses suggested that the introduction of the Ag NBs to the system may have enhanced the fraction of conductive fillers at the surface, even though the total amount of silver fillers is still similar to that of the conventional ECA. This enrichment of silver fillers in the hybrid ECA can also explain the better electrical conductivity of the hybrid ECA in comparison to that of the conventional ones.

4.4 Summary

High aspect-ratio Ag NBs were synthesized and utilized to develop a nano and micro hybrid filler system for the epoxy-based conductive adhesive composites. The synthesis of the Ag NBs is based on a chemical reduction of silver nitride in the presence of PMAA. It involves an innovative process of the self-assembling and room-temperature joining of hexagonal and triangular structural blocks formed at the initial stages of the synthesis to fabricate high aspect-ratio NBs. The DSC and TGA analyzed showed that only a small amount of PMAA physically adsorbed on the NBs surface, while the attached polymer can be detached from

the surface at 150 °C. The high aspect-ratio NBs were successfully incorporated to the system of conventional ECAs, consisting of silver flakes and epoxy, to make hybrid ECAs of superior electrical properties. It was found that the hybrid ECAs always displayed lower electrical resistivity than the conventional ECAs. In particular, the introduction of a small amount of the Ag NBs (weight ratio of the NBs to flakes $K = 0.03$) into a conventional ECA with 60 wt% micron-sized silver flakes resulted in an electrical conductivity enhancement by 1550% in comparison to that of the conventional ECAs with the same total silver weight fraction (61 wt%). The conductivity enhancement comes from the bridging of Ag NBs among the silver micro flakes. The addition of a larger amount of Ag NBs did not improve the conductivity further because it increased the number of contact points and subsequently the contact resistance among the fillers, which might cancel out the positive effect of bridging on the quality of filler network. Other than the bridging effect of Ag NBs in the hybrid ECAs, the SEM and the water contact angle analyses suggested that the introduction of the Ag NBs to the system may have enhanced the fraction of conductive fillers at the surface, even though the total amount of silver fillers is still similar to that of the conventional ECA. This might be another reason for the electrical conductivity improvement of the ECAs. Moreover, it was found that adding a 2 wt % ($K = 0.03$) of the NBs into a conventional ECA with 80 wt% Ag flakes improved the electrical conductivity of ECAs by 240%, implying the importance of the NBs in improving the electrical conductivity of ECAs at concentrations close to the percolation threshold, where the electrical network is not fully formed and silver flakes are not in the complete contact with one another.

Chapter 5. Electrically Conductive Adhesives Using Ag NP-decorated graphene: The Effect of NPs Sintering on the Electrical Conductivity Improvement

5.1 Introduction

In Chapters 3 and 4 we explained electrical conductivity improvement of conventional ECAs by implementing hybrid filler system (using spherical Ag NPs and high aspect-ratio Ag NBs). We showed that spherical Ag NPs can be melted at temperatures far less than their bulk melting point (due to the depressed melting point effect) and provide metallurgical connection between silver flakes. One dimensional (1-D) silver nanostructures (e.g., NWs, NBs, etc.) were found to be more effective than spherical NPs at enhancing the electrical conductivity of ECAs. The 1-D nanostructures can provide more electrical pathways inside ECAs and establish a percolated network at lower filler contents while still taking advantage of the depressed melting point effect due to their nano size.

Since the discovery of graphene nanosheets, they have drawn an intensive attention towards a variety of research fields to utilize their exceptional thermal, mechanical, optical and electrical properties. These nanosheets are flat monolayers of carbon atoms, 0.335 nm thick, densely packed into a honeycomb 2-D lattice structure [52,53,61]. Possessing the largest aspect-ratio among all the nano-structured materials and also having 2-D structure, graphene nanosheets are promising nanomaterials, able to establish a percolated network at very low

concentrations. Luan et al., demonstrated the significant potential of graphene to reduce the percolation threshold of ECA by decreasing the tunnelling resistance in the electrical network [54]. However, one challenge with the use of graphene is its aggregation during mixing with polymers, as graphene nanosheets tends to attract one another with strong van der Waals forces [55,56]. In order to harness the characteristic properties of graphene, its unique single layer structure must be preserved during nanocomposite fabrication [57]. Pasricha et al., reported that the decoration of graphene with Ag NPs is an effective way to exfoliate graphene nanosheets, and to prevent their aggregation [58]. Apart from the aggregation problem, the quality of filler-filler contact is another important issue [23,58]. Oh et al., reported a significant contact resistance reduction when they decorated carbon nanotubes (CNTs) with glutaric acid-functionalized Ag NPs [23]. Considering the higher aspect-ratio of graphene than CNTs [59], the Ag NP-decorated graphene should be more promising nanofiller to improve the electrical conductivity of conventional ECAs as Peng et al, recently reported the electrical conductivity improvement of ECAs via addition of Ag NP-decorated graphene to the conventional ECAs [60]. If sintering of Ag NPs on the graphene surface occurs, it can significantly decrease the contact resistance between neighboring fillers via the formation of metallurgical contacts between silver flakes and graphene nanosheets. It should be noted that the organic layer over the surface of the Ag NPs has an important impact on their sintering behavior [21,101]. The smaller amount of organic material and the shorter organic chain length help the sintering at lower temperature, as well as electron transfer inside the network [20–22,34]. Recently, Liu's research group developed new *in situ* approaches to decorate the graphene surface with Ag NPs for ECAs application [113,114]. In

their method, the formation of Ag NPs on graphene surface occurs during the curing process of epoxy, making the NPs size very sensitive to curing temperature. Although *in situ* approaches eliminate the use of organic layer over NPs surface, it makes it difficult to keep the NPs size constant as the curing temperature changes. Furthermore, at temperatures less than NPs formation temperature, there would be no Ag NPs inside the nanocomposites, thereby limiting the applications of the ECAs to those operating at temperatures higher than NPs formation temperature.

In this chapter, we report a simple wet chemistry approach to decorate the graphene surface with Ag NPs for ECAs applications and carried out a systematic investigation on the effect of NPs sintering on the electrical conductivity improvement of hybrid ECAs. The NPs were functionalized with MPA to control their size and to prevent their oxidation. The small size of the NPs covered by very short chain length organic layer (MPA with 3 carbon atoms chain length) makes the NPs dispersible in organic solvent and possible to sinter at low temperatures. By decorating the graphene surface with small size MPA-functionalized Ag NPs and introducing them into epoxy/silver composite, we can provide metallurgical connection between neighboring fillers at low temperatures and also increase the surface area for electron transportation inside the electrical network. The electrical conductivity of the hybrid ECAs were measured at different curing temperatures and compared to those of conventional ECAs and hybrid ECAs with non-modified graphene. The mechanism of electrical conductivity improvement was discussed according to the quality of filler-filler interaction at different temperatures. The sintering behavior of conductive fillers was

investigated using morphological, electrical, and thermal studies. A highly conductive hybrid ECA was prepared by introducing a small amount of Ag NP-decorated graphene nanosheets (1 wt%) to the conventional formulation of ECAs. The resultant hybrid ECAs were found to have a bulk resistivity of 4.6×10^{-5} Ω.cm which is close to that of lead-based solders [14].

5.2 Experimental

5.2.1 The decoration of graphene with MPA-functionalized Ag NPs

Graphene oxide (GrO) was first prepared before the deposition of Ag NPs. For this, 50 mg of graphene nanosheets (ACS material, USA) with an average size of 1 μm was dispersed into a solution (100 ml) of sulfuric and nitric acids (3:1 volume ratio) and stirred at 70 °C for 20 min. The solution was then filtered using a polycarbonate (PC) membrane (with a pore size of 100 nm) and washed several times with de-ionized (DI) water until the pH became neutral. The filtrate was dried in a vacuum oven overnight.

The deposition of Ag NPs on the surface of graphene oxide nanosheets is based on the direct reduction of Ag ions (adsorbed on the surface of graphene oxide) using a strong reducing agent ($NaBH_4$) in the presence of MPA. First, 20 mg of GrO was dispersed in 50 ml DI water using a bath sonicator for 30 min. Second, a solution of 170 mg $AgNO_3$ (≥ 99 wt%, Sigma-Aldrich) in THF and DI water (5:1 volume ratio) was added to GrO solution and stirred for 1 hr. Third, a solution of 0.4 ml MPA (≥ 99 wt%, Sigma-Aldrich) in 20 ml THF

was added to the mixture in a drop wise fashion. Finally, 10 ml aqueous solution of $NaBH_4$ (≥ 99 wt%, Sigma-Aldrich) was added to the mixture, leading to an abrupt precipitation of a dark solid. To remove the un-attached Ag NPs from system, the mixture was filtered using a PC membrane (with a pore size of 400 nm) and continuously washed with DI water.

5.2.2 Preparation of conductive filler "thin-films"

To prepare a "thin-film" of silver flakes and Ag NP-decorated graphene for "thin-film" conductivity measurements, the decorated graphene was dispersed into 5 ml of ethanol using a bath sonicator for 30 min. 100 mg of silver flakes (Aldrich, 10 μm) was then added; and, the solution was sonicated for a further 30 min. The solution was then deposited on a glass slide and heated at different temperatures for 1 hr to evaporate the solvent. The same procedure was performed to prepare pure silver flake "thin-film" as well as silver flakes and non-modified graphene "thin-film".

5.2.3 ECA nanocomposite preparation

The Ag NP-decorated graphene along with silver flakes were added to epoxy (diglycidyl ether of bisphenol A, DERTM 322, DOW chemical company, USA). To ensure a good dispersion of the decorated graphene in the viscous epoxy, the decorated graphene was first dispersed into ethanol for 30 min using a bath sonicator. Ag flakes and epoxy were then

added to the decorated graphene dispersion; the mixture was further mixed using a vortex mixer for 20 min followed by ultrasonication for 1 hr. The mixture was then degassed under vacuum for 1.5 hr to remove the solvent from the system. After degassing, the curing agent, triethylenetetramine (TETA, DOW chemical company, USA), was added to the mixture. The weight ratio of the curing agent to epoxy was 0.13. The final mixture was filled into a mold of 7 × 7 × 0.5 mm^3 (L × W × D) made on a pre-cleaned microscope glass slide using pieces of adhesive tape. To fabricate a smooth surface and control the sample thickness, a clean copper plate was placed on top of the mold; the extra material was squeezed out. The samples were pre-cured for 30 min at 60 °C and then post cured at different curing temperatures (i.e., 150 °C, 190 °C, and 220 °C) for 2 hr. After curing, the copper plate and adhesive tape were peeled off. Similar mixing and curing procedures were applied to prepare hybrid ECAs with non-modified graphene and conventional ECAs except that for conventional ECA there was no graphene in the system. It should be noted that in hybrid ECAs, the weight fraction of both modified and non-modified graphene was kept at 1 wt%.

5.2.4 Characterization

Fourier transform infrared spectroscopy (FTIR) (Tensor 27, Bruker Co.) was performed to verify the functionalization of Ag NPs on the surface of graphene nanosheets. A high resolution transmission electron microscope (HRTEM, JEOL 2010 F FEG), operated at 200 kV and equipped with Gatan ultra scan imaging filter, was used to characterize the size of Ag NPs on graphene surface. The morphologies of the decorated graphene and conductive “thin-

films" were examined by scanning electron microscope (SEM, LEO FE-SEM 1530, Carl Zeiss NTS) operated at 10 kV. Ultraviolet-visible spectroscopy (UV-vis) (UV-2501 pc, Shimadzu) was performed to confirm both the synthesis and the quality of size distribution of the synthesized Ag NPs on the graphene surface. X-ray diffraction (XRD) patterns of the decorated graphene were collected on a D8 Discover Bruker instrument equipped with Cu-Kα radiation. To collect the XRD patterns, samples were deposited on a glass sample holder. The weight-loss of Ag NPs and the decorated graphene were studied using thermogravimetric analysis (TGA, TA instrument, Q500-1254). A sample of approximately 3 mg was placed into the TGA sample pan, and a dynamic scan was performed from 40 °C to 800 °C with a heating rate of 10 °C/min under a 50 mL/min nitrogen purge atmosphere. The sheet resistance of samples was measured using a four-point probe setup consisting of a probe fixture (Cascade microtech Inc.) and a source meter (Keithley 2440 5A Source Meter, Keithley Instruments Inc.). The sheet resistance was converted to the bulk resistivity according to:

$$\rho = F.t\frac{\pi}{ln2}\left(\frac{V}{I}\right) \qquad \textbf{Equation 5.1}$$

where *t* is samples thickness, *I* is the applied current, and *V* is the voltage drop measured by the source meter. In equation 1, *F* is a correction factor for a finite sample with finite thickness. *F* is a function of the ratio of sample thickness (*t*) to probe spacing (*s*). For $0.4 < \frac{t}{s} < 1$, *F* is close to 1. In our system, in which the samples thickness is 0.5 mm and the probe spacing is 1 mm, *F* can be safely considered as 1.

5.3 Results and discussion

5.3.1 Ag NP decoration of graphene nanosheets

The schematic mechanism of Ag NP decoration of graphene is illustrated in Figure 5.1. In order to decorate graphene with Ag NP, the graphene nanosheets were first oxidized to generate polar functional groups (hydroxyl and carboxylic groups) on their surface (shown in Figure 5-1A) using a typical acid treatment process with a mixture of sulfuric and nitric acids (3:1 volume ratio).

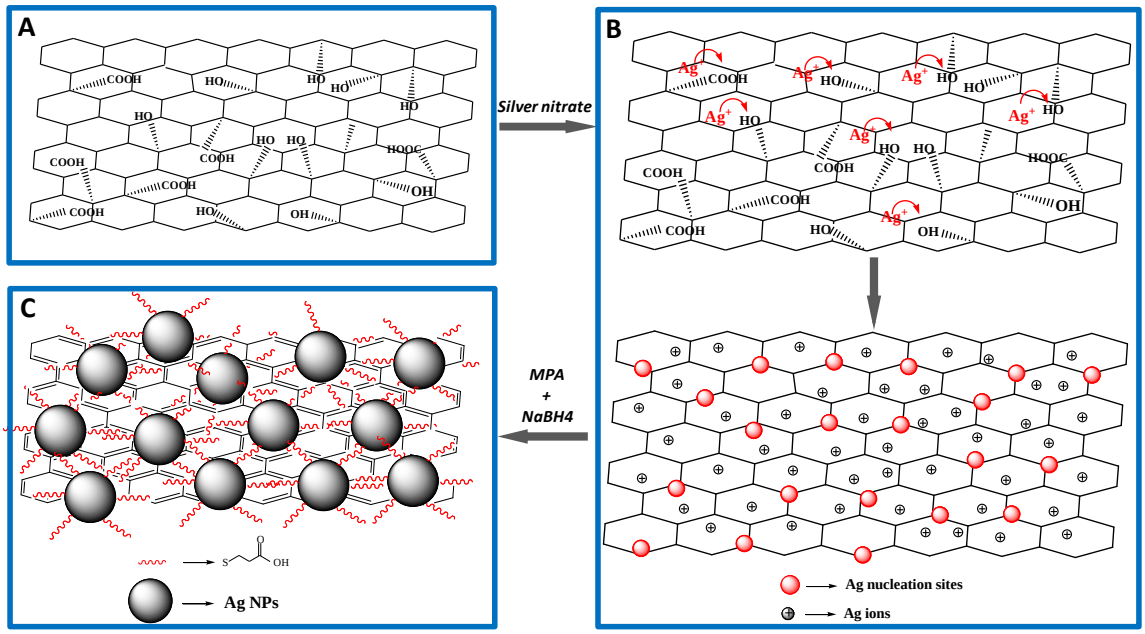

Figure 5-1. A schematic of silver decoration over the surface of graphene; A) GrO with oxygen functionalities; B) adsorption of Ag ions on the oxygen functionalities of the graphene surface to form nucleation sites for Ag NPs; C) graphene decorated with MPA-functionalized Ag NPs.

The resultant GrO was dispersible in water, which is needed for further surface modification, as the synthesis of Ag NPs on the graphene surface is performed in an aqueous medium. Comparing the FTIR spectra of the non-modified graphene and GrO (Figure 5-2A) confirms the presence of polar functional groups on acid-treated graphene surface. The peak at 1704 cm^{-1} is attributed to the C=O carbonyl stretching vibrations of carboxylic groups, while this peak is damped before acid treatment [152]. The strong and broad peak around 3400 cm^{-1} is assigned to O-H stretching vibrations due to hydroxyl groups of GrO [58]. In addition, the peaks at 1617 cm^{-1}, and 1228 cm^{-1} in the GrO spectrum are attributed to the C=C stretching and C-OH stretching bands, respectively [153]. Similar peaks with a slight shift are observed in the spectrum of the non-modified graphene. The FTIR results confirm that the graphene is successfully functionalized with hydroxyl and carboxylic groups through the acid treatment process. The functionalization can be further verified by comparing the dispersion qualities of graphene in polar solvents, i.e., ethanol and water, before and after acid treatment. Graphene before the treatment was not dispersible in ethanol and water while the GrO was dispersible and stable in both solutions for more than 8 hours (see Figure 5-2B).

Ag NPs were synthesized on GrO surface through a two-step process as illustrated in Scheme 1B and C. In the first step, GrO and $AgNO_3$ aqueous solutions were stirred together for 1 hr to provide initial active nucleation sites on the surface of graphene. The carboxylic groups, uniformly distributed on the graphene surface [154], form a complex with the Ag ions and attach them to the surface of graphene [58]. The reduction of Ag ions on GrO surface has been reported in recent literature [58,152,154].

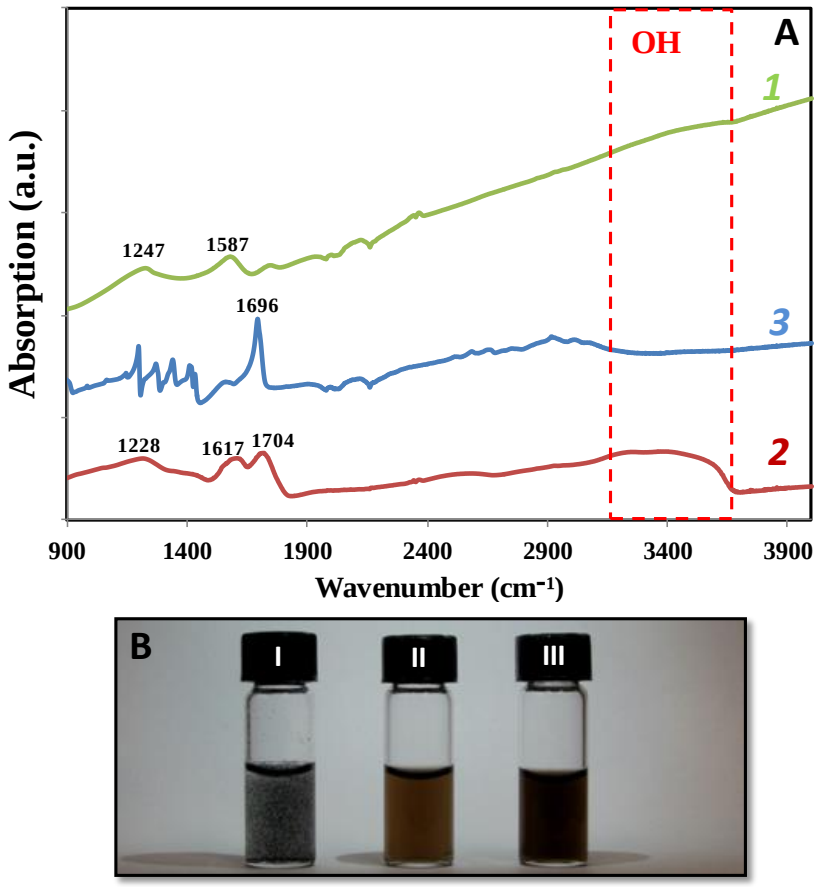

Figure 5-2. A) The infrared spectrum of non-modified graphene (curve 1), GrO (curve 2) and Ag NP-decorated graphene (curve 3); B) digital images of the dispersion of I) non-modified graphene, II) GrO, and III) Ag NP-decorated graphene in ethanol.

Figure 5-3A shows a representative SEM image of graphene oxide nanosheets before decoration. Figure 5-3B shows the Ag NPs, formed in the first step, on the graphene surface. As can be observed in this figure, very small NPs are homogeneously distributed on the graphene surface which is related to the uniform distribution of oxygen functionalities over GrO surface. As observed in Figure 5.3C, there is no agglomeration of Ag NPs on the surface

of graphene. The size of individual NPs, formed in this step, is less than 5 nm. Figure 5-3D shows the EDX spectrum of the elemental state of Ag NPs on graphene surface (i.e., first step of Ag NP decoration of graphene). A relatively strong peak for Ag (indicated by the black arrow) in this spectrum along with the peaks of carbon and oxygen confirms the formation of Ag NPs in this stage. The presence of the oxygen peak implies oxygen functionalities still exist on the graphene surface.

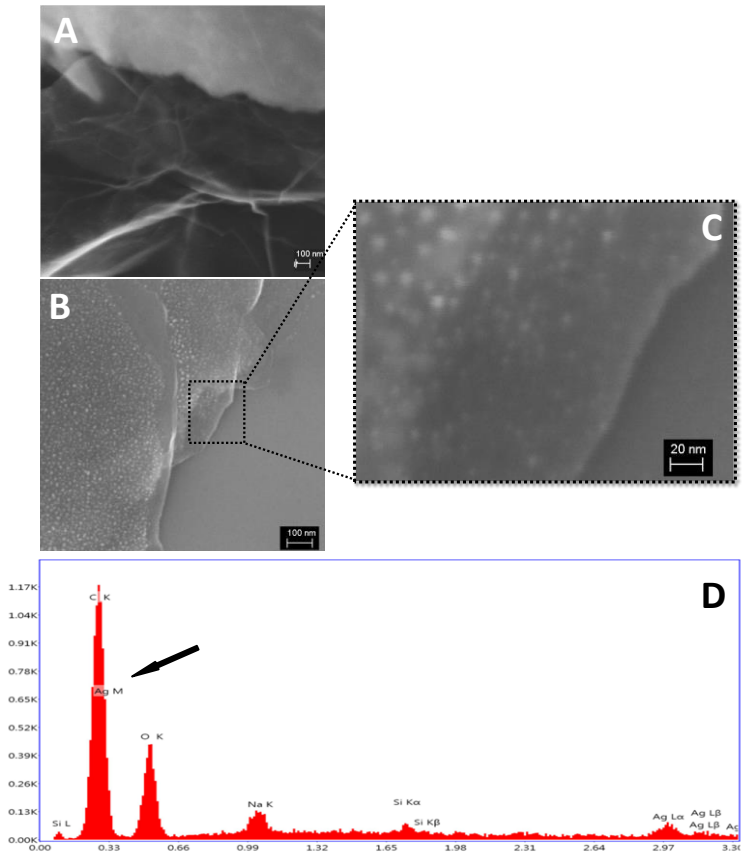

Figure 5-3. A) A representative SEM image of GrO before decoration B) A representative SEM image of silver nucleation on the graphene surface; C) a magnified image of the selected area of Figure B; D) EDX diagram of the elemental state of Ag NPs on the surface of graphene (the black arrow indicates the relatively a strong peak for Ag).

The second step of Ag NP decoration of graphene is based on direct reduction of the remaining Ag ions by $NaBH_4$ in the presence of MPA as a capping agent. MPA chains, with a sulfur group at one end and a carboxylic group at the other, form micellar structures at the nucleation sites in THF/water medium and trap the remaining Ag ions [20]. When MPA was added to the solution of GrO and $AgNO_3$, the initial dark solution became greyish along with the formation of small clusters in the solution. In Chapter 3, we explained that the color change is associated with the formation of Ag-S bands [20,130]. Upon the addition of $NaBH_4$, all the ions are reduced to Ag° and form Ag NPs covered by MPA on the graphene surface. The role of MPA is to control the size and shape of NPs and to prevent them from oxidation [20]. As shown in Figure 5-2A, the strong and sharp peak at 1696 cm^{-1} in the FTIR spectrum of the Ag NP-decorated graphene is attributed to the carbonyl stretching frequency resulting from the semiquinone moieties on Ag NPs surface [58]. The MPA on Ag NPs surface makes the decorated graphene dispersible in polar solvents (i.e., ethanol and water); Figure 5-2B (sample 3) shows a stable dispersion of the Ag NP-decorated graphene in ethanol. The same quality of stability was observed for the decorated graphene in water.

Apart from reducing Ag ions, $NaBH_4$ plays an important role in restoring the conjugated sp^2 network. Some research groups reported the contribution of $NaBH_4$ in reducing GrO to graphene and increasing its conductivity [65,155]. The diminished spectra of Figure 5-2A at 3400 cm^{-1} for Ag NP-decorated graphene implies there is no oxygen moiety on the surface of graphene after the completion of the decoration of graphene, which in turn confirms the restoration of π-π carbon bonds after the decoration of the graphene surface.

UV-vis spectroscopy was performed to confirm the synthesis of the individual Ag NPs on the graphene surface. It is well known that Ag NPs larger than 2 nm show a strong and broad peak in the UV-visible range (390 to 460 nm) due to the excitation of surface plasmon bonds (SPB) [132]. The position and symmetrical feature of this peak give useful information about both the size and size distribution of the NPs. Figure 5-4A shows the UV-vis spectra of GrO, Ag NP-decorated graphene, and the individual Ag NPs fabricated with a similar procedure (as described in Chapter 3) [20]. The UV-vis spectrum of GrO shows a peak around 223 nm corresponding to $\pi \rightarrow \pi^*$ transitions of aromatic C-C bonds [153]. For the Ag NP-decorated graphene, the presence of the characteristic peak at 394 nm clearly indicates the formation of Ag NPs on the graphene surface. The symmetry of this peak implies a homogeneous size distribution of the NPs. Compared to the spectrum of the individual Ag NPs, the spectrum of the Ag NP-decorated graphene shows a shoulder at 270 nm which is attributed to graphene aromatic C-C bonds. The presence of this peak further confirms the decoration of graphene with Ag NPs. The XRD pattern of the Ag NP-decorated graphene is shown in Figure 5-4B. The dominant peaks are observed at 38.2°, 44.3°, 64.6°, and 77.6° with corresponding to 2θ values. According to JCPDS card No. 07-0783, these peaks correspond to the (1 1 1), (2 0 0), (2 2 0) and (3 1 1) crystallographic planes of face center cubic (*fcc*) of the Ag NPs. The highest diffraction intensity is found for the peak at 38.2°, which indicates that the surface of Ag NPs is preliminary (1 1 1) planes that are considered the most stable crystalline structure [51]. Graphene nanosheets usually show a diffraction peak at 26° which corresponds to the 0.335 nm interlayer spacing of graphite [108]. In the diffraction pattern of GrO, another peak is observed at 13.6°, suggesting possible partial structural damage of graphene after

oxidation. Others have observed similar trends in the shift of the XRD peak to lower angles due to the chemical oxidation of graphene [156,157]. However, this peak has been dampened and shifted to 12.2° indicating the effectiveness of $NaBH_4$ in restoring the conjugated sp^2 bands of graphene aromatic structure.

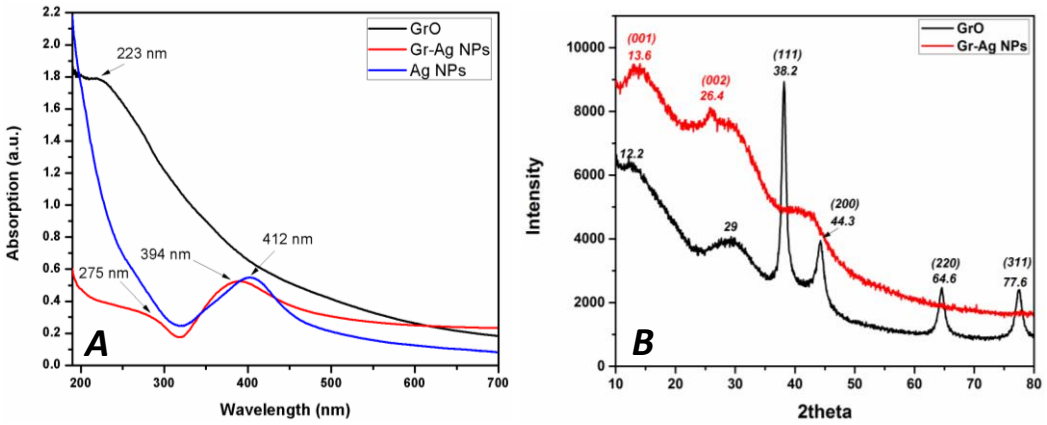

Figure 5-4. A) UV-vis spectra of GrO, individual Ag NPs (synthesized with the same procedure as the Ag NPs on graphene surface), and Ag NP-decorated graphene; B) XRD pattern of GrO and the Ag NP-decorated graphene.

Figure 5-5A shows a representative TEM image of graphene sheets before treatment. A representative TEM image of the Ag NP-decorated graphene can be observed in Figure 5-5B where the black arrow indicates to the graphene edge. As can be seen in this image, spherical Ag NPs with an average size of 9.1 nm ± 3.1 nm formed on the graphene surface along with some small particles (less than 2 nm). The small NPs are those formed in the first step and did not grow further. This image confirms that graphene maintained its smooth and very thin structure. Figure 5-5C displays a SEM image of the Ag NP-decorated graphene showing two

layers of the decorated graphene beside one another. Figure 5-5D shows a HRTEM image of the selected area of Figure 5-5B. The amorphous structure over the surface of the NPs (as indicated by red arrows) clearly shows the surface coverage of Ag NPs by MPA. This image supports the FTIR results.

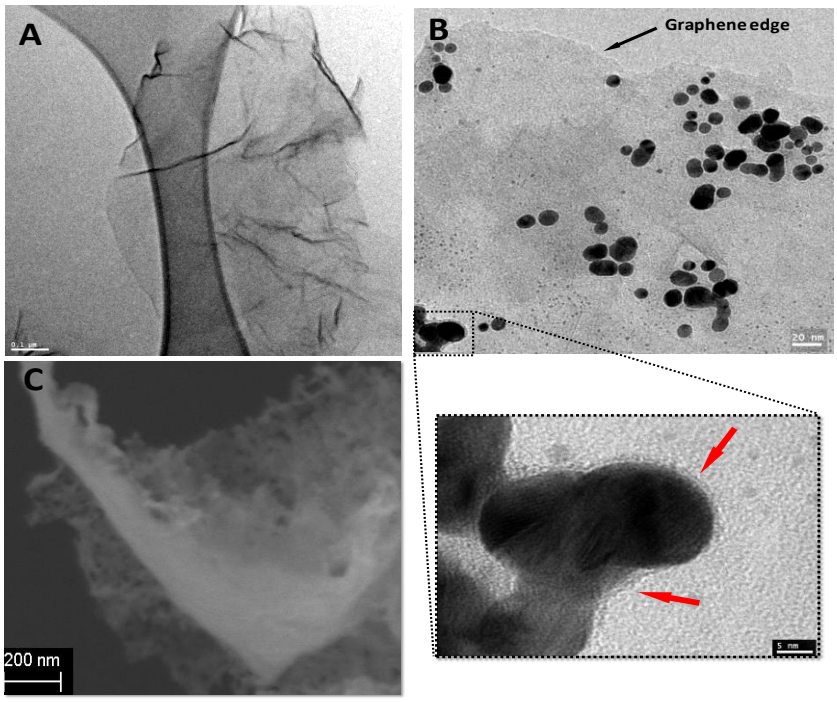

Figure 5-5. A) a representative TEM image of non-modified graphene; B) a representative TEM image of the decorated graphene with MPA-functionalized Ag NP, the edge of graphene single layer are pointed by a black arrow, C) a representative SEM image of the decorated graphene; D) a HRTEM images of the selected area of Figure B, showing the presence of an amorphous structure (pointed by arrows) of MPA on Ag NPs surface.

5.3.2 Electrical conductivity measurements of conductive filler “thin films” and ECA nanocomposites

To investigate the effectiveness of the Ag NP-decorated graphene as a co-filler inside the electrical network, we first performed “thin-film” conductivity studies to examine the inter-filler interaction prior to adding them into epoxy matrix. The electrical resistivity of a “thin-film” of silver flakes and the decorated graphene as a novel hybrid filler system was measured and compared to those of pure silver flakes and silver flakes with non-modified graphene “thin-films” at varied temperatures. In each sample the total amount of silver was constant. The results are shown in Figure 5-6. The electrical resistivity of hybrid filler system with both the decorated graphene (Ag flakes & Gr-Ag NPs) and non-modified graphene (Ag flakes & Gr) were decreased over the pure silver flake films (Ag flakes) for all measured temperatures. Due to its 2-D structure and high aspect-ratio, graphene provides more surface area for electron transport inside the network and displays improved electrical conductivity with the hybrid filler system [54,113].

As can be observed in Figure 5-6, the electrical resistivity of all three film samples decreased as the temperature increased. However, the electrical conductivity improvement for hybrid filler film with the decorated graphene was more significant at higher temperatures than the other two. The increase in the electrical conductivity of both the pure silver flakes film and the hybrid filler films with non-modified graphene at higher temperature can be attributed to the increased packing density of silver flakes that enhanced the connection between

conductive fillers. The significant improvements of the electrical conductivity for the hybrid filler film with the decorated graphene at higher temperatures (i.e., 150 °C and 220 °C) is related to the contribution of the Ag NPs in the system. The presence of small Ag NPs on the graphene surface provides an opportunity to take advantage of the "melting depression effect". At higher temperatures, some Ag NPs began to sinter to each other as well as to the silver flakes. This situation provides metallurgical contacts between silver flakes and graphene which facilitates electron transportation throughout the electrical network.

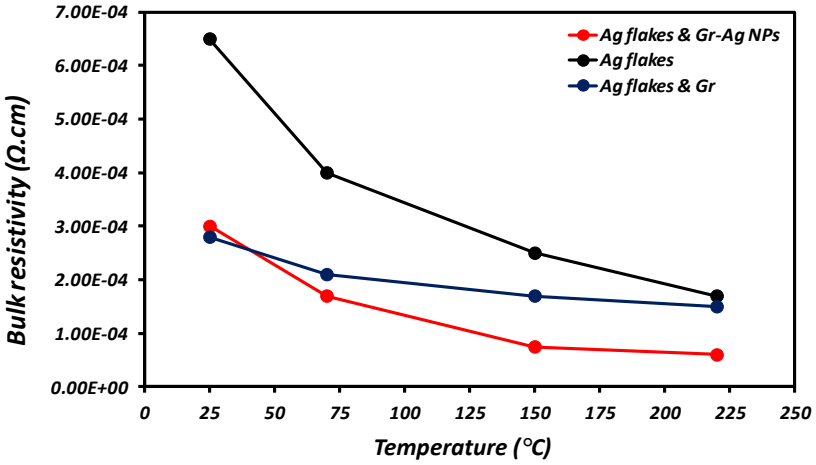

Figure 5-6. The effect of temperature on the electrical conductivity of conductive fillers "thin-films" before their addition into epoxy.

Sintering of Ag NPs is largely affected by the amount of organic layer present on their surface and also by the temperature at which this layer is decomposed from the surface [34]. Thus, the thermal behavior of the Ag NP-decorated graphene was studied using TGA to

evaluate the phase transition of the Ag NPs on the graphene surface. Figure 5-7A shows the TGA results for Ag NP-decorated graphene and Ag NPs synthesized with a similar procedure (As explained in Chapter 3). For the individual Ag NPs, thermal decomposition began at 130 °C. The weight of the NPs decreased by 3 wt% until 285 °C due to the decomposition of un-bonded MPA and/or absorbed water in the system [20]. As the temperature increased, the NPs displayed two main thermal decomposition steps. The first transition occurred between 290 °C and 380 °C, displaying an approximate weight-loss of 8 wt% that may be attributed to the amount of MPA physisorbed on the surface of Ag NPs (as explained in Chapter 3). The second transition with a 10 wt% weight-loss was observed at 385 °C, and continued up to 455 °C. This large weight-loss is attributed to the decomposition of chemisorbed organic materials [139]. Conversely, the thermal decomposition of surface residue for the Ag NP-decorated graphene occurs with a slight transition step, starting from 145 °C and ending at 375 °C, which can be attributed to the thermal decomposition of MPA adsorbed on the surface of the Ag NPs [20]. Comparing the TGA results of the decorated graphene with individual NPs indicates the thermal decomposition of MPA from the NPs surface occurs at lower temperature for the decorated graphene than individual NPs. These results also show a lower amount of MPA (< 3.5% for the Ag NP-decorated graphene compared to 22% for the individual Ag NPs) covering the surface of the Ag NPs on the graphene surface, which helps with occurrence of sintering at lower temperature. TGA results suggest that at temperatures higher than 145 °C, Ag NPs on the surface of graphene started to sinter with each other.

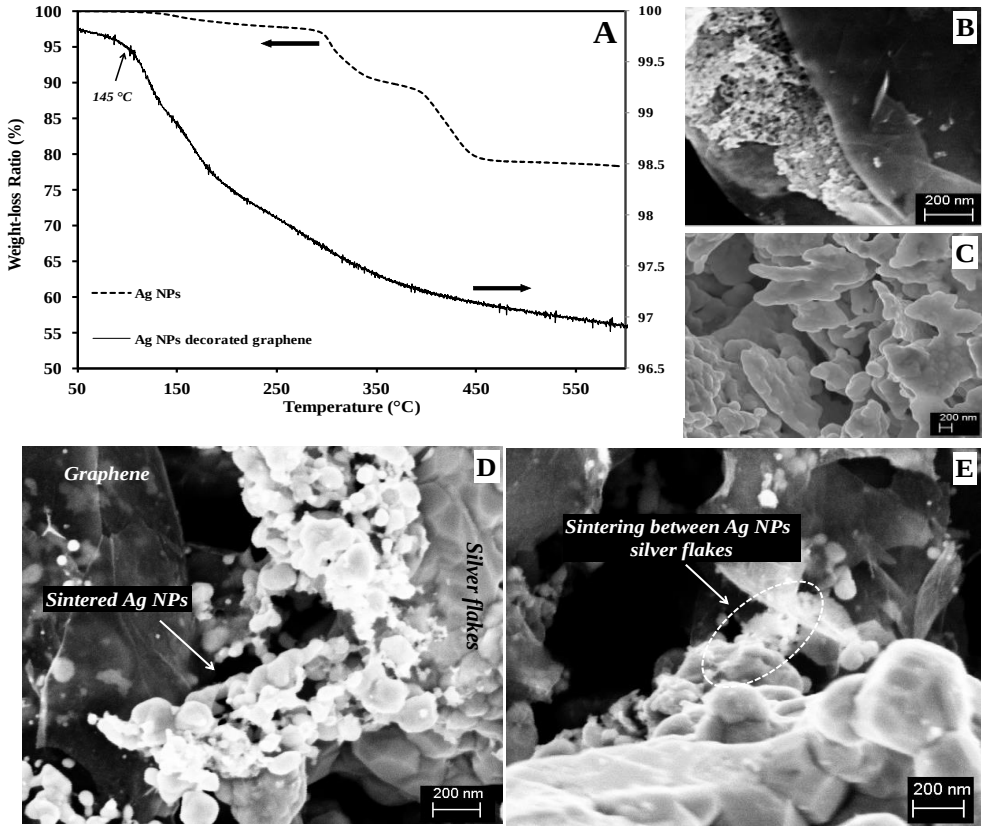

Figure 5-7. A) TGA analysis of the Ag NP-decorated graphene and the individual Ag NPs, synthesized with a similar procedure; B) an SEM image of the "thin-film" of the Ag NP-decorated graphene and silver flakes mixture at room temperature; C) SEM image of silver flakes "thin-film" at 220 °C; D and E) SEM images of the Ag NP-decorated graphene and silver flakes "thin-films" at 150 °C, and 220 °C, respectively, showing the sintering between the Ag NPs and flakes.

The sintering of the NPs on the surface of graphene was further confirmed using SEM. Figures 5-7B shows an SEM image of a "thin-film" of Ag NP-decorated graphene and silver flakes mixture at room temperature. An SEM image of silver flakes "thin-film" at 220 °C is shown in Figure 5-7C. Figures 5-7D and 5-7E show the SEM images of a "thin-film" of Ag

NP-decorated graphene and silver flakes mixture at 150 °C, and 220 °C, respectively. Comparison between the morphologies of the NPs in each case shows that sintering occurred between the NPs for the both samples annealed at 150 °C, and 220 °C where they became whitish due to the removal of the organic layer from the surface [21]. In contrast, the NPs at room temperature did not sinter to each other, and instead had a dark color. Figures 5-7D and 5-7E also indicate the formation of metallurgical connections between the silver flakes and the decorated graphene, which can significantly improve the conductivity of the electrical network.

Hybrid ECAs were fabricated by adding a small amount of the Ag NP-decorated graphene (1 wt%) to the conventional ECAs, consisting of silver micron flakes and epoxy. The decorated graphene was incorporated into conventional ECAs at two different silver contents, i.e., near and after the percolation threshold (60 wt% and 80 wt%, respectively) and the final composites were cured at 150 °C. The bulk resistivity of the hybrid ECAs with the decorated graphene were compared to those of conventional ECAs (epoxy-silver flakes) and hybrid ECAs with non-modified graphene (epoxy-silver flakes-non-modified graphene). Figure 5-8 shows the bulk resistivity of the samples cured at 150 °C. As can be seen in this figure, the resistivity of the hybrid ECAs with both decorated and non-modified graphene are less than that of the conventional ECAs for the both filler concentrations. The bulk resistivity of the hybrid ECA with the decorated graphene at 60 wt% of total silver content is 7.6×10^{-4} Ω.cm, which shows 90 % reduction (equal to 1362 % electrical conductivity improvement) compared to the bulk resistivity of conventional ECA with the same filler content (1.1×10^{-2}

Ω.cm). This resistivity is close to that of the conventional ECA with 80 wt% of silver flakes. Also, the resistivity of the hybrid ECA with the decorated graphene at 80 wt% showed 67 % reduction (equal to 200 % electrical conductivity improvement) compared to that of the conventional ECA with an equivalent silver content, although the final electrical conductivity was not significantly high.

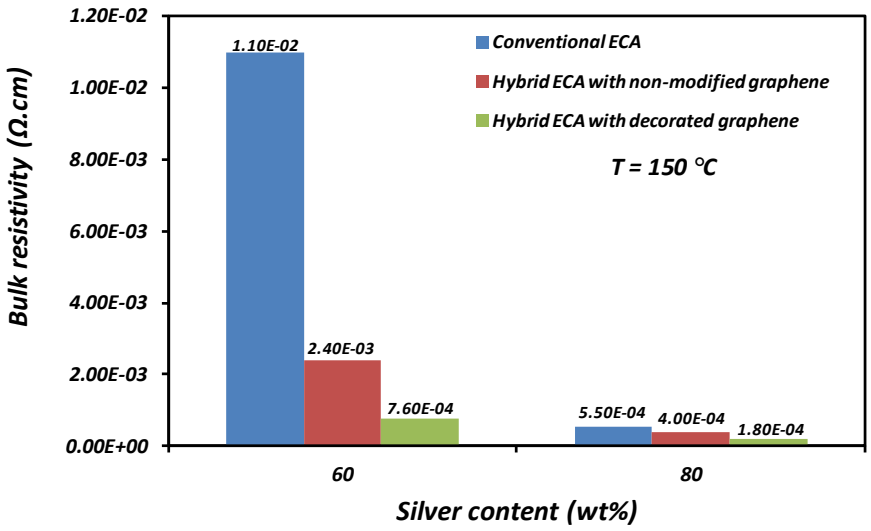

Figure 5-8. The comparison between the electrical conductivity of conventional and hybrid ECAs at different filler concentrations of 60 and 80 wt% (for hybrid ECAs 1 wt% of nanofillers was used).

As electrons are transferred through the electrical pathways created by conductive fillers inside the ECAs, the morphology and quality of contact between fillers are crucial for the electrical conductivity of ECAs. As explained in previous chapters, the quality of contact between conductive fillers is related to the contact resistance which is a combination of

constriction and tunnelling resistances [77]. The reduced electrical resistivity of the hybrid ECAs with both of non-modified and decorated graphene in comparison to that of conventional ECAs suggested that graphene nanosheets provide larger surface area than an equivalent amount of silver flakes for electron transportation within the network, which decreases the tunnelling resistance, significantly. This situation is more pronounced at concentrations close to the percolation where the silver flakes are not fully in contact with each other. However, the increased number of contact points because of the presence of Ag NPs may cancel out the reduced tunnelling resistance.

To shed further light on the effect of Ag NPs on the electrical conductivity of the hybrid ECAs, the samples with 80 wt% of silver flakes were cured at different temperatures. The bulk resistivity data, shown in Figure 5-9, revealed a much more significant resistivity reduction for the hybrid ECAs with the decorated graphene than for conventional ECAs and hybrid ECAs with non-modified graphene as curing temperature increased. A low bulk resistivity of 4.6×10^{-5} Ω.cm was achieved for the hybrid ECAs with the decorated graphene and cured at 220 °C, which is comparable to that of a typical eutectic solder (2×10^{-5} Ω.cm) [14]. It demonstrates a great potential for this hybrid ECA to be used as an alternative electrical interconnect material. These results imply that although the Ag NPs on the surface of graphene improve the electrical conductivity of conventional ECA at low curing temperatures, their influence is more pronounced at higher curing temperatures. The presence of Ag NPs at low temperatures may increase the number of contact points in the filler system which in turn increases the contact resistance [21]. However, when the temperature increases

they start to sinter with each other as well as with the silver flakes so as to provide direct metallurgical contacts between the silver flakes and graphene to form flake-NP-graphene-NP-flake conduction paths inside ECAs. This situation makes electron transport more prevalent through the electrical network and decreases the contact resistance among fillers.

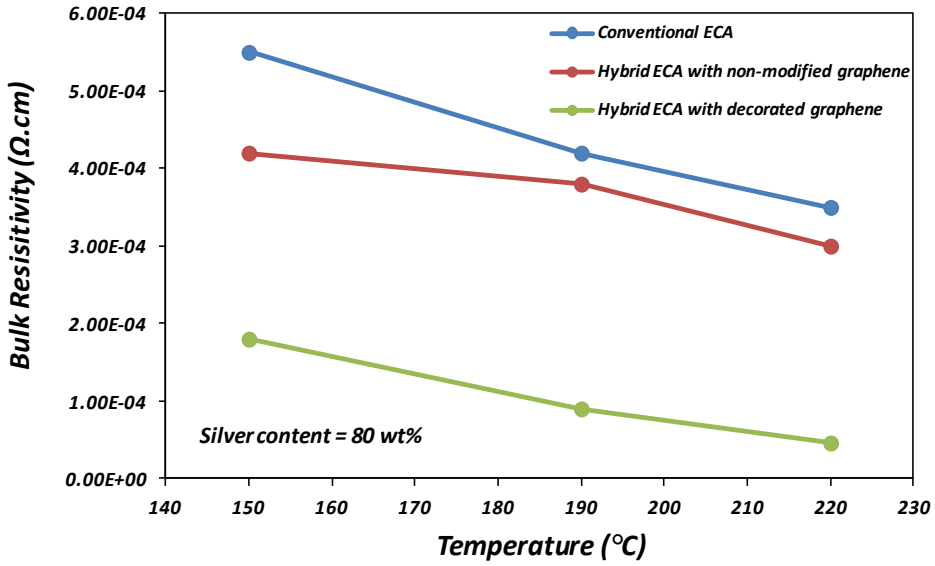

Figure 5-9. The effect of curing temperature on the electrical conductivity of ECAs.

5.4 Summary

In this chapter, we reported a simple novel room temperature wet chemistry approach to decorate graphene nanosheets with MPA-functionalized Ag NPs to be utilized as auxiliary fillers inside ECA nanocomposites and investigated the role of Ag NPs sintering on electrical conductivity of ECAs. The deposition of Ag NPs was based on the direct reduction of Ag

ions, adsorbed on the surface of graphene oxide, using a strong reducing agent ($NaBH_4$) in the presence of MPA; $NaBH_4$ was also found to be able to reduce the graphene oxide back to graphene. FTIR, UV-vis, XRD, and TEM confirmed the decoration of graphene with MPA-functionalized Ag NPs. The surface functionalization of Ag NPs made the decorated graphene dispersible in water and ethanol, and facilitated their dispersion in epoxy nanocomposite. TGA analysis of the decorated graphene showed that the MPA starts to decompose from the NPs surface at temperatures close to 150 °C. SEM images confirmed the sintering of Ag NPs at this temperature which resulted in significant reduction of bulk resistivity of the decorated graphene and silver flakes mixture "thin-film" at temperatures higher than 150 °C. The addition of a small amount of the decorated graphene into the conventional ECA remarkably decreased its bulk resistivity, especially at concentrations near the percolation content. The bulk resistivity of hybrid ECAs with the decorated graphene significantly decreased as the curing temperature increased to 220 °C. A highly conductive ECA with a very low electrical resistivity of 4.6×10^{-5} Ω.cm (close to that of eutectic solders) was achieved by incorporating a small amount of the Ag NP-decorated graphene (1 wt%) into the conventional ECAs (total silver content of 80 wt%). The high electrical conductivity of the fabricated ECA is attributed to the metallurgical connection between graphene and silver flakes inside the electrical network because of the sintering of small Ag NPs on the graphene surface.

Chapter 6. SDS-modification of graphene nanosheets; the effect of size and surface property of graphene on the electrical conductivity of ECAs

6.1 Introduction

As discussed in previous chapters, the key parameter in electrical conductivity improvement of an ECA is the quality of electrical network. The conductive nanofillers, depending on their type and morphology, affect the quality of network through their morphology or the quality of junction between silver flakes. In chapters 4 and 5, we demonstrated that the tunnelling resistance is a dominant parameter at low silver content and can be remarkably reduced by introducing high aspect-ratio nanomaterials [54]. Many research groups, including us, have studied the effects of different high aspect-ratio nanomaterials such as Ag NWs [40,54], Ag NBs [101], and carbon nanotubes (CNTs) [17,42] on the electrical properties of ECAs and reported the establishment of a percolated network at low silver content.

As mentioned in Chapter 5, graphene has attracted great interest as a promising nanofiller for ECAs application because graphene has the highest aspect-ratio among all the nano-structure materials, enabling establishment of a more complete electrical network at lower filler content [52,55,61,158]. Pu et al. used nitrogen-doped graphene inside the system of epoxy and silver powder and reported that the percolation of silver powder reduced to 30 wt% [59]. Their results confirmed that 2-D graphene is much more effective than other types of high aspect-ratio carbon-based fillers such as carbon nanotubes and carbon black. However, the

challenge of attaining a homogeneous dispersion, as well as preserving its single-layer structure acts as bottlenecks in ECA fabrication.

Surface modification of graphene using organic materials is one approach to exfoliate graphene in which the interaction occurs via either covalent bonding or via π-π stacking. Although this technique is shown to be effective to exfoliate graphene layers, it hinders their electrical properties because it disturbs the π-electrons delocalization of graphene surface [56,62,63,111]. The surface decoration of graphene with inorganic nanoparticles (NPs) such as Ag NPs is another approach that can effectively exfoliate graphene nanosheets [58]. Some research groups applied this idea for ECA applications and used the Ag NP-decorated graphene for the formulation of ECAs; they reported a positive effect of Ag NP-decorated graphene on the electrical conductivity of ECAs [60,112,113]. Based on our research finding, presented in Chapter 5, we believe that the improved electrical conductivity of ECAs via addition of Ag NP-decorated graphene is mainly because of the establishment of more electrical pathways inside the electrical network; however, the increased number of contact points (due to the presence of Ag NPs on the graphene surface) may cancel out this positive effect [61]. We showed that to decrease the number of contact points sintering of NPs must occur which requires elevated curing temperatures (higher than 150 °C). We speculate the single layer graphene without metallic decoration is a better option as auxiliary filler for ECA application if a proper exfoliation technique is applied to preserve its single layer structure within the epoxy matrix.

Another method to exfoliate and stabilize graphene nanosheets is based on the use a surfactant. In this approach, graphene layers are exfoliated by the mechanical energy provided by bath or horn sonication which overcomes the van der Waals interactions between graphene layers. At the same time, surfactant molecules are adsorbed onto the graphene surface and prevent their re-stacking via steric repulsions [56,64,65] (see Figure 6-1A). Some research groups implemented this method to produce surfactant-stabilized graphene from graphite powder. For instance, Lotya et al. reported the production of a high-concentration aqueous solution of graphene, stabilized by sodium cholate surfactant, using a long time low power sonication of graphite, followed by centrifugation [64]. In this chapter, we report a simple surfactant-assisted approach to stabilize graphene nanosheets and disperse them inside the conventional formulation of ECAs (consisting of epoxy and silver micro flake) based on the use of an ionic surfactant, sodium dodecyl sulfate (SDS). The main advantage is we are able to preserve the single layer structure of graphene inside the nanocomposite without disturbing its structure. The single layer graphene nanosheets can effectively bridge between separated silver flakes and provide more surface area for electron transportation inside the electrical network (as illustrated in Figure 6.1B). To shed further light on the effect of graphene aspect-ratio we used graphene nanosheets with two different sizes (1 μm, and 5μm diameter) and applied the same SDS modification approach to exfoliate and disperse them inside the conventional ECAs. The electrical resistivities of the hybrid ECAs with small and large SDS-modified graphene were measured at different silver contents and compared to those of conventional and hybrid ECAs with non-modified

graphene. The effect of SDS modification on curing behavior of epoxy and the thermal stability of hybrid composite was also investigated.

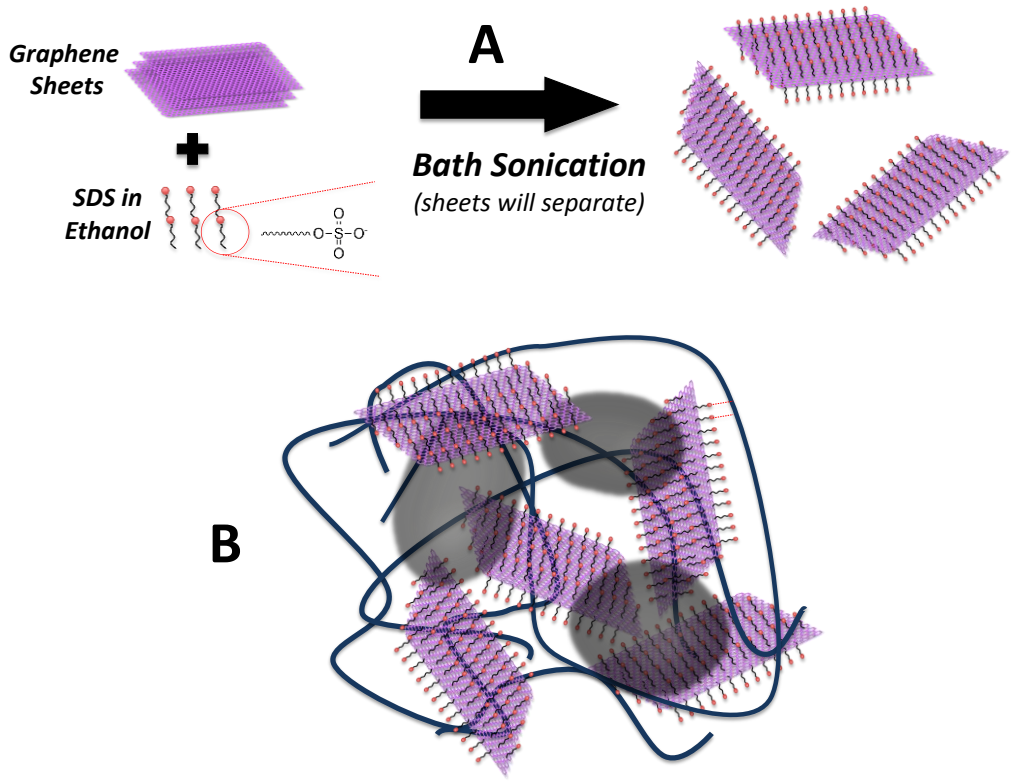

Figure 6-1. A) SDS modification of graphene leads to exfoliation of graphene flakes, B) the bridging of SDS-modified graphene between separated silver flakes establishes a compete electrical network inside epoxy

6.2 Experimental

6.2.1 Synthesis of large graphene

Large size graphene was produced using graphene oxide (GrO) which was synthesized by modified Hummers' method [159,160]. The GrO was prepared from large graphene pellets

with the average size of 1 mm to 5 mm. The reduction of GrO to produce graphene was achieved by pre-heating of GrO in vacuum oven for 6 hours followed by thermal annealing in a furnace protected with Ar at 900 °C for 10 minutes. This process is to ensure the total removal of the oxygen functionality and restoration of the graphitic surface, so that the highest electrical conductivity can be achieved for the resulting large size graphene. Small size graphene was purchased from ACS material (USA).

6.2.2 SDS modification of graphene

In order to modify the graphene surface with SDS, both large and small graphene powders were dispersed into a solution of SDS (Sigma-Aldrich, ≥99.0%) and ethanol. The concentration of SDS in ethanol was 0.06 mol/L. Then the solution was ultrasonicated using a low power sonic bath (Branson 2510R-MT) for 30 min. In order to remove the un-bonded SDS, the graphene dispersion was washed four times by repeatedly dispersing in fresh ethanol and applying centrifugation at 8000 rpm for 10 min to remove the supernatant. The final solution was then filtered using a polycarbonate (PC) membrane (with a pore size of 400 nm) and dried overnight at room temperature in a vacuum oven.

6.2.3 Nanocomposite preparation

Diglycidyl ether of bisphenol A epoxy (DER^{TM} 322) and triethylenetetramine (TETA), supplied by Dow Chemical company (USA), were used as the adhesive base and hardener,

respectively. The weight ratio of hardener to epoxy was 0.13. Two general types of sample (conventional and hybrid ECAs) were prepared as listed in Table 6.1. The conventional ECA contained only silver flakes (Aldrich, 10 mm) and epoxy whereas the hybrid ECAs contained epoxy and a mixture of the graphene (either SDS-modified or non-modified) and silver flakes at different weight percent. To make a hybrid ECA with SDS-modified graphene (either small or large size), silver flakes were mixed with the dispersion of modified graphene in ethanol for 30 min and then epoxy was added to the mixture. The composite was mixed using a vortex mixer for one hour. In order to remove ethanol from the composite, the mixture was placed inside a desiccator and degassed for 30 minutes followed by 5 minutes vortex mixing until ethanol was fairly removed. Then the TETA was added to the mixture and the resultant paste was filled into a mold (7 mm × 7 mm × 0.5 mm) made using a glass slide and pieces of adhesive tape. A clean copper sheet was placed on top of the mold in order to ensure that the thickness of the sample remained constant, as well as to consistently produce a smooth surface. The samples were then pre-cured inside an oven at 60 °C for 30 minutes, and then cured at 150 °C for 2 hours. After curing, the copper plate and the adhesive tape were removed. The schematic of nanocomposite preparation is presented in Figure 6-2. A similar procedure was followed for the preparation of the hybrid ECA with non-modified graphene.

6.2.4 Characterization

Fourier Transform Infrared Spectroscopy (FTIR) (Tensor 27, Bruker Co.) was carried out to confirm the SDS modification of graphene. An X-ray Diffractometer (XRD) (D8 Discover

Bruker) equipped with Cu-Kα radiation was used to characterize the interlayer spacing of graphene layers before and after modification. A High Resolution Transmission Electron Microscope (HRTEM, JEOL 2010 F FEG) equipped with a field emission gun running at high resolution was used to determine the quality of exfoliation of graphene layers. Bulk resistivity of samples was tested through sheet resistance measurements using a four-point probe configuration. The setup is comprised of a probe unit (Cascade Microtech Inc.) and a source meter (Keithley 2440 5A Source meter, Keithley Instruments Inc.) The acquired sheet resistance was then converted into bulk resistivity using the following equation:

$$\rho = Ft\frac{\pi}{ln2}\left(\frac{V}{I}\right) \qquad \textbf{Equation 6.1}$$

Table 6-1. Conductive fillers for each type of electrical conductive adhesive.

Type of ECA	Abbreviation	Conductive filler system
Conventional ECA	CCA	Silver flakes
Hybrid ECA	HCA-SGS	Silver flakes and SDS-modified small graphene
	HCA-SGN	Silver flakes and non-modified small graphene
	HCA-LGS	Silver flakes and SDS-modified large graphene
	HCA-LGN	Silver flakes and non-modified large graphene

where *F* is a correction factor used for samples with finite thicknesses, *t* is the sample thickness, *I* is the applied current and *V* is the voltage drop measured by the source meter. The correction factor is defined as a function of the ratio of the sample thickness-to-probe spacing denoted as *s* and so, for situations where the ratio between *t* and *s* is $0.4 < t/s < 1.0$, *F*

can be approximated to 1 [61]. For our measurements, the sample thickness is ~ 0.5 mm and the spacing is 1 mm, therefore it is safe to assume that $F = 1$.

Using a Scanning Electron Microscope (SEM, LEO 1530, Carl Zeiss NTS), a study was carried out on the morphology of the electrical network inside the composites, as well as the filler-filler interaction between the graphene and the silver flakes. Differential Scanning Calorimetry (DSC) was performed for pure epoxy and composite to determine the rate of curing and their glass transient temperature (Tg). Polymer and composite DSC samples were encapsulated in hermetically sealed aluminum pans and cured during a 3 °C/min ramp to 180°C in a TA4600 differential scanning calorimeter. The area under the exothermal peak was taken as the specific cure reaction enthalpy (ΔH_{tot}), in accordance with ASTM E2160-04. Samples were then cooled to 50 °C at 3 °C/min, and a second-heating scan performed to 180 °C using a modulation of ±0.477 °C every 60 seconds and an underlying heating rate of 3°C/min.

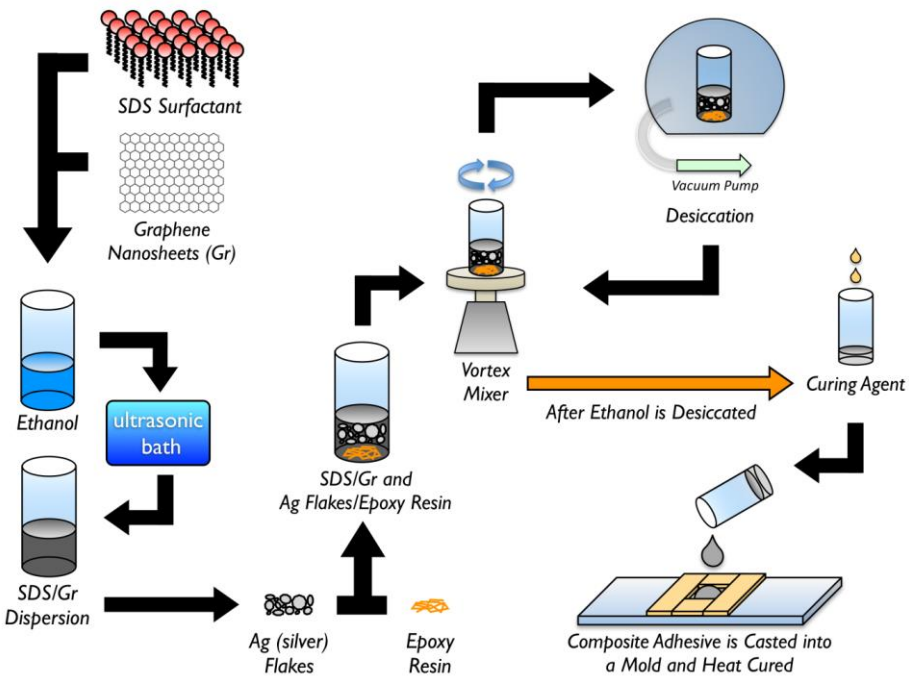

Figure 6-2. A schematic of a hybrid ECA nanocomposite preparation.

The glass transition (T_g) of polymer and composite samples was determined from the reversing heat capacity (*Rev Cp*) signal of the second scan, using the methodology described by ASTM D7426-08. No residual cure signal was observed, confirming completion of the detectable enthalpic cure in the first heating scan [161]. Samples were then cooled to 50 °C at 3 °C/min before post-curing. Polymer and composite samples were post-cured using heat-treatment cycles, applied by DSC. Each cycle consisted of heating the sample to 150 °C with an underlying heating rate of 3 °C/min, holding isothermally for 60 minutes, then cooling to 50 °C at 3 °C/min. Heating was modulated at 0.477 °C amplitude every 60 seconds to obtain the reversing *Cp* component of the signal, determining the T_g at the beginning of each post-cure cycle. The $T_{g\infty}$ value reported is the value obtained when T_g stopped changing

significantly between post-cure cycles, indicating post-cure was complete. Each sample was cycled 10 times to assure they reached a completely post-cured state. The thermogravimetric Analysis (TGA, TA instruments Q5000-1254) was used to study the thermal stability of the nanocomposites. Samples of about 10 mg were placed in the TGA sample pan. Dynamic scan was performed from 40 to 800 °C with a heating rate of 10 °C/min under nitrogen atmosphere.

6.3 Results and discussion

FTIR was used to verify the interaction between SDS and graphene layers. The FTIR was performed for pure SDS, non-modified graphene, and the SDS-modified graphene; the results are shown in Figure 6-3A. To make sure there was no un-bonded SDS left in the system, the mixture of SDS and graphene after sonication was vigorously washed with fresh ethanol using sonication and centrifugation. In the FTIR spectrum of non-modified graphene, the peaks at 1589 and 1740 cm^{-1} are related to the stretching vibration of C=C and C=O bands, respectively [162]. Both of these peaks can be seen in the spectrum of SDS-modified graphene with slightly reduced intensities. Also, the peak at 1240 cm^{-1} in the spectrum of non-modified graphene is considered to be C–H in plane bending [163]. This peak is too weak and in the most cases cannot be seen, as it was diminished in the spectrum of the SDS-modified graphene. The spectrum of pure SDS shows peaks at 1248 cm^{-1}, 1219 cm^{-1}, and 1084 cm^{-1} which correspond to asymmetric and symmetric stretching modes of SO_4^{-1}, respectively. Furthermore, pure SDS spectrum shows CH_3 asymmetric, symmetric (2955 cm^{-}

[1], 2873 cm^{-1}) and CH_2 asymmetric, symmetric (2917 cm^{-1}, 2850 cm^{-1}) stretching vibrational frequencies [164]. The same peaks are observed in the spectrum of SDS-modified graphene (as highlighted in red and green), implying the presence of SDS on the graphene surface even after vigorous washing for several times. These results confirm the interaction between SDS and graphene layers.

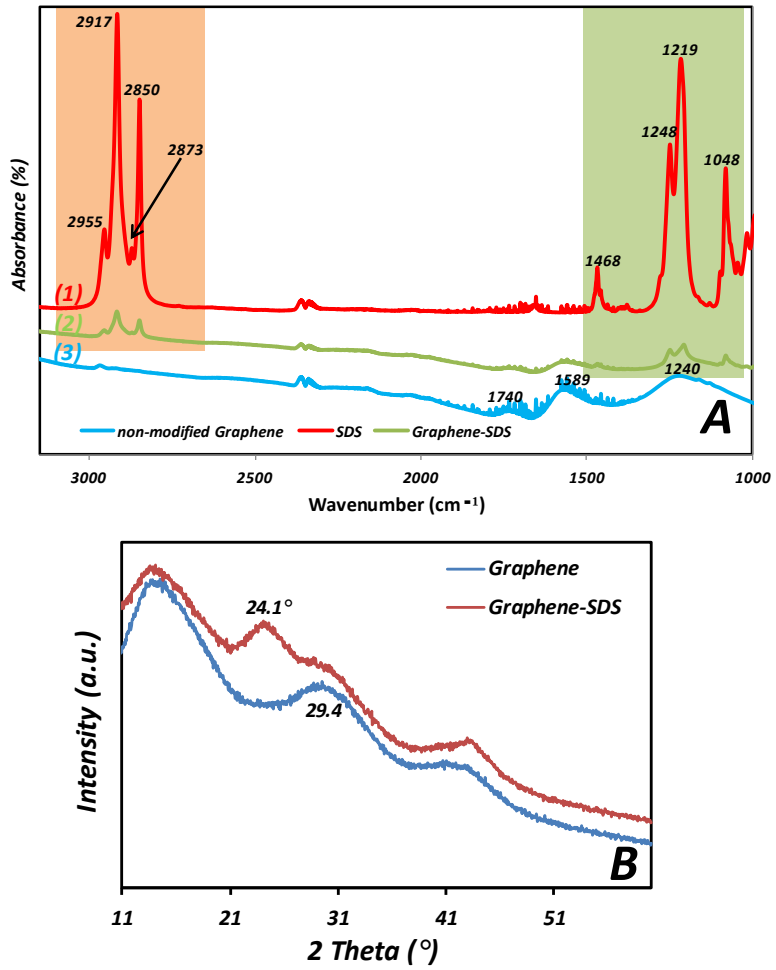

Figure 6-3. A) FTIR spectra of pure SDS (1), SDS-modified graphene (2), and non-modified graphene (3); B) XRD spectra of non-modified and SDS-modified graphene.

Figure 6-3B shows the XRD pattern of small graphene before and after treatment with SDS. As can be observed in this figure, there is a peak at 29.4° before treatment, corresponding to 0.3 nm d-spacing of graphene layers. However, after SDS treatment this peak was shifted to 24.1° which is corresponded to 0.38 nm d-spacing between graphene layers. This observation indicates that SDS adsorption on graphene surface expanded the graphene interlayer spacing.

TEM was carried out to examine the effectiveness of SDS modification on exfoliation of both small and large graphenes. The transparency of flakes to the electron beam implies the level of exfoliation [64]. The number of graphene layers can be indicated by counting the number of distinguishable edges in TEM images [114]. Figure 6-4A and 6-4B are representative TEM images of non-modified and SDS-modified small graphene, respectively. The opaque feature of non-modified graphene implies the stacking of graphene layers which hindered the electron beam to pass through the sample. However, after SDS modification we see a bright and transparent graphene layer with a single distinguishable edge. The HRTEM image of the red square-marked area of Figure 6-4B clearly shows that the graphene layers are exfoliated to individual layers. Electron diffraction (ED) pattern of black square-marked area also confirms the single layer feature of the selected area, as the inner set of spots are more intense than the secondary set [107,114]. The blurry ring in the ED pattern is attributed to the amorphous structure of SDS covering the graphene surface. A representative TEM image of non-modified large graphene flakes is shown in Figure 6-4C which have a similar dark structure as small graphene. However, as can be seen in Figure 6.4D, after SDS treatment, the large graphene flake is transparent to the electron beams. The HRTEM image

of the red square-marked area of Figure 6-4D also shows there is only a single layer at the edge of the large flake.

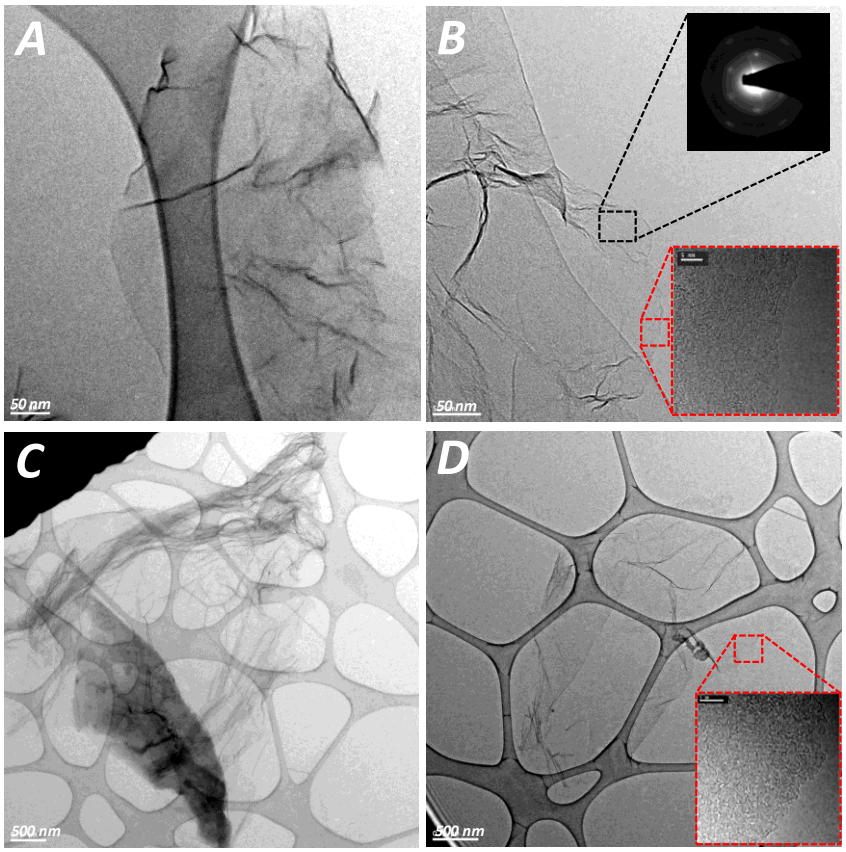

Figure 6-4. A) a representative TEM image of graphene without SDS; B) a representative TEM image of graphene after SDS treatment, the black inset is an electron diffraction pattern of the black marked area, the red inset is a HRTEM image of the red marked area of graphene edge; C) a representative TEM image of large graphene flake before SDS treatment; D) a representative TEM image of large graphene after SDS treatment.

As the first attempt to investigate the electrical properties of the nanocomposites, small graphene (1.5 wt%) was added into the conventional formulation of ECAs (CCAs) as a conductive co-filler to produce a customized hybrid ECAs (HCAs). The effect of SDS on electrical conductivity of ECAs was investigated by comparing the bulk resistivity of HCAs containing SDS-modified small graphene (HCA-SGSs) to that of HCAs with non-modified graphene (HCA-SGNs). The electrical resistivities of both the CCA and the HCA-SGNs until 30 wt% (equal to 5.4 vol%) silver flake were higher than the upper limit of our four-probe electrometer while a relatively low electrical resistivity of 0.4 Ω.cm was achieved for HCA-SGSs at 30 wt% silver flakes. As can be seen in Figure 6-5A, the percolation threshold for both the CCAs and the HCA-SGNs was 30 wt%, and the HCA-SGNs rendered lower bulk resistivity compared to the conventional ECAs. The lower bulk resistivity of the HCA-SGNs is because of the bridging effect of the graphene layers between the silver flakes. However, when SDS was used to disperse graphene layers inside the composite the percolation threshold was decreased to 10 wt%. A low bulk resistivity of 3×10^{-5} Ω.cm was achieved for the HCA-SGS with 80 wt% (equal to 32.8 vol%) silver flakes and 1.5 wt% (equal to 6.4 vol%) SDS-modified graphene. The difference between the bulk resistivity of HCA-SGSs and HCA-SGNs is much more pronounced at low silver content, indicating the effectiveness of SDS to exfoliate and stabilize the graphene sheet. The SDS modification of graphene provides the opportunity to fully take advantage of its high aspect-ratio which is crucial to decrease the tunnelling resistance by bridging between separated silver flakes.

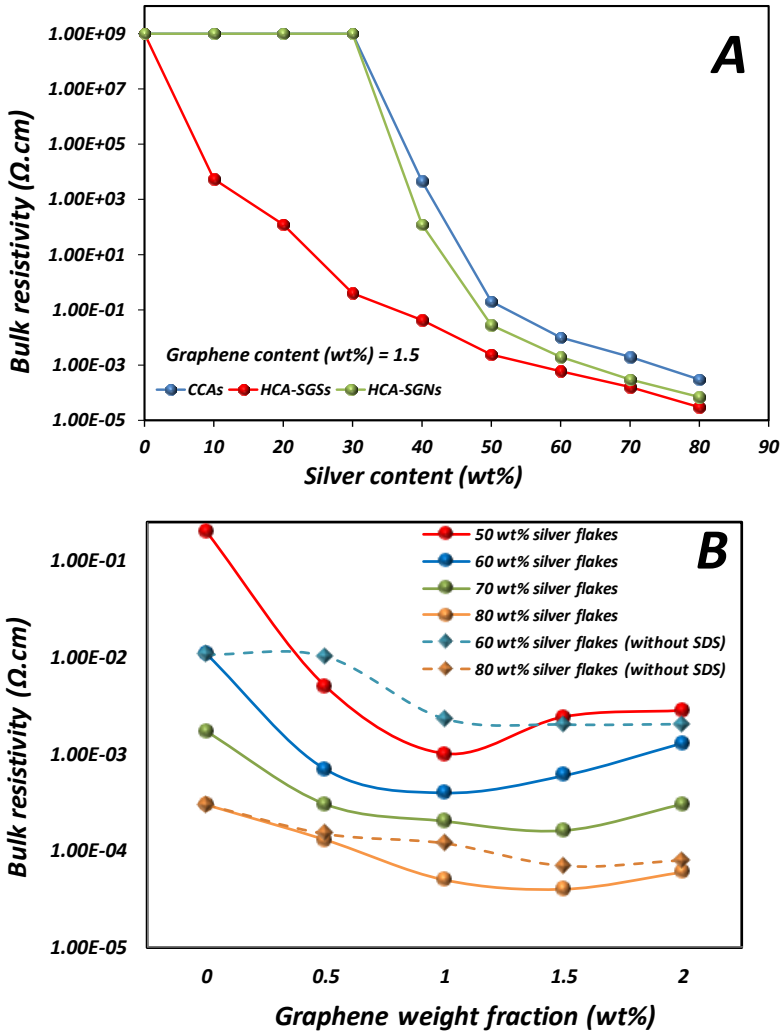

Figure 6-5. A) bulk resistivity of conventional ECAs (CCAs), hybrid ECAs with non-modified small graphene (HCA-SGNs), and hybrid ECAs with SDS-modified small graphene (HCA-SGSs), B) the effect of SDS-modified small graphene concentration on the bulk resistivity of hybrid ECAs with different silver contents.

In order to investigate the effect of graphene concentration on the electrical conductivity of hybrid ECAs, SDS-modified graphene of varying concentrations were added into the CCAs and the bulk resistivities of the HCA-SGSs were measured. The same ranges of graphene concentrations were applied for CCAs with different silver concentrations to identify the optimal graphene content at each silver concentration (see Figure 6-5B). The optimum graphene content was 1 wt% for the HCA-SGSs with 50 and 60 wt% of silver flakes while that concentration was 1.5 wt% for the HCA-SGSs with 70 and 80 wt% of silver flakes, indicating the importance of the weight ratio between silver micro flakes and graphene nanosheets on the electrical performance of HCAs. The increased bulk resistivity of the HCA-SGSs after the optimum concentration may attribute to the agglomeration of graphene at higher concentration. The dashed lines of Figure 5B show the bulk resistivity of the HCA-SGNs at 60 and 80 wt% of silver flakes. The higher bulk resistivity of these samples compared to the HCA-SGSs with the same filler content is in agreement with our previous discussion on the positive effect of SDS treatment on the electrical conductivity of ECAs.

To study the effect of graphene size and SDS modification, hybrid ECAs with various silver contents were produced containing large graphene, either unmodified or modified with SDS (HCA-LGN and HCA-LGS, respectively). Figure 6-6 presents the bulk resistivity of these, in comparison with those of HCA-SGSs with comparable silver contents. As can be observed in Figure 6-6, the bulk resistivity of the HCA-LGSs is noticeably lower than that of the HCA-SGSs, especially at low silver concentrations, when the silver flakes would be separated and rarely in direct contact. This demonstrates that when either are well distributed by SDS

modification, the large graphene sheets are better able to bridge the gaps between the silver flakes than the small graphene sheets, allowing further reductions in silver content. Addition of 1.5 wt% of large SDS-modified graphene into CCAs with 10 wt%, 20 wt%, and 30 wt% led to bulk resistivities of 35 Ω.cm, 0.5 Ω.cm, and 7.6×10^{-3} Ω.cm, respectively, while those resistivities for the HCA-SGSs were 5.5×10^{3} Ω.cm, 122 Ω.cm, and 0.4 Ω.cm, respectively. Figure 6-6 also confirms the effectiveness of SDS in improving the electrical conductivity of the hybrid ECAs. Although the bulk resistivity of the HCA-LGNs was lower than that of the CCAs in all the silver content, those resistivity values were higher than those of HCA-LGSs.

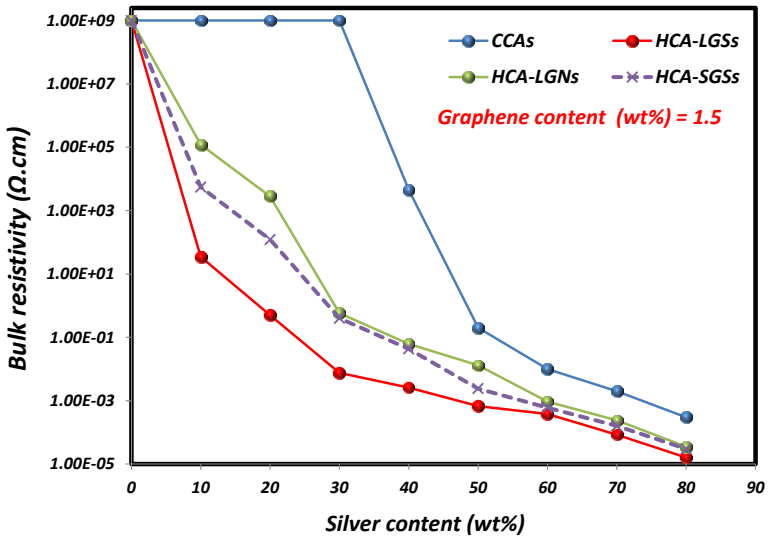

Figure 6-6. The effect of the aspect-ratio of SDS-modified graphene on the electrical conductivity of ECAs.

It should be noted that a highly conductive ECA with a very low electrical resistivity of 1.6×10^{-5} Ω.cm was prepared by adding 1.5 wt% of SDS-modified large graphene into the CCA with 80 wt% of silver flakes. This bulk resistivity is even lower than that of eutectic lead-

based solders [14]. Figure 6-6 also shows that the electrical resistivity of HCA-LGNs is higher than that of HCA-SGSs in all the silver contents, indicating that the SDS modification effect is more dominant in electrical conductivity improvement of ECAs than the effect of the aspect-ratio of conductive fillers.

The SEM images of the CCA, HCA-SGS, HCA-LGS, and HCA-LGN with 30 wt% silver flakes were shown in Figure 6-7 A-D, respectively. For the hybrid ECAs, the concentration of graphene was 1.5 wt%. As can be observed in Figure 6-7A, a large portion of silver flakes are separated by epoxy resin and the electrical network is not fully formed, as evidenced by electrical resistivity measurements (see Figure 6-5A). However, the high aspect-ratio of graphene nanosheets helps to construct new electrical pathways for electron transportation inside the network. The yellow arrows of Figure 6-7B identify small SDS-modified graphene sheets spanning gaps between separated flakes to form a connected network. As can be seen in this figure, the small graphene layers were reasonably dispersed inside the epoxy and no noticeable form of aggregation of graphene was observed. Figure 6-7C also shows large SDS-modified graphene well dispersed inside epoxy. Because of the large size of graphene nanosheets more parts of the composite are covered by a conductive material. The yellow arrows of Figure 6-7C representatively indicate a conductive path inside the conductive composite. Finally, Figure 6-7D shows the SEM image of the HCA-LGN. As can be seen in this figure, the large graphene was not well dispersed inside the composite and large graphitic agglomerates formed, which explains the high electrical resistivity of this type of ECA compared to that with SDS-modified graphene.

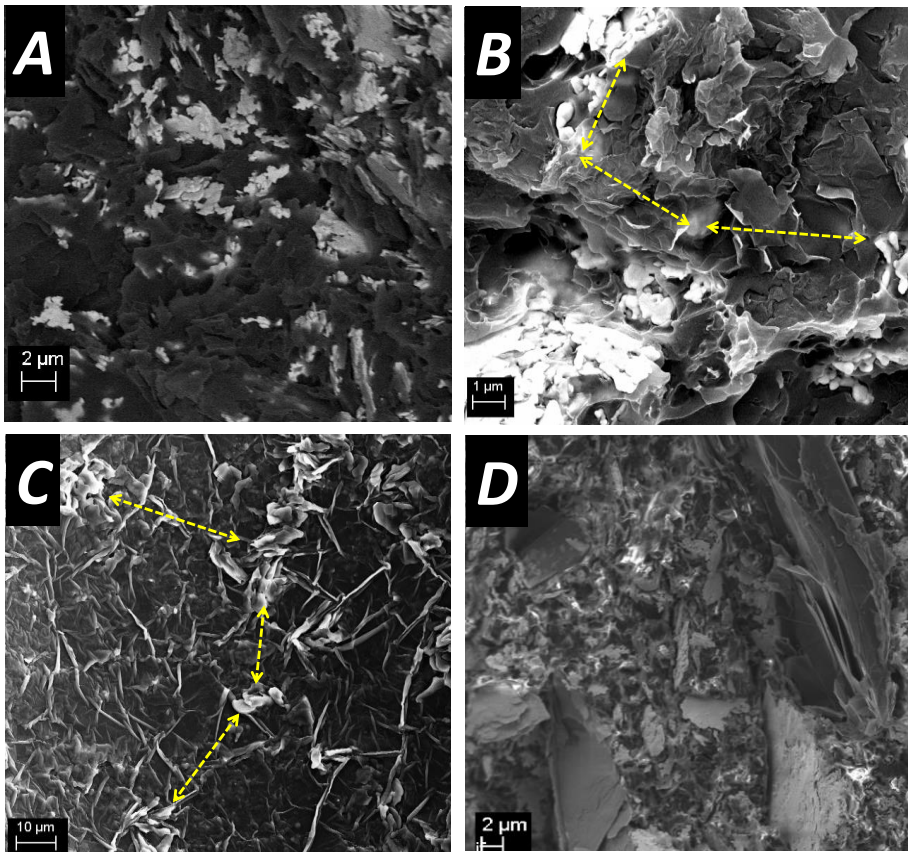

Figure 6-7. A) an SEM image of the conventional ECA; B) an SEM image of the hybrid ECAs with 1.5 wt% of SDS-modified small graphene; C) an SEM image of the hybrid ECA with 1.5 wt% of SDS-modified large graphene; D) and an SEM image of the hybrid ECA with 1.5 wt% of non-modified large graphene. Note: for all the ECAs the content of silver flakes was 30 wt%.

DSC was performed to examine the effect of graphene and its SDS modification on the curing behavior of epoxy and the T_g of the final nanocomposite. Characteristic DSC data are presented in Table 6-2, collected from the cure and post cure of two control group samples and two graphene composites (HCA-SGN and HCA-SGS). The control group samples are pure epoxy, and epoxy diluted with the same solvent content as the two nanocomposites. ΔH_{norm} represents the reported enthalpy normalized to only the mass of the hardened epoxy

matrix [22]. Solvent masses for each composition have been presented using both the ethanol wt% in the total composite and the ethanol PHR (resin mass as reference), referencing the amount of ethanol present after degassing and at the start of curing. DSC traces for cure and post cure of HCA-SGS are presented in Figures 6-8A and 6-8B, respectively, as examples to demonstrate the means by which the characteristic data was obtained. From the data of both control groups in Table 6-2, we see that the addition of ethanol reduced ΔH_{tot}, and reduced $T_{g\infty}$ by 12°C, indicating a reduction in epoxy crosslinking. This is likely partially due to the typical dilution effects of solvents during cure [161]. However, contrasting the reduced ΔH_{tot} and the increase in ΔH_{norm} implies that the ethanol also reduced the crosslinking by taking part in the matrix cure reaction and competing with the main stoichiometric epoxy/TETA reaction.

Table 6-2. Characteristic Cure and Tg data from DSC.

		Composition			
Name Description		**Control 1 (Neat Epoxy)**	**Control 2 (Ethanol Diluted)**	**HCA-SGN**	**HCA-SGS**
Ethanol Content	PHR	0 PHR	40.8 PHR	40.4 PHR	40.4 PHR
	wt%	0 wt%	26.5 wt%	12.5 wt%	12.5 wt%
ΔH_{tot}	J/g	452.7	380.5	132.7	148.3
ΔH_{norm}	J/g_{matrix}	452.7	517.5	380.9	436.2
$T_{g\infty}$	°C	129.7	117.8	111.9	111.9

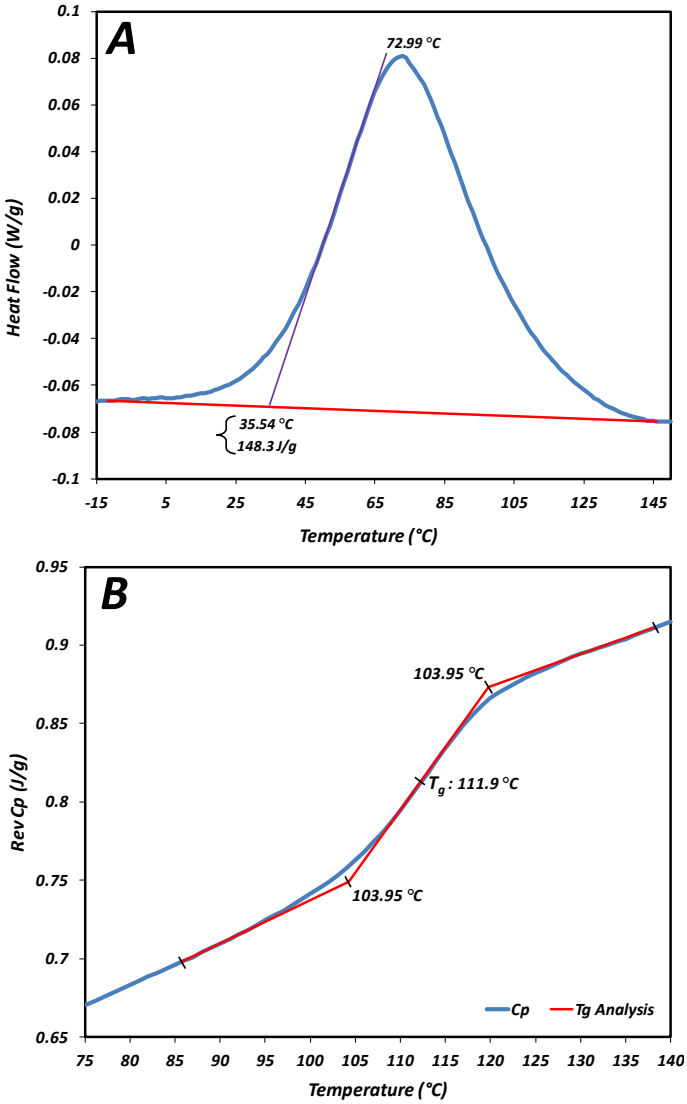

Figure 6-8. DSC data for HCA-SGS, demonstrating methods by which characteristic data was determined for A) composite cure from heat flow; B) composite T_g from Reversing *Cp*. Each trace was performed at 3°C/min underlying heating rate. Modulation of ±0.477 °C every 60 seconds used in B) only.

From the composite containing silver flake and graphene without SDS (HCA-SGN) in Table 6-2, we can see that the addition of filler substantially reduces ΔH_{norm} compared to that of the

representative ethanol diluted epoxy control. In addition, the $T_{g\infty}$ was reduced by 5°C by the addition of filler. Since it is known that silver microflake has no significant effect on $T_{g\infty}$ [161], it appears that the addition of graphene produced both of these effects. Comparing the data for composites HCA-SGN and HCA-SGS from Table 6-2, where the only difference is the modification of graphene by SDS, we see no change in $T_{g\infty}$. However, the addition of SDS-modified graphene does not reduce the ΔH_{norm} as much as the addition of untreated graphene did. This result may be interpreted in a number of ways, one of which can be as follows. The presence of graphene reduces crosslinking density, ΔH_{norm} and $T_{g\infty}$ regardless of the presence of SDS. The reduction of ΔH_{norm} may be partly due to the moiety of oxygen functionality on graphene surfaces (i.e., C=O characteristic peak of carboxylic group at 1740 cm^{-1} in Figure 6.3) acting catalytically on the reactions of epoxides and amines, or the reaction of epoxides and hydroxyls (from ethanol and the epoxy autocatalytic reaction) as discussed by others [165–167]. These would lead to an unaccounted fraction of the total reaction heat being released before the sample is placed in the DSC, reducing the reported ΔH_{norm}. However, in the case of HCA-SGS, SDS would have covered a large fraction of the graphene surface, reducing the ability of graphene to act as a catalyst. This would slow the unintended reactions of the composite before it enters the DSC, increasing the fraction of enthalpy captured. However, further investigations are needed to clarify the exact mechanism by which the graphene and the SDS influence the reaction enthalpy.

TGA was used to characterize the thermal stability of the final nanocomposites. The experiment was performed for pure epoxy, pure SDS, CCA, HCA-SGN, and HCA-SGS. For

all the composites, the concentration of silver flakes was 60 wt% and the graphene content was 1.5 wt% for the hybrid ECAs. As the TGA results show that pure epoxy decomposition started slowly around 300 °C, then greatly accelerated at around 325 °C (see Figure 6-9). The pure SDS degraded at a much lower temperature of 200 °C. HCA-SGNs began its decomposition rapidly at approximately 325 °C, demonstrating a small but noticeable reinforcement effect from the presence of the graphene surface. HCA-SGS has a relatively lower decomposition temperature than the HCA-SGNs, perhaps because of the SDS layer between the graphene and epoxy that may weaken the reinforcement effect of graphene surface. It was noted that HCA-SGS had 12 wt% more residue after TGA degradation than the SDS-free CCA and HCA-SGN composites. This is consistent with results reported by Wang et al.; they studied composites of epoxy and SDS and observed an increase in residual wt% in the SDS-containing epoxy [168]. It is possibly due to the formation of SO_2 or a sulfonate, during SDS degradation, which would then be available to promote formation of stable char [169,170].

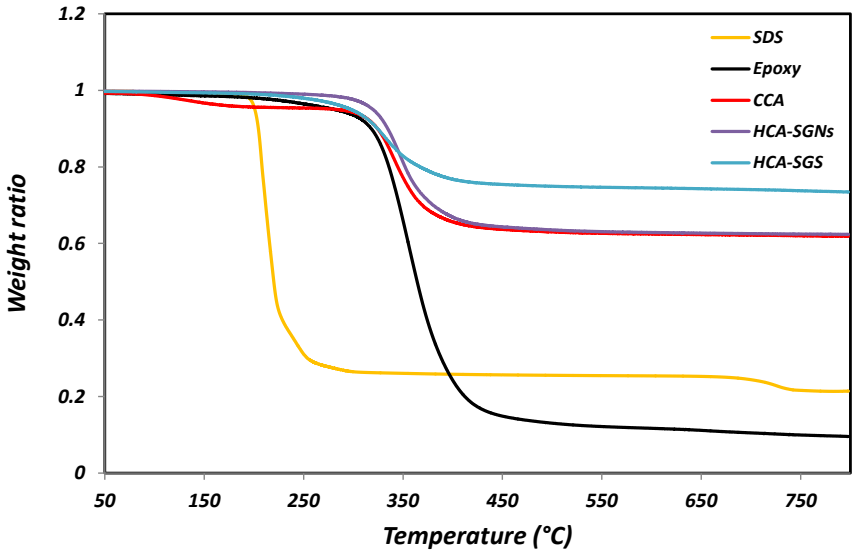

Figure 6-9. The TGA results for pure SDS, pure epoxy, the conventional ECA, hybrid ECA with non-modified graphene, and hybrid ECA with SDS-modified graphene.

6.4 Summary

Graphene nanosheets with two different sizes (1 μm and 5 μm) were modified with SDS and introduced into the conventional formulation of ECAs; the effect of the graphene surface modification and graphene size on the electrical conductivity of ECAs was investigated. FTIR results confirmed the surface modification of graphene with SDS. TEM imaging and XRD confirmed the effectiveness of SDS on exfoliation of graphene nanosheets. The SDS modification of graphene decreased the percolation threshold of silver content from 30 wt% to the remarkably low value of 10 wt% while the percolation value did not change for the hybrid ECA with non-modified graphene. The electrical conductivity measurements also showed that the larger graphene is more effective in improving the electrical conductivity of

ECAs and reducing the amount silver flakes than small graphene. The bulk resistivity of HCA-LGS with 10 wt% silver flakes and 1.5 wt% graphene was 35 Ω.cm while the bulk resistivity for the HCA-SGS with the same filler composition was 5.5×10^3 Ω.cm. According to DSC results, additions of both SDS-modified and unmodified graphene reduced the crosslinking of the epoxy matrix based on the reduction in T_g compared to an appropriate control group. However, the modification of the graphene filler surface by SDS had a definite effect on the apparent normalized enthalpy (ΔH_{norm}) of the resulting nanocomposite (HCA-SDS), possibly demonstrating the suppression by the SDS of premature reactions that would be otherwise promoted by the presence of the bare graphene surfaces.

Chapter 7. Concluding Remarks, Main Thesis Contributions, and Recommendations

7.1 Summary and concluding remarks

In this thesis, we first explained the fundamentals of electrically conductive adhesives (ECAs) and discussed their working mechanism based on the quality of inter-filler interactions. Following these principles, the drawbacks of conventional ECA (consisting of epoxy and silver micro flakes) were addressed and the importance of the application of conductive nanofillers inside the conventional formulation of ECAs to overcome those drawbacks were highlighted. Different types of conductive nanofillers were implemented to develop customized hybrid ECAs and proper surface modifications were applied to facilitate the dispersion of nanofillers inside the polymeric matrix and to improve the quality of inter-filler interaction. The details of the electrical conductivity enhancement mechanism via the introduction of the surface modified nanofillers were investigated for each case.

The concluding remarks which were demonstrated in this thesis are:

- First, spherical Ag NPs were synthesized and simultaneously functionalized with two thiocarboxylic acids with similar chemical structure but two different chain lengths (MPA with 3 carbons in its backbone, and MUA with 11 carbons). For the first time, we demonstrated that the chain length of organic layer significantly influences the

NPs size and their electrical properties; we showed that Ag NPs with longer organic chain-length were bigger (4.49 ± 1.28 nm) and electrically insulating while the surface functionalization of the NPs with short chain-length led to smaller size (2.09 ± 0.66 nm) NPs which were electrically conductive.

- MPA functionalized Ag NPs were incorporated into the conventional formulation of ECA and the effect of the Ag NPs to silver flakes weight ratio on the electrical conductivity of the ECAs was studied. The results showed that the electrical conductivity of the ECAs improved via addition of Ag NPs. However, after specific concentration, adding more Ag NPs decreased the electrical conductivity. The bridging of Ag NPs between separated silver flakes is the main reason for the observed electrical conductivity improvement. Besides, the very small size of the NPs enables them to fill the interstitial spaces between silver flakes and also provide the opportunity to trigger the sintering at a relatively low curing temperature of 150 °C.

- By understanding the importance of the bridging of the NPs on the electrical conductivity enhancement of ECAs, we used a new type of high aspect-ratio silver NPs, Ag NBs, which can readily connect separated silver flakes at low silver content. The wavy belt morphology of the NBs provides more surface area for electron transportation inside the electrical network compared to the commonly used Ag NWs. Our results showed that addition of a small amount of the NBs (1 wt%) to the conventional ECA with relatively low silver flakes content (close to the percolation threshold) increased the electrical conductivity by 1550%, while at higher silver content the electrical conductivity enhancement was not significant.

- Taking into account the significance of the aspect-ratio of the nanofiller, we used graphene as co-filler to generate a novel type of hybrid ECAs. The 2D structure of graphene, along with its remarkably high surface area, provides a large surface area for electron transportation inside the electrical network which in turn can noticeably reduce the minimum required amount of silver materials. Using a novel wet chemistry approach, we decorated the surface of graphene with the same Ag NPs as reported in Chapter 3 as an attempt to preserve the single layer feature of graphene layers and to reduce the contact resistance between graphene and silver flakes. Our results showed that although addition of the Ag NP-decorated graphene improves the electrical conductivity of the conventional ECAs, the final electrical conductivity is not high enough, mostly because of the increased number of contact points. High curing temperature is required to achieve high electrical conductivity comparable to that of eutectic solders. We demonstrated that by increasing the curing temperature up to 220 °C, electrical conductivities close to those of eutectic solders can be achieved when the Ag NPs on graphene surface sinter to silver flakes.

- Despite all the efforts to keep the chemical structure of graphene intact during decoration of graphene, its surface still experiences partial damage. In order to exfoliate graphene layers and facilitate their dispersion inside epoxy without disturbing their chemical structure, we used a non-covalent technique using SDS surfactant to stabilize graphene layers and incorporated them inside the conventional ECAs. To shed further light on the effect of co-filler's aspect-ratio on the electrical performance of hybrid ECAs, we used two graphenes with different sizes. Our results

revealed that addition of 1.5 wt% of SDS-modified small graphene decreased the silver flakes percolation threshold to a significantly low value of 10 wt% while this value for the conventional ECA was 40 wt%. It should be noted that larger graphene was more effective in improving the electrical conductivity of ECAs than the smaller graphene. We reached a very low electrical resistivity of 1.6×10^{-5} Ω.cm for the hybrid ECA with 80 wt% silver flakes and 1.5 wt% SDS-modified large graphene which is lower than that of eutectic lead-based solders.

7.2 Main thesis contributions

In this project, we have developed new generations of hybrid ECAs through the incorporation of novel conductive nanofillers i.e., spherical thicarboxylate-functionalized Ag NPs, high aspect-Ratio Ag NBs, Ag NP-decorated graphene, and SDS-stabilized single layer graphene, into the conventional formulation of ECAs. We have succeeded in properly functionalizing and dispersing these conductive nanofillers inside epoxy.

In Chapter 3, we functionalized spherical Ag NPs with thiocarboxylic acids with two different sizes and for the first time reported the effect of organic layer chain length on the size and electrical conductivity of the NPs. We successfully prepared very small NPs with low organic coverage content which enable the NPs to be sintered at low curing temperatures (i.e., < 150 °C). Despite the fact that the most of the literature report use of large Ag NPs

(larger than 20 nm), we demonstrated that very small NPs can be also effective for improving the electrical conductivity of ECAs, although the ratio of the NPs to the silver micro flakes is crucial for electrical conductivity enhancement.

Although spherical Ag NPs have positive effect on the electrical conductivity of ECAs, a large amount of NPs is needed for this purpose. In Chapter 4, we reported the application of a novel high aspect-ratio type of Ag NPs, Ag NBs, which provide high surface area for electron transportation throughout the composite and as result significantly reduces the total amount of silver flake content. Compared to the previously used Ag NWs, (which are synthesized at high temperatures and long reaction times), the fabrication of the NBs is fast and occurs at room temperature. Besides, the Ag NBs have a low "weight to length" ratio, which can form a percolated network at low concentrations which consequently reduce the total mass of composites. The NBs had tiny amount of organic layer enabling them to be sintered at low curing temperatures. We showed that the hybrid ECA with 1 wt% Ag NBs and 60 wt% silver flakes render almost the same bulk resistivity as the conventional ECA with 80 wt% silver flakes does.

By understanding the important role that the aspect-ratio of nanofillers plays on reducing the amount of silver flakes, we implemented graphene as conductive co-filler inside conventional ECAs. Two covalent (Ag NP-decoration) and non-covalent (SDS modification) approaches were applied to exfoliate graphene layers inside epoxy (Chapters 5 and 6, respectively). We

showed that although Ag NP modification of graphene was effective to improve the electrical conductivity of ECAs, achieving high electrical conductivity requires high curing temperature because of the increased number of contact points. By conducting the non-covalent SDS modification of graphene, we demonstrated that the common thought that believes the metallization of graphene is the best way to improve the electrical conductivity of ECAs filled with graphene may not be true and the characteristic electrical conductivity of graphene can be exploited if a proper technique is employed to disperse it inside epoxy and preserve its single layer structure.

7.2.1 List of Peer-reviewed Journal Publications

- **Behnam Meschi Amoli**; A. Hu; Y. N. Zhou; B. Zhao, "Recent Progress on Hybrid Micro-nano filler Systems for Electrical Conductive Adhesives (ECAs) Applications", *Journal of Materials Science: Materials in Electronics (JMSE),* accepted.
- **Behnam Meschi Amoli**; J. Trinidad; A. Hu; Y. N. Zhou; B. Zhao, "Highly Electrically Conductive Adhesives Using Silver Nanoparticle (Ag NP)-decorated graphene: The Effect of NPs Sintering on the Electrical Conductivity Improvement", *Journal of Materials Science: Materials in Electronics (JMSE)*, **2015**, 26, 590-600.
- **Behnam Meschi Amoli**; E. Marzbanrad; A. Hu; Y. N. Zhou; B. Zhao, "Electrical Conductive Adhesives Enhanced with High-Aspect-Ratio Silver Nanobelts", *Journal of Macromolecular Materials and Engineering*, **2014**, 299, 739-747.

- S. Gumfekar; **Behnam Meschi Amoli**; A. Chen; B. Zhao, "Polyaniline-Tailored Electromechanical Responses of the Silver/Epoxy Conductive Adhesive Composites", *Journal of Polymer Science, Part B: Polymer Physics*, **2013**, 51, 1448–1455.
- **Behnam Meschi Amoli**; S. Gumfekar; A. Hu; Y. N. Zhou; B. Zhao, "Thiocarboxylate Functionalization of Silver Nanoparticles: Effect of Chain Length on the Electrical Conductivity of Nanoparticles and their Polymer Composites", *Journal of Materials Chemistry*, **2012**, 22, 20048–20056.

7.3 Recommendations for future steps

7.3.1 Short-term recommendations

There are several short-term studies which can be carried out to address some of the unanswered questions regarding the mechanism of electron transformation inside the electrical network

- In Chapter 3, we reported the use of MPA and MUA with 3 and 11 carbon as the covering layer of Ag NPs and demonstrated that the chain length of these thiocarboxylic acids changes the size of the NPs. Further study can be performed for other thiocarboxylic acids with different chain length to figure out if there is an optimum chain length for the size of the Ag NPs.

- Since the electrons are transferred inside the polymeric matrix when the conductive fillers come to contact with one another, the quality of inter-filler interaction is crucial. For each hybrid system, one can monitor how the electrical conductivity of hybrid ECAs would change as the curing temperature varies. Our preliminary DSC results for the hybrid ECA with SDS modified graphene showed that the curing of epoxy is completed at temperatures close to 110 °C. This temperature can be chosen as the minimum curing temperature for all the cases. At the same time, the quality of interaction between silver flakes and nanofillers, specifically for those with Ag NPs, can be monitored using SEM imaging. This study would provide a comprehensive understanding about how thermal treatment of composite affects the quality of filler-filler interaction and eventually the electrical conductivity of the final composites.

As for composite itself, there are some additional questions that need to be answered.

- First and foremost, although the synergistic effect of each type of nanofiller in improving the electrical conductivity of the ECAs has been well studied, the mechanical and adhesive properties of the hybrid ECAs needs to be investigated. More specifically this study for the hybrid ECAs with Ag NBs and graphene can be very informative since upon the addition of these nanofillers the amount of silver flakes reduced significantly, which is most likely to exhibit mechanical property changes.

- Although the curing behavior of the hybrid ECA with SDS modified graphene was investigated in this project (Chapter 6), this study also can be carried out for other hybrid systems to investigate how the curing behavior of epoxy is changed upon addition of nanofillers, more specifically to see if there is any change on T_g or the degree of curing after addition of nanofillers.

7.3.2 Long-term recommendations

There are also several additional questions that can be answered as long-term future work that can help broaden the understanding regarding the potential application as well as the performance of the next generation of ECAs.

- Since the invention of ECAs, silver flakes have been widely used as conductive fillers for commercial ECAs due to their excellent electrical conductivity and stability. However, a high amount of silver flakes (>33 vol.%) is usually required to achieve the minimum desired electrical conductivity, which in turn increases the final cost of the commercial ECAs. Besides, the high concentration of silver flakes jeopardies the mechanical strength of the final composites. Therefore, to enhance the electrical conductivity of the ECAs, lower the cost of the products, and to improve the mechanical properties of the final composite silver particles loading should be reduced. Finding alternative silver type fillers with the same conductivity but

offering higher surface area than silver flakes is one scientific aspect that could open new research pathways in this field.

- As mentioned earlier, one of the most important applications of ECAs is on electronic packaging industries. The printing ability of the fabricated ECAs can be examined to see how they can be applicable for real industrial applications. For example, the fabricated ECAs can be examined for applications such as electrical interconnections for multi-layer circuit boards.
- It is also important to study the reliability of the fabricated ECAs for long term applications. One of the major drawbacks of commercial ECAs is the change in their electrical conductivity as they are exposed to harsh environments. One can monitor the electrical conductivity of the fabricated ECAs at humid and elevated conditions during different aging times.

References

[1] Y. Li, K. Moon, C.P. Wong, Electronics without lead, Science (80-.). 308 (2005) 1419–1420.

[2] W. Jillek, W.K.C. Yung, Embedded components in printed circuit boards: a processing technology review, Int. J. Adv. Manuf. Technol. 25 (2004) 350–360. doi:10.1007/s00170-003-1872-y.

[3] H.-J. Yun, K.-H. Baek, L.-M. Do, K.-S. Jeong, Y.-M. Kim, S.-D. Yang, et al., Additive Effect of Poly(4-vinylphenol) Gate Dielectric in Organic Thin Film Transistor at Low Temperature Process, J. Nanosci. Nanotechnol. 13 (2013) 3313–3316. doi:10.1166/jnn.2013.7272.

[4] T. Akter, W.S. Kim, Reversibly stretchable transparent conductive coatings of spray-deposited silver nanowires., ACS Appl. Mater. Interfaces. 4 (2012) 1855–9. doi:10.1021/am300058j.

[5] Y. Zemen, S.C. Schulz, H. Trommler, S.T. Buschhorn, W. Bauhofer, K. Schulte, Comparison of new conductive adhesives based on silver and carbon nanotubes for solar cells interconnection, Sol. Energy Mater. Sol. Cells. 109 (2013) 155–159. doi:10.1016/j.solmat.2012.10.020.

[6] Y. Li, K.J. Moon, C.P. Wong, Nano-Bio- Electronic, Photonic and MEMS Packaging, Nano-Bio- Electron. Photonic MEMS Packag. (2010). doi:10.1007/978-1-4419-0040-1.

[7] S. Qi, R. Litchfield, D. a. Hutt, B. Vaidhyanathan, C. Liu, P. Webb, et al., Copper conductive adhesives for printed circuit interconnects, in: 2012 IEEE 62nd Electron. Components Technol. Conf., Ieee, 2012: pp. 1651–1655. doi:10.1109/ECTC.2012.6249059.

[8] I.N. Kholmanov, S.H. Domingues, H. Chou, X. Wang, C. Tan, J.-Y. Kim, et al., Reduced graphene oxide/copper nanowire hybrid films as high-performance transparent electrodes., ACS Nano. 7 (2013) 1811–6. doi:10.1021/nn3060175.

[9] I. Halaciuga, J.I. Njagi, K. Redford, D. V Goia, Deposition of continuous nickel shells on polymer microspheres., J. Colloid Interface Sci. 383 (2012) 215–221. doi:10.1016/j.jcis.2012.05.055.

[10] N. Hansen, D.O. Adams, K.L. DeVries, A. Goff, G. Hansen, Investigation of Electrically Conductive Structural Adhesives using Nickel Nanostrands, J. Adhes. Sci. Technol. 25 (2011) 2659–2670. doi:10.1163/016942411X556033.

[11] Y. Li, C.P. Wong, Recent advances of conductive adhesives as a lead-free alternative in electronic packaging: Materials, processing, reliability and applications, Mater. Sci. Eng. R Reports. 51 (2006) 1–35. doi:10.1016/j.mser.2006.01.001.

[12] W. S., Bohm, E. Stammen, M., G. (Technical University of Braunchweig, Microjoining and NanoJoining, Elsevier, 2008.

[13] S. Nam, H. Woo Cho, T. Kim, D. Kim, B. June Sung, S. Lim, et al., Effects of silica particles on the electrical percolation threshold and thermomechanical properties of epoxy/silver nanocomposites, Appl. Phys. Lett. 99 (2011) 043104. doi:10.1063/1.3615690.

[14] C. Yang, C.P. Wong, M.M.F. Yuen, Printed electrically conductive composites: conductive filler designs and surface engineering, J. Mater. Chem. C. 1 (2013) 4052–69. doi:10.1039/c3tc00572k.

[15] W. Jeong, H. Nishikawa, D. Itou, T. Takemoto, Electrical Characteristics of a New Class of Conductive Adhesive, Mater. Trans. 46 (2005) 2276–2281.

[16] C. Chen, L. Wang, R. Li, G. Jiang, H. Yu, T. Chen, Effect of silver nanowires on electrical conductance of system composed of silver particles, J. Mater. Sci. 42 (2007) 3172–3176. doi:10.1007/s10853-007-1594-x.

[17] K.-Y. Chun, Y. Oh, J. Rho, J.-H. Ahn, Y.-J. Kim, H.R. Choi, et al., Highly conductive, printable and stretchable composite films of carbon nanotubes and silver., Nat. Nanotechnol. 5 (2010) 853–7. doi:10.1038/nnano.2010.232.

[18] Y. Tao, Y.P. Xia, G.Q. Zhang, H.P. Wu, G.L. Tao, Isotropical Conductive Adhesives Filled with Silver Nanowires, Proc SPIE. 7493 (2009) 74933Q1–74933Q–7. doi:10.1117/12.840597.

[19] R. Zhang, J.C. Agar, C.P.P. Wong, Recent Advances on Electrically Conductive Adhesives 1, Proc 12th Electron. Packag. Technol. (2010) 696–704.

[20] B. Meschi Amoli, S. Gumfekar, A. Hu, Y.N. Zhou, B. Zhao, Thiocarboxylate functionalization of silver nanoparticles: effect of chain length on the electrical conductivity of nanoparticles and their polymer composites, J. Mater. Chem. 22 (2012) 20048–20056. doi:10.1039/c2jm33280a.

[21] H. Jiang, K. Moon, Y. Li, C.P. Wong, Surface Functionalized Silver Nanoparticles for Ultrahigh Conductive Polymer Composites, Chem. Mater. 18 (2006) 2969–2973.

[22] H. Jiang, K. Moon, J. Lu, Conductivity Enhancement of Nano Silver-Filled Conductive Adhesives by Particle Surface Functionalization, J. Electron. Mater. 34 (2005) 1432–1439.

[23] Y. Oh, K.-Y. Chun, E. Lee, Y.-J. Kim, S. Baik, Functionalized nano-silver particles assembled on one-dimensional nanotube scaffolds for ultra-highly conductive silver/polymer composites, J. Mater. Chem. 20 (2010) 3579–3582. doi:10.1039/c0jm00086h.

[24] M. Cherrington, T.C. Claypole, D. Deganello, I. Mabbett, T. Watson, D. Worsley, Ultrafast near-infrared sintering of a slot-die coated nano-silver conducting ink, J. Mater. Chem. 21 (2011) 7562–7564. doi:10.1039/c1jm10630a.

[25] J. Liu, X. Li, X. Zeng, Silver nanoparticles prepared by chemical reduction-protection method, and their application in electrically conductive silver nanopaste, J. Alloys Compd. 494 (2010) 84–87. doi:10.1016/j.jallcom.2010.01.079.

[26] Y. Long, J. Wu, H. Wang, X. Zhang, N. Zhao, J. Xu, Rapid sintering of silver nanoparticles in an electrolyte solution at room temperature and its application to fabricate conductive silver films using polydopamine as adhesive layers, J. Mater. Chem. 21 (2011) 4875–4881. doi:10.1039/c0jm03838e.

[27] Q. Song, Y. Li, J. Xing, J.Y. Hu, Y. Marcus, Thermal stability of composite phase change material microcapsules incorporated with silver nano-particles, Polymer (Guildf). 48 (2007) 3317–3323. doi:10.1016/j.polymer.2007.03.045.

[28] M. Farrag, M. Tha, M. Tschurl, T. Bu, U. Heiz, Preparation and Spectroscopic Properties of Monolayer-Protected Silver Nanoclusters, J. Phys. Chem. 116 (2012) 8034–8043.

[29] A. Saxena, R.M. Tripathi, F. Zafar, P. Singh, Green synthesis of silver nanoparticles using aqueous solution of Ficus benghalensis leaf extract and characterization of their antibacterial activity, Mater. Lett. 67 (2012) 91–94. doi:10.1016/j.matlet.2011.09.038.

[30] M.J. Yim, Y. Li, K. Moon, K.W. Paik, C.P. Wong, Review of Recent Advances in Electrically Conductive Adhesive Materials and Technologies in Electronic Packaging, J. Adhes. Sci. Technol. 22 (2008) 1593–1630. doi:10.1163/156856108X320519.

[31] F. Liu, J.-M. Nunzi, Phosphorescent organic light emitting diode efficiency enhancement using functionalized silver nanoparticles, Appl. Phys. Lett. 99 (2011) 123302. doi:10.1063/1.3640892.

[32] J.C. Ramos, A. Ledezma, E. Arias, I. Moggio, C.A. Martínez, F. Castillon, Optical and morphological characterisation of a silver nanoparticle/fluorescent poly(phenylenethynylene) composite for optical biosensors, Vacuum. 84 (2010) 1244–1249. doi:10.1016/j.vacuum.2009.10.034.

[33] R.N. Das, F.D. Egitto, V.R. Markovich, Nano- and micro-filled conducting adhesives for <IT>z</IT>-axis interconnections: new direction for high-speed, high-density, organic microelectronics packaging, Circuit World. 34 (2008) 3–12. doi:10.1108/03056120810848743.

[34] R. Zhang, K. Moon, W. Lin, C.P. Wong, Preparation of highly conductive polymer nanocomposites by low temperature sintering of silver nanoparticles, J. Mater. Chem. 20 (2010) 2018–2023. doi:10.1039/b921072e.

[35] H. Gao, L. Liu, K. Liu, Y. Luo, D. Jia, J. Lu, Preparation of highly conductive adhesives by in situ generated and sintered silver nanoparticles during curing process, J. Mater. Sci. Mater. Electron. 23 (2011) 22–30. doi:10.1007/s10854-011-0388-8.

[36] L. Ye, Z. Lai, J. Liu, Effect of Ag Particle Size on Electrical Conductivity of Isotropically, IEEE Trans. Electron. Packag. Manuf. 22 (1999) 299–302.

[37] R. Zhang, W. Lin, K. Moon, C.P. Wong, Fast preparation of printable highly conductive polymer nanocomposites by thermal decomposition of silver carboxylate and sintering of silver nanoparticles., ACS Appl. Mater. Interfaces. 2 (2010) 2637–45. doi:10.1021/am100456m.

[38] P. Peng, A. Hu, H. Huang, A.P. Gerlich, B. Zhao, Y.N. Zhou, Room-temperature pressureless bonding with silver nanowire paste: towards organic electronic and heat-sensitive functional devices packaging, J. Mater. Chem. 22 (2012) 12997–13001. doi:10.1039/c2jm31979a.

[39] R. Zhang, K. Moon, W. Lin, J.C. Agar, C.-P. Wong, A simple, low-cost approach to prepare flexible highly conductive polymer composites by in situ reduction of silver carboxylate for flexible electronic applications, Compos. Sci. Technol. 71 (2011) 528–534. doi:10.1016/j.compscitech.2011.01.001.

[40] H.P. Wu, J.F. Liu, X.J. Wu, M.Y. Ge, Y.W. Wang, G.Q. Zhang, et al., High conductivity of isotropic conductive adhesives filled with silver nanowires, Int. J. Adhes. Adhes. 26 (2006) 617–621. doi:10.1016/j.ijadhadh.2005.10.001.

[41] Y. Oh, D. Suh, Y. Kim, E. Lee, J.S. Mok, J. Choi, et al., Silver-plated carbon nanotubes for silver/conducting polymer composites., Nanotechnology. 19 (2008) 495602. doi:10.1088/0957-4484/19/49/495602.

[42] R. Ma, S. Kwon, Q. Zheng, H.Y. Kwon, J. Il Kim, H.R. Choi, et al., Carbon-nanotube/silver networks in nitrile butadiene rubber for highly conductive flexible adhesives., Adv. Mater. 24 (2012) 3344–9. doi:10.1002/adma.201201273.

[43] F. Marcq, P. Demont, P. Monfraix, a. Peigney, C. Laurent, T. Falat, et al., Carbon nanotubes and silver flakes filled epoxy resin for new hybrid conductive adhesives, Microelectron. Reliab. 51 (2011) 1230–1234. doi:10.1016/j.microrel.2011.03.020.

[44] J. Feng, X. Ma, H. Mao, B. Liu, X. Zhao, Ag/epoxy nanocomposite film with aligned Ag nanowires and their polarization property, J. Mater. Res. 26 (2011) 2691–2700. doi:10.1557/jmr.2011.254.

[45] D. Chen, X. Qiao, X. Qiu, F. Tan, J. Chen, R. Jiang, Effect of silver nanostructures on the resistivity of electrically conductive adhesives composed of silver flakes, J. Mater. Sci. Mater. Electron. 21 (2010) 486–490. doi:10.1007/s10854-009-9943-y.

[46] Y.-H. Yu, C.-C.M. Ma, S.-M. Yuen, C.-C. Teng, Y.-L. Huang, I. Wang, et al., Morphology, Electrical, and Rheological Properties of Silane-Modified Silver Nanowire/Polymer Composites, Macromol. Mater. Eng. 295 (2010) 1017–1024. doi:10.1002/mame.201000180.

[47] T. Yu, Y. ZhenGuo, L. XiaoLu, T. GuoLiang, X. YanPing, W. HaiPing, Influence of filler morphology on percolation threshold of isotropical conductive adhesives (ICA), Sci. China Technol. Sci. 55 (2011) 28–33. doi:10.1007/s11431-011-4651-2.

[48] H. Wu, X. Wu, M. Ge, G. Zhang, Y. Wang, J. Jiang, Properties investigation on isotropical conductive adhesives filled with silver coated carbon nanotubes, Compos. Sci. Technol. 67 (2007) 1182–1186. doi:10.1016/j.compscitech.2006.05.010.

[49] Y. Tao, Y. Xia, H. Wang, F. Gong, H. Wu, G. Tao, Novel Isotropical Conductive Adhesives for, IEEE Trans. Adv. Packag. 32 (2009) 589–592.

[50] Z.X. Zhang, X.Y. Chen, F. Xiao, The Sintering Behavior of Electrically Conductive Adhesives Filled with Surface Modified Silver Nanowires, J. Adhes. Sci. Technol. 25 (2011) 1465–1480. doi:10.1163/016942410X549924.

[51] E. Marzbanrad, a. Hu, B. Zhao, Y. Zhou, Room Temperature Nanojoining of Triangular and Hexagonal Silver Nanodisks, J. Phys. Chem. C. 117 (2013) 16665–16676. doi:10.1021/jp403712x.

[52] S. Stankovich, D. a Dikin, G.H.B. Dommett, K.M. Kohlhaas, E.J. Zimney, E. a Stach, et al., Graphene-based composite materials., Nature. 442 (2006) 282–6. doi:10.1038/nature04969.

[53] K.S. Novoselov, a K. Geim, S. V Morozov, D. Jiang, M.I. Katsnelson, I. V Grigorieva, et al., Two-dimensional gas of massless Dirac fermions in graphene., Nature. 438 (2005) 197–200. doi:10.1038/nature04233.

[54] V.H. Luan, H.N. Tien, T.V. Cuong, B. Kong, J.S. Chung, E.J. Kim, et al., Novel conductive epoxy composites composed of 2-D chemically reduced graphene and 1-D silver nanowire hybrid fillers, J. Mater. Chem. 22 (2012) 8649. doi:10.1039/c2jm16910j.

[55] K.P. Loh, Q. Bao, P.K. Ang, J. Yang, The chemistry of graphene, J. Mater. Chem. 20 (2010) 2277–2289. doi:10.1039/b920539j.

[56] E.E. Tkalya, M. Ghislandi, G. de With, C.E. Koning, The use of surfactants for dispersing carbon nanotubes and graphene to make conductive nanocomposites, Curr. Opin. Colloid Interface Sci. 17 (2012) 225–232. doi:10.1016/j.cocis.2012.03.001.

[57] Y. Jin, M. Jia, M. Zhang, Q. Wen, Preparation of stable aqueous dispersion of graphene nanosheets and their electrochemical capacitive properties, Appl. Surf. Sci. 264 (2013) 787–793. doi:10.1016/j.apsusc.2012.10.130.

[58] R. Pasricha, S. Gupta, A.K. Srivastava, A facile and novel synthesis of Ag-graphene-based nanocomposites., Small. 5 (2009) 2253–9. doi:10.1002/smll.200900726.

[59] N.-W. Pu, Y.-Y. Peng, P.-C. Wang, C.-Y. Chen, J.-N. Shi, Y.-M. Liu, et al., Application of nitrogen-doped graphene nanosheets in electrically conductive adhesives, Carbon N. Y. 67 (2014) 449–456. doi:10.1016/j.carbon.2013.10.017.

[60] X. Peng, F. Tan, W. Wang, X. Qiu, F. Sun, X. Qiao, et al., Conductivity improvement of silver flakes filled electrical conductive adhesives via introducing silver–graphene nanocomposites, J. Mater. Sci. Mater. Electron. 25 (2014) 1149–1155. doi:10.1007/s10854-013-1671-7.

[61] B. Meschi Amoli, J. Trinidad, A. Hu, Y.N. Zhou, B. Zhao, Highly electrically conductive adhesives using silver nanoparticle (Ag NP)-decorated graphene: the effect of NPs sintering on the electrical conductivity improvement, J. Mater. Sci. Mater. Electron. 26 (2015) 590–600. doi:10.1007/s10854-014-2440-y.

[62] C. Bao, Y. Guo, L. Song, Y. Kan, X. Qian, Y. Hu, In situ preparation of functionalized graphene oxide/epoxy nanocomposites with effective reinforcements, J. Mater. Chem. 21 (2011) 13290–13298. doi:10.1039/c1jm11434d.

[63] H. Kim, Y. Miura, C.W. Macosko, Graphene/Polyurethane Nanocomposites for Improved Gas Barrier and Electrical Conductivity, Chem. Mater. 22 (2010) 3441–3450. doi:10.1021/cm100477v.

[64] M. Lotya, P.J. King, U. Khan, S. De, J.N. Coleman, High-concentration, surfactant-stabilized graphene dispersions., ACS Nano. 4 (2010) 3155–62. doi:10.1021/nn1005304.

[65] Y. Si, E.T. Samulski, Synthesis of Water Soluble Graphene, Nano Lett. 8 (2008) 1679–1682.

[66] Y. Li, D. Lu, C.P. Wong, Electrical Conductive Adhesives with Nanotechnologies, Springer US, Boston, MA, 2010. doi:10.1007/978-0-387-88783-8.

[67] J.J. Licari, D.W. Swanson, ADHESIVES TECHNOLOGY FOR by, William Andrew Publishing, Norwich, 2005.

[68] I.. Lau, John H (Agilent Technology, C.P. (Georgia I. of T. Wong, N.-C. (Indium C. of A. Lee, S.W.R. (Hong K.U. of S. and T. Lee, ELECTRONICS MANUFACTURING WITH LEAD-FREE, HALOGEN-FREE, AND CONDUCTIVE-ADHESIVE MATERIALS, The McGraw Hill, Inc, 2003. doi:10.1201/b12518.

[69] J.C. Jagt, Reliability of electrically conductive adhesive joints for surface mount applications: a summary of the state of the art, IEEE Trans. Components, Packag. Manuf. Technol. Part A. 21 (1998) 215–225. doi:10.1109/95.705467.

[70] A. Mikrajuddin, F.G. Shi, S. Chungpaiboonpatana, K. Okuyama, C. Davidson, J.M. Adams, Onset of electrical conduction in isotropic conductive adhesives : a general theory, Mater. Sci. Semicond. Process. 2 (1999) 309–319.

[71] A.J. Lovinger, Development of Electrical Conduction in Silver-filled Epoxy Adhesives I Development of Electrical r Conduction in Silver-filled Epoxy f Adhesives, J. Adhes. 10 (1979) 1–15.

[72] H. Wu, X. Wu, M. Ge, G. Zhang, Y. Wang, J. Jiang, Effect analysis of filler sizes on percolation threshold of isotropical conductive adhesives, Compos. Sci. Technol. 67 (2007) 1116–1120. doi:10.1016/j.compscitech.2006.05.017.

[73] J. Li, J.K. Lumpp, R. Andrews, D. Jacques, Aspect Ratio and Loading Effects of Multiwall Carbon Nanotubes in Epoxy for Electrically Conductive Adhesives, J. Adhes. Sci. Technol. 22 (2008) 1659–1671. doi:10.1163/156856108X320528.

[74] L. Li, J.E. Morris, Electrical Conduction Models for Isotropically Conductive Adhesive Joints, IEEE Trans. Components, Packag. Manuf. Technol. Part A. 20 (1997) 3–8.

[75] C. a. Martin, J.K.W. Sandler, M.S.P. Shaffer, M.-K. Schwarz, W. Bauhofer, K. Schulte, et al., Formation of percolating networks in multi-wall carbon-nanotube–epoxy composites, Compos. Sci. Technol. 64 (2004) 2309–2316. doi:10.1016/j.compscitech.2004.01.025.

[76] J. Li, P.C. Ma, W.S. Chow, C.K. To, B.Z. Tang, J.-K. Kim, Correlations between Percolation Threshold, Dispersion State, and Aspect Ratio of Carbon Nanotubes, Adv. Funct. Mater. 17 (2007) 3207–3215. doi:10.1002/adfm.200700065.

[77] G.R. Ruschau, S. Yoshikawa, R.E. Newnham, Resistivities of conductive composites, J. Appl. Phys. 72 (1992) 953. doi:10.1063/1.352350.

[78] M. Amjadi, A. Pichitpajongkit, S. Lee, S. Ryu, I. Park, Highly stretchable and sensitive strain sensor based on silver nanowire-elastomer nanocomposite., ACS Nano. 8 (2014) 5154–63. doi:10.1021/nn501204t.

[79] N. Hu, Y. Karube, C. Yan, Z. Masuda, H. Fukunaga, Tunneling effect in a polymer/carbon nanotube nanocomposite strain sensor, Acta Mater. 56 (2008) 2929–2936. doi:10.1016/j.actamat.2008.02.030.

[80] J.G. Simmons, Generalized Formula for the Electric Tunnel Effect between Similar Electrodes Separated by a Thin Insulating Film, J. Appl. Phys. 34 (1963) 1793. doi:10.1063/1.1702682.

[81] D. Lu, Q.K. Tong, C.P. Wong, Conductivity mechanisms of isotropic conductive adhesives (ICAs), in: Int. Symp. Adv. Packag. Mater., 1999: pp. 223–227. doi:10.1109/6104.795857.

[82] Y. Li, K. Moon, C.P. Wong, Electrical Property Improvement of Electrically Conductive Adhesives Through In-Situ Replacement by Short-Chain Difunctional Acids, IEEE Electron. Componenets Technol. Conf. 29 (2006) 173–178.

[83] C. Yang, Y.-T. Xie, M.M.-F. Yuen, B. Xu, B. Gao, X. Xiong, et al., Silver Surface Iodination for Enhancing the Conductivity of Conductive Composites, Adv. Funct. Mater. 20 (2010) 2580–2587. doi:10.1002/adfm.201000673.

[84] C. Yang, W. Lin, Z. Li, R. Zhang, H. Wen, B. Gao, et al., Water-Based Isotropically Conductive Adhesives: Towards Green and Low-Cost Flexible Electronics, Adv. Funct. Mater. 21 (2011) 4582–4588. doi:10.1002/adfm.201101433.

[85] C. Gallagher, G. Matijasevic, J.F. Maguire, Transient Liquid Phase Sintering Conductive Adhesives, in: IEEE Electron. Componenets Technol. Conf., 1997: pp. 554–560.

[86] S. Khairul Anuar, M. Mariatti, a. Azizan, N. Chee Mang, W.T. Tham, Effect of different types of silver and epoxy systems on the properties of silver/epoxy conductive adhesives, J. Mater. Sci. Mater. Electron. 22 (2010) 757–764. doi:10.1007/s10854-010-0207-7.

[87] Y. Li, K. Moon, A. Whitman, C.P. Wong, Enhancement of Electrical Properties of Electrically Conductive Adhesives (ECAs) by Using Novel Aldehydes, IEEE Trans. Components Packag. Technol. 29 (2006) 758–763.

[88] H.-W. Cui, A. Kowalczyk, D.-S. Li, Q. Fan, High performance electrically conductive adhesives from functional epoxy, micron silver flakes, micron silver spheres and acidified single wall carbon nanotube for electronic package, Int. J. Adhes. Adhes. 44 (2013) 220–225. doi:10.1016/j.ijadhadh.2013.03.004.

[89] H.-H. Lee, K.-S. Chou, Z.-W. Shih, Effect of nano-sized silver particles on the resistivity of polymeric conductive adhesives, Int. J. Adhes. Adhes. 25 (2005) 437–441. doi:10.1016/j.ijadhadh.2004.11.008.

[90] S.-S. Chee, J.-H. Lee, Reduction synthesis of silver nanoparticles anchored on silver micro-flakes and electrical resistivity of isotropic conductive adhesives at percolation threshold, Electron. Mater. Lett. 8 (2012) 315–320. doi:10.1007/s13391-012-1105-3.

[91] L. Fan, B. Su, J. Qu, C.P. Wong, Electrical and Thermal Conductivities of Polymer Composites Containing Nano-Sized Particles, in: Electron. Components Technol. Conf., 2004: pp. 148–154.

[92] P. Mach, R. Radev, A. Pietrikova, Electrically Conductive Adhesive Filled with Mixture of Silver Nano and Microparticles, in: Electron. Syst. Technol. Conf., IEEE, Greenwich, 2008: pp. 1141–1146.

[93] D. Wakuda, K. Kim, K. Suganuma, Room temperature sintering of Ag nanoparticles by drying solvent, Scr. Mater. 59 (2008) 649–652. doi:10.1016/j.scriptamat.2008.05.028.

[94] A. Hu, J.Y. Guo, H. Alarifi, G. Patane, Y. Zhou, G. Compagnini, et al., Low temperature sintering of Ag nanoparticles for flexible electronics packaging, Appl. Phys. Lett. 97 (2010) 153117. doi:10.1063/1.3502604.

[95] S.. Lai, J.. Guo, V. Petrova, G. Ramanath, L.. Allen, Size-dependent melting properties of small tin particles: nanocalorimetric measurements, Phys. Rev. Lett. 77 (1996) 99–102. http://www.ncbi.nlm.nih.gov/pubmed/20482218.

[96] B.J. Perelaer, A.W.M. de Laat, C.E. Hendriks, U.S. Schubert, Inkjet-printed silver tracks: low temperature curing and thermal stability investigation, J. Mater. Chem. 18 (2008) 3209. doi:10.1039/b720032c.

[97] Z.Z. Fang, H. Wang, Densification and grain growth during sintering of nanosized particles, Int. Mater. Rev. 53 (2008) 326–352. doi:10.1179/174328008X353538.

[98] J.G. Bai, T.G. Lei, J.N. Calata, G.-Q. Lu, Control of nanosilver sintering attained through organic binder burnout, J. Mater. Res. 22 (2011) 3494–3500. doi:10.1557/JMR.2007.0440.

[99] S. Magdassi, M. Grouchko, O. Berezin, A. Kamyshny, Triggering the sintering of silver nanoparticles at room temperature., ACS Nano. 4 (2010) 1943–8. doi:10.1021/nn901868t.

[100] L. Polavarapu, K.K. Manga, H.D. Cao, K.P. Loh, Q. Xu, Preparation of Conductive Silver Films at Mild Temperatures for, Chem. Mater. 23 (2011) 3273–3276.

[101] B. Meschi Amoli, E. Marzbanrad, A. Hu, Y.N. Zhou, B. Zhao, Electrical Conductive Adhesives Enhanced with High-Aspect-Ratio Silver Nanobelts, Macromol. Mater. Eng. 299 (2014) 739–747. doi:10.1002/mame.201300295.

[102] Z. Zhang, X. Chen, H. Yang, H. Fu, F. Xiao, Electrically conductive adhesives with sintered silver nanowires, 2009 Int. Conf. Electron. Packag. Technol. High Density Packag. (2009) 834–837. doi:10.1109/ICEPT.2009.5270629.

[103] M. Moskovits, J.S. Suh, Conformation of Mono- and Dicarboxylic Acids Adsorbed on Silver Surfaces, J. Am. Chem. Soc. 107 (1985) 6826–6829.

[104] S. Iijima, Iijima 1991, Helical microtubules of graphitic carbon.pdf, Nature. 354 (1991) 56–58.

[105] T.W. Odom, J. Huang, Atomic structure and electronic properties of single-walled carbon nanotubes, Nature. 391 (1998) 1997–1999.

[106] J. Lu, I. Do, L.T. Drzal, R.M. Worden, I. Lee, Nanometal-decorated exfoliated graphite nanoplatelet based glucose biosensors with high sensitivity and fast response., ACS Nano. 2 (2008) 1825–32. doi:10.1021/nn800244k.

[107] A. O'Neill, U. Khan, P.N. Nirmalraj, J. Boland, J.N. Coleman, Graphene Dispersion and Exfoliation in Low Boiling Point Solvents, J. Phys. Chem. C. 115 (2011) 5422–5428. doi:10.1021/jp110942e.

[108] V.H. Pham, T.V. Cuong, S.H. Hur, E. Oh, E.J. Kim, E.W. Shin, et al., Chemical functionalization of graphene sheets by solvothermal reduction of a graphene oxide suspension in N-methyl-2-pyrrolidone, J. Mater. Chem. 21 (2011) 3371. doi:10.1039/c0jm02790a.

[109] A.S. Wajid, H.S.T. Ahmed, S. Das, F. Irin, A.F. Jankowski, M.J. Green, High-Performance Pristine Graphene/Epoxy Composites With Enhanced Mechanical and Electrical Properties, Macromol. Mater. Eng. 298 (2013) 339–347. doi:10.1002/mame.201200043.

[110] L. Xuechun, L. Feng, The improvement on the properties of silver-containing conductive adhesives by the addition of carbon nanotube, in: Proc. Sixth IEEE CPMT Conf. High Density Microsyst. Des. Packag. Compon. Fail. Anal. (HDP '04), Ieee, 2004: pp. 382–384. doi:10.1109/HPD.2004.1346734.

[111] J. Kim, B. Yim, J. Kim, J. Kim, The effects of functionalized graphene nanosheets on the thermal and mechanical properties of epoxy composites for anisotropic conductive adhesives (ACAs), Microelectron. Reliab. 52 (2012) 595–602. doi:10.1016/j.microrel.2011.11.002.

[112] K. Liu, S. Chen, Y. Luo, D. Jia, H. Gao, G. Hu, et al., Edge-functionalized graphene as reinforcement of epoxy-based conductive composite for electrical interconnects, Compos. Sci. Technol. 88 (2013) 84–91. doi:10.1016/j.compscitech.2013.08.032.

[113] K. Liu, L. Liu, Y. Luo, D. Jia, One-step synthesis of metal nanoparticle decorated graphene by liquid phase exfoliation, J. Mater. Chem. 22 (2012) 20342–20352. doi:10.1039/c2jm34617f.

[114] K. Liu, S. Chen, Y. Luo, D. Jia, H. Gao, G. Hu, et al., Noncovalently functionalized pristine graphene/metal nanoparticle hybrid for conductive composites, Compos. Sci. Technol. 94 (2014) 1–7. doi:10.1016/j.compscitech.2014.01.006.

[115] R. Brenier, Enhancement of Light Transmission through Silver Nanoparticles, J. Phys. Chem. C. 116 (2012) 5358–5366. doi:10.1021/jp210374j.

[116] R. Bryaskova, D. Pencheva, G.M. Kale, U. Lad, T. Kantardjiev, Synthesis, characterisation and antibacterial activity of PVA/TEOS/Ag-Np hybrid thin films., J. Colloid Interface Sci. 349 (2010) 77–85. doi:10.1016/j.jcis.2010.04.091.

[117] M. Layani, S. Magdassi, Flexible transparent conductive coatings by combining self-assembly with sintering of silver nanoparticles performed at room temperature, J. Mater. Chem. 21 (2011) 15378. doi:10.1039/c1jm13174e.

[118] L. Bao, B. Wei, A.Y. Xiao, Conductive Coating Formulations with silver content, Electron. Components Technol. Conf. (2007) 494–500.

[119] C. Shen, C. Hui, T. Yang, C. Xiao, J. Tian, L. Bao, et al., Monodisperse Noble-Metal Nanoparticles and Their Surface Enhanced Raman Scattering Properties, Chem. Mater. 20 (2008) 6939–6944.

[120] C.J. Sandroff, S. Garoff, K.P. Leung, Surface-Enhanced Raman Study of The Solid-Liquid Interface: Conformational Changes in Adsorbed Molecules, Chem. Phys. 96 (1983) 547–551.

[121] C.D. Bain, B.E. Troughton, Y.-T. Tao, J. Evail, G.M. Whitesides, R.G. Nuzzo, Formation of Monolayer Films by the Spontaneous Assembly of Organic Thiols from Solution onto Gold', 335 (1989) 321–335.

[122] M. Brust, M. Walker, D. Bethell, D.J. Schiffrin, R. Whyman, Synthesis of Thiol-derivatised Gold Nanoparticles in, J. Chem. Soc., Chem. Commun. (1994) 801–802.

[123] Q. Zhang, J. Xie, Y. Yu, J.Y. Lee, Monodispersity control in the synthesis of monometallic and bimetallic quasi-spherical gold and silver nanoparticles., Nanoscale. 2 (2010) 1962–75. doi:10.1039/c0nr00155d.

[124] A.N. Parikh, S.D. Gillmor, J.D. Beers, K.M. Beardmore, R.W. Cutts, B.I. Swanson, Characterization of Chain Molecular Assemblies in Long-Chain , Layered Silver Thiolates : A Joint Infrared Spectroscopy and X-ray Diffraction Study, J. Phys. Chem. B. 103 (1999) 2850–2861.

[125] J.C. Love, L. a Estroff, J.K. Kriebel, R.G. Nuzzo, G.M. Whitesides, Self-assembled monolayers of thiolates on metals as a form of nanotechnology., Chem. Rev. 105 (2005) 1103–69. doi:10.1021/cr0300789.

[126] M.D. Malinsky, K.L. Kelly, G.C. Schatz, R.P. Van Duyne, Chain Length Dependence and Sensing Capabilities of the Localized Surface Plasmon Resonance of Silver Nanoparticles Chemically Modified with Alkanethiol Self-Assembled Monolayers, J. Am. Chem. Soc. 123 (2001) 1471–1482.

[127] S. Chen, K. Kimura, Synthesis and Characterization of Carboxylate-Modified Gold Nanoparticle Powders Dispersible in Water, Langmuir. 15 (1999) 1075–1082.

[128] S. Chen, K. Kimura, Water soluble nanoparticles functionalized with thiolate.pdf, Chem. Lett. (1999) 1169–1170.

[129] C. Ma, J.M. Harris, Surface-enhanced Raman scattering study of the kinetics of self-assembly of carboxylate-terminated n-alkanethiols on silver., Langmuir. 28 (2012) 2628–36. doi:10.1021/la2037444.

[130] I.E. Dell'Erba, C.E. Hoppe, R.J.J. Williams, Synthesis of silver nanoparticles coated with OH-functionalized organic groups: dispersion and covalent bonding in epoxy networks., Langmuir. 26 (2010) 2042–2049. doi:10.1021/la902568v.

[131] T. Yonezawa, T. Sutoh, M. Kunitake, practical preparation of size controlled gold nanoparticles in water.pdf, Chem. Lett. (n.d.) 619–620.

[132] F. Moores, A. Goettmann, The plasmon band in noble metal nanoparticles : an introduction to theory and applications, New J. Chem. 30 (2006) 1121–1132. doi:10.1039/b604038c.

[133] L. Kvıtek, A. Panacek, J. Soukupova, M. Kolar, R. Vecerova, R. Prucek, et al., Effect of Surfactants and Polymers on Stability and Antibacterial Activity of Silver Nanoparticles (NPs), J. Phys. Chem. C. 112 (2008) 5825–5834.

[134] A. Henglein, D. Meisel, Spectrophotometric Observations of the Adsorption of Organosulfur Compounds on Colloidal Silver Nanoparticles, J. Phys. Chem. B. 102 (1998) 8364–8366.

[135] S. He, J. Yao, P. Jiang, D. Shi, H. Zhang, S. Xie, et al., Formation of Silver Nanoparticles and Self-Assembled Two-Dimensional Ordered Superlattice, Langmuir. 17 (2001) 1571–1575.

[136] Y. Badr, M. Wahed, M. Mahmoud, On 308nm photofragmentation of the silver nanoparticles, Appl. Surf. Sci. 253 (2006) 2502–2507. doi:10.1016/j.apsusc.2006.05.021.

[137] A. Manna, B.D. Kulkarni, K. Bandyopadhyay, K. Vijayamohanan, Synthesis and Characterization of Hydrophobic , Approtically-Dispersible , Silver Nanoparticles in Winsor II Type Microemulsions, Chem. Mater. 9 (1997) 3032–3036.

[138] L.A. Porter, D. Ji, S.L. Westcott, M. Graupe, R.S. Czernuszewicz, N.J. Halas, et al., Gold and Silver Nanoparticles Functionalized by the Adsorption of Dialkyl Disulfides, Langmuir. 14 (1998) 7378–7386.

[139] D.E. Cliffel, F.P. Zamborini, S.M. Gross, R.W. Murray, Gold , Silver , and Palladium Clusters, Langmuir. 16 (2000) 9699–9702.

[140] J.C. Agar, K.J. Lin, R. Zhang, J. Durden, K. Lawrence, K. Moon, et al., Deconstructing the Myth of Percolation in Electrically Conductive Adhesives and Its Implications, in: Proc 60th Electron. Components Technol. Conf., 2010: pp. 1713–1718.

[141] W. Songping, M. Shuyuan, Preparation of ultrafine silver powder using ascorbic acid as reducing agent and its application in MLCI, Mater. Chem. Phys. 89 (2005) 423–427. doi:10.1016/j.matchemphys.2004.09.026.

[142] A.R. Tao, S. Habas, P. Yang, Shape Control of Colloidal Metal Nanocrystals, Small. 4 (2008) 310–325. doi:10.1002/smll.200701295.

[143] D. Spadaro, E. Barletta, F. Barreca, G. Currò, F. Neri, Synthesis of PMA stabilized silver nanoparticles by chemical reduction process under a two-step UV irradiation, Appl. Surf. Sci. 256 (2010) 3812–3816. doi:10.1016/j.apsusc.2010.01.031.

[144] J.L. Elechiguerra, J. Reyes-Gasga, M.J. Yacaman, The role of twinning in shape evolution of anisotropic noble metal nanostructures, J. Mater. Chem. 16 (2006) 3906. doi:10.1039/b607128g.

[145] D. Aherne, D.M. Ledwith, M. Gara, J.M. Kelly, Optical Properties and Growth Aspects of Silver Nanoprisms Produced by a Highly Reproducible and Rapid Synthesis at Room Temperature, Adv. Funct. Mater. 18 (2008) 2005–2016. doi:10.1002/adfm.200800233.

[146] X. Lu, M. Rycenga, S.E. Skrabalak, B. Wiley, Y. Xia, Chemical synthesis of novel plasmonic nanoparticles., Annu. Rev. Phys. Chem. 60 (2009) 167–92. doi:10.1146/annurev.physchem.040808.090434.

[147] M. Maillard, S. Giorgio, M.-P. Pileni, Silver Nanodisks, Adv. Mater. 14 (2002) 1084. doi:10.1002/1521-4095(20020805)14:15<1084::AID-ADMA1084>3.0.CO;2-L.

[148] V. Germain, J. Li, D. Ingert, Z.L. Wang, M.P. Pileni, Stacking Faults in Formation of Silver Nanodisks, J. Phys. Chem. B. 107 (2003) 8717–8720. doi:10.1021/jp0303826.

[149] F.. Bartell, P.H. Cardwell, secondary reactions of these radicals . Reproducible Contact Angles on Reproducible Metal Surfaces . I . Contact Angles of Water against Silver and Gold ' AND PAUL, JACS. 64 (1942) 494–497.

[150] A. Safaee, D.K. Sarkar, M. Farzaneh, Superhydrophobic properties of silver-coated films on copper surface by galvanic exchange reaction, Appl. Surf. Sci. 254 (2008) 2493–2498. doi:10.1016/j.apsusc.2007.09.073.

[151] R. Heeb, R.M. Bielecki, S. Lee, N.D. Spencer, Room-Temperature, Aqueous-Phase Fabrication of Poly(methacrylic acid) Brushes by UV-LED-Induced, Controlled Radical Polymerization with High Selectivity for Surface-Bound Species, Macromolecules. 42 (2009) 9124–9132. doi:10.1021/ma901607w.

[152] M.K. Singh, E. Titus, R. Krishna, R.R. Hawaldar, G. Goncalves, P. a. a. P. Marques, et al., Direct Nucleation of Silver Nanoparticles on Graphene Sheet, J. Nanosci. Nanotechnol. 12 (2012) 6731–6736. doi:10.1166/jnn.2012.4572.

[153] G. Goncalves, P.A.A.P. Marques, C.M. Granadeiro, H.I.S. Nogueira, M.K. Singh, J. Grácio, Surface Modification of Graphene Nanosheets with Gold Nanoparticles: The Role of Oxygen Moieties at Graphene Surface on Gold Nucleation and Growth, Chem. Mater. 21 (2009) 4796–4802. doi:10.1021/cm901052s.

[154] J.I. Paredes, S. Villar-Rodil, a Martínez-Alonso, J.M.D. Tascón, Graphene oxide dispersions in organic solvents., Langmuir. 24 (2008) 10560–4. doi:10.1021/la801744a.

[155] A.B. Bourlinos, D. Gournis, D. Petridis, T. Szabó, A. Szeri, I. Dékány, Graphite Oxide: Chemical Reduction to Graphite and Surface Modification with Primary Aliphatic Amines and Amino Acids, Langmuir. 19 (2003) 6050–6055. doi:10.1021/la026525h.

[156] L. Zhou, H. Gu, C. Wang, J. Zhang, M. Lv, R. He, Study on the synthesis and surface enhanced Raman spectroscopy of graphene-based nanocomposites decorated with noble metal nanoparticles, Colloids Surfaces A Physicochem. Eng. Asp. 430 (2013) 103–109. doi:10.1016/j.colsurfa.2013.04.012.

[157] H.C. Schniepp, J.-L. Li, M.J. McAllister, H. Sai, M. Herrera-Alonso, D.H. Adamson, et al., Functionalized single graphene sheets derived from splitting graphite oxide., J. Phys. Chem. B. 110 (2006) 8535–9. doi:10.1021/jp060936f.

[158] V. Georgakilas, M. Otyepka, A.B. Bourlinos, V. Chandra, N. Kim, K.C. Kemp, et al., Functionalization of graphene: covalent and non-covalent approaches, derivatives and applications., Chem. Rev. 112 (2012) 6156–214. doi:10.1021/cr3000412.

[159] A. Yu, I. Roes, A. Davies, Z. Chen, Ultrathin, transparent, and flexible graphene films for supercapacitor application, Appl. Phys. Lett. 96 (2010) 253105. doi:10.1063/1.3455879.

[160] A. Davies, P. Audette, B. Farrow, F. Hassan, Z. Chen, J.-Y. Choi, et al., Graphene-Based Flexible Supercapacitors: Pulse-Electropolymerization of Polypyrrole on Free-Standing Graphene Films, J. Phys. Chem. C. 115 (2011) 17612–17620. doi:10.1021/jp205568v.

[161] G. Rivers, A. Rogalsky, P. Lee-Sullivan, B. Zhao, Thermal analysis of epoxy-based nanocomposites: Have solvent effects been overlooked?, J. Therm. Anal. Calorim. 119 (2015) 797–805. doi:10.1007/s10973-013-3613-2.

[162] D.C. Marcano, D. V Kosynkin, J.M. Berlin, A. Sinitskii, Z. Sun, A. Slesarev, et al., Improved synthesis of graphene oxide., ACS Nano. 4 (2010) 4806–14. doi:10.1021/nn1006368.

[163] M. Wojtoniszak, D. Rogińska, B. Machaliński, M. Drozdzik, E. Mijowska, Graphene oxide functionalized with methylene blue and its performance in singlet oxygen generation, Mater. Res. Bull. 48 (2013) 2636–2639. doi:10.1016/j.materresbull.2013.03.040.

[164] R.B. Viana, A.B.F. da Silva, A.S. Pimentel, Infrared Spectroscopy of Anionic, Cationic, and Zwitterionic Surfactants, Adv. Phys. Chem. 2012 (2012) 1–14. doi:10.1155/2012/903272.

[165] S.L. Qiu, C.S. Wang, Y.T. Wang, C.G. Liu, X.Y. Chen, H.F. Xie, et al., Effects of graphene oxides on the cure behaviors of a tetrafunctional epoxy resin, Express Polym. Lett. 5 (2011) 809–818. doi:10.3144/expresspolymlett.2011.79.

[166] D.W. Boukhvalov, D.R. Dreyer, C.W. Bielawski, Y.W. Son, A Computational Investigation of the Catalytic Properties of Graphene Oxide: Exploring Mechanisms by using DFT Methods, ChemCatChem. 4 (2012) 1844–1849. doi:10.1002/cctc.201200210.

[167] R.E. Parker, N.S. Isaacs, Mechanisms Of Epoxide Reactions, Chem. Rev. 59 (1959) 737–799. doi:10.1021/cr50028a006.

[168] W. Wang, H. Lu, Y. Liu, J. Leng, Sodium dodecyl sulfate/epoxy composite: water-induced shape memory effect and its mechanism, J. Mater. Chem. A. 2 (2014) 5441. doi:10.1039/c3ta15204a.

[169] J.M. Patterson, Z. Kortylewicz, W.T. Smith, Thermal Degradation of Sodium Dodecyl Sulfate, J. Agric. Food Chem. 32 (1984) 782–784.

[170] Y.C. Chiu, I.C. Chou, W.C. Tseng, C.C.M. Ma, Preparation and thermal properties of diglycidylether sulfone epoxy, Polym. Degrad. Stab. 93 (2008) 668–676. doi:10.1016/j.polymdegradstab.2007.12.014.